Molecular and Cellular Control of Intrathymic T-Cell Development

Dissertation

zur Erlangung des Doktorgrades

der Naturwissenschaften

vorgelegt beim Fachbereich 14

Biochemie, Chemie und Pharmazie

der Johann Wolfgang Goethe-Universität

in Frankfurt am Main

von

Heike Kunze-Schumacher

aus Westerstede

Frankfurt am Main, 2021

(D30)

vom Fachbereich Biochemie, Chemie und Pharmazie (14)
der Johann Wolfgang Goethe-Universität als Dissertation angenommen.

Dekan: Prof. Dr. Clemens Glaubitz

Erstgutachter: Prof. Dr. Robert Tampé
Zweitgutachter: Prof. Dr. Andreas Krueger

Datum der Disputation:

Results and parts of this work were published in:

1. **Kunze-Schumacher, H.**, Winter, S.J., Imelmann, E., and Krueger, A. (2018). miRNA miR-21 Is Largely Dispensable for Intrathymic T-Cell Development. *Frontiers in immunology* 9, 2497

2. **Kunze-Schumacher, H.**, and Krueger, A. (2020). The Role of MicroRNAs in Development and Function of Regulatory T Cells - Lessons for a Better Understanding of MicroRNA Biology. *Frontiers in immunology* 11, 2185

3. Robert, P.A., **Kunze-Schumacher, H.**, Greiff, V., and Krueger, A. (2021). Modeling the Dynamics of T-Cell Development in the Thymus. *Entropy (Basel, Switzerland)* 23

Additional scientific contributions during doctoral studies (2016-2021):

4. Abels, W.C., Manandhar, T., **Kunze-Schumacher, H**., Blasczyk, R., and Bade-Döding, C. (2018). The polymorphism at residue 156 determines the HLA-B*35 restricted peptide repertoire during HCMV infection. *Immunogenetics* 70, 639-646
5. Simper, G.S., Hò, G.-G.T., Celik, A.A., Huyton, T., Kuhn, J., **Kunze-Schumacher, H.**, Blasczyk, R., and Bade-Döding, C. (2018). Carbamazepine-Mediated Adverse Drug Reactions: CBZ-10,11-epoxide but Not Carbamazepine Induces the Alteration of Peptides Presented by HLA-B∗15:02. *Journal of immunology research* 2018, 5086503
6. Blume, J., Ziętara, N., Witzlau, K., Liu, Y., Sanchez, O.O., Puchałka, J., Winter, S.J., **Kunze-Schumacher, H.**, Saran, N., and Düber, S., et al. (2019). miR-191 modulates B-cell development and targets transcription factors E2A, Foxp1, and Egr1. *European journal of immunology* 49, 121-132
7. Brune, T., **Kunze-Schumacher, H.**, and Kölling, R. (2019). Interactions in the ESCRT-III network of the yeast Saccharomyces cerevisiae. *Current genetics* 65, 607-619
8. Cossarizza, A., …, **Kunze-Schumacher, H.**, et al. (2019). Guidelines for the use of flow cytometry and cell sorting in immunological studies (second edition). *European journal of immunology* 49, 1457-1973
9. Łyszkiewicz, M., Winter, S.J., Witzlau, K., Föhse, L., Brownlie, R., Puchałka, J., Verheyden, N.A., **Kunze-Schumacher, H.**, Imelmann, E., and Blume, J., et al. (2019). miR-181a/b-1 controls thymic selection of Treg cells and tunes their suppressive capacity. *PLoS biology* 17, e2006716
10. Pump, W.C., Schulz, R., Huyton, T., **Kunze-Schumacher, H.**, Martens, J., Hò, G.-G.T., Blasczyk, R., and Bade-Doeding, C. (2019). Releasing the concept of HLA-allele specific peptide anchors in viral infections: A non-canonical naturally presented human cytomegalovirus-derived HLA-A*24:02 restricted peptide drives exquisite immunogenicity. *HLA* 94, 25-38

11. Ronkina, N., Schuster-Gossler, K., Hansmann, F., **Kunze-Schumacher, H.**, Sandrock, I., Yakovleva, T., Lafera, J., Baumgärtner, W., Krueger, A., and Prinz, I., et al. (2019). Germ Line Deletion Reveals a Nonessential Role of Atypical Mitogen-Activated Protein Kinase 6/Extracellular Signal-Regulated Kinase 3. *Molecular and cellular biology* 39
12. Simper, G.S., Gräser, L.S., Celik, A.A., Kuhn, J., **Kunze-Schumacher, H.**, Hò, G.-G.T., Blasczyk, R., Pich, A., and Bade-Doeding, C. (2019). The Mechanistic Differences in HLA-Associated Carbamazepine Hypersensitivity. *Pharmaceutics* 11
13. Winter, S.J., **Kunze-Schumacher, H.**, Imelmann, E., Grewers, Z., Osthues, T., and Krueger, A. (2019). MicroRNA miR-181a/b-1 controls MAIT cell development. *Immunology and cell biology* 97, 190-202
14. Meyer, A., Herkt, S., **Kunze-Schumacher, H.**, Kohrs, N., Ringleb, J., Schneider, L., Kuvardina, O.N., Oellerich, T., Häupl, B., and Krueger, A., et al. (2020). The transcription factor TAL1 and miR-17-92 create a regulatory loop in hematopoiesis. *Scientific reports* 10, 21438
15. Cossarizza, A., …, **Kunze-Schumacher, H.**, et al. 2021. Guidelines for the use of flow cytometry and cell sorting in immunological studies (third edition). *European journal of immunology* online version

.

Contents

Declaration

Except where stated otherwise by reference or acknowledgment, the work presented was generated by myself under the supervision of my advisors during my doctoral studies. All contributions from colleagues are explicitly referenced in the thesis.

The plasmid MDH1-PGK-GFP_2.0-miR-21 was generated by Dr. Namita Saran, Krueger laboratory, Institute for Immunology, Hannover Medical School. All subsequent experiments were performed by myself.

Figure 31, **Figure 41**, **Figure 42**, **Figure 43**: Cell sorting was performed by Praveen Mathorr, Brüne laboratory, Institute of Biochemistry I, Faculty of Medicine, Goethe University, Frankfurt. Preparation, staining of cells and sorter settings were performed by myself.

Figure 23, Figure 24, Figure 25, Figure 52: scRNA-seq was done on a collaborative basis with the laboratory of Dr. Mir Farzin Mashreghi (Therapeutic Gene Regulation) at the Deutsches Rheuma Forschungszentrum (DRFZ) in Berlin. Preparation, staining of cells and sorting were performed by myself. All steps upon sorting were done by Dr. Gitta Heinz. Bioinformatic analyses were done in consultation and applied by Dr. Pawel Durek and Dr. Frederik Heinrich.

The following parts of the thesis have been previously published: Figure 31 - Figure 47 of section 4.2 were published in Kunze-Schumacher et al. 2018.

The rights have been granted by co-authors to include the material in this dissertation.

Summary

T-cell development is a highly dynamic and stepwise process comprimising T-lineage commitment, T-cell receptor (TCR) gene rearrangements and subsequent selection. From a quantitative point of view, only a few hundred progenitor cells migrate from the bone marrow into the thymus. Developing thymocytes (termed double negative (DN), $CD4^{-}CD8^{-}$) can be further divided into DN1-4 cells based on the expression of CD25 and CD44. These developmental events are interspersed by proliferative bursts which ultimately lead to the generation of millions of double positive (DP, $CD4^{+}CD8^{+}$) thymocytes that then undergo selection. As a consequence, a proportion of naïve T cells evolves to ensure adaptive, but not autoreactive immunity.

Previous studies of our lab focused on the quantification of thymus colonization and identified thymus entry to be dependent on expression of the chemokine receptors CCR7 and CCR9 (Krueger et al., 2010; Ziętara et al., 2015). CCR7/9 double knockout (DKO) mice are almost completely devoid of the most immature thymocyte populations (DN1 and DN2), but show near normal DN3 cellularity. Interestingly, a similar defect during early development but a virtually complete recovery of later stages and total thymocyte numbers was also observed in thymi of miR-17~92-deficient mice. Here, a failure of prethymic IL-7 signaling dampens early T-cell development (Regelin et al., 2015). For this reason, we hypothesized a tight regulation of thymocyte population size through alterations in the underlying cell cycle kinetics.

In this thesis, we employed *in vivo* single- and dual-nucleoside pulse labeling combined with determination of DNA replication over time in different WT thymocyte subsets at steady-state. Based on this, we assessed alterations in cell cycle kinetics of CCR7/9- and miR-17~92-defcicient mice and identified compensatory mechanisms of thymocytes on the level of cell cycle phase distribution and cell cycle speed. In addition, single-cell RNA sequencing helped to obtain information on cell cycle dynamics of early thymocyte subsets, exemplarily shown for WT and CCR7/9 DKO mice. Lastly, we performed cell cycle analyses in a model of endogenous thymic repair upon sublethal total body irradiation which provided insight into intrathymic cell cycle regulation as an adjustable system to re-establish normal thymus cellularity.

In the second part of the thesis, we addressed the role of miR-21 in the thymus. In various studies, we and others identified miRNAs as key posttranscriptional regulators of the immune system and especially for T-cell development (Regelin et al. 2015; Mildner et al. 2017; Li et al. 2007; Ebert et al. 2009; Ziętara et al. 2013; Schaffert

et al. 2015). The dynamic expression of miR-21 during T-cell development (Neilson et al. 2007; Kirigin et al. 2012; Kuchen et al. 2010) prompted us to hypothesize that miR-21 has a regulatory function in the thymus. A miR-21 knockout mouse model allowed us to study the role of this miRNA for the development of T cells in the thymus and the maintenance of T cells in the periphery. In addition, we performed competitive bone marrow chimera experiments in the context of miR-21 deficiency and overexpression. Further insights were provided by exploring the function of miR-21 in negative selection *in vivo* as well as in T-cell differentiation in coculture experiments *in vitro*. To unravel implications of miR-21 to regulate cellular stress responses, we assessed the contribution of miR-21 in a model of endogenous regeneration of the thymus after sublethal irradiation. We could not provide evidence for a prominent role for miR-21 during T-cell development. Together, our experiments revealed that miR-21 is largely dispensable for physiologic T-cell development despite high and dynamic expression in the thymus (Kunze-Schumacher et al., 2018). The apparent discrepancy between dynamic expression but lack of a regulatory function in the thymus led us to conclude that miR-21 is rather fine-tuning T-cell responses than controlling a developmental event.

Deutsche Zusammenfassung

Das adaptive Immunsystem ist von elementarer Bedeutung für die Eliminierung von Infektionserregern. T-Zellen stellen dabei das zentrale Glied der erworbenen Immunantwort dar, da sie Effektormechanismen lenken, die zur Bekämpfung von verschiedenen Krankheitserregern beitragen. Insbesondere für die Regeneration nach einer hämatopoetischen Stammzelltransplantation sind T-Zellen von zentraler Bedeutung, denn durch die vorausgehende myeloablative Therapie (Chemotherapie und/oder Bestrahlung) werden nicht nur Tumorzellen, sondern auch das Immunsystem supprimiert. Dies zieht als Konsequenz eine langanhaltende Phase der Immundefizienz nach sich. Ein besseres Verständnis der molekularen und zellulären Prozesse, die die T-Zellentwicklung und -regeneration beeinflussen, ist daher dringend notwendig, um die Wiederherstellung des erworbenen Immunsystems weiter zu verbessern und zu beschleunigen. Die Entwicklung der T-Zellen findet in einem hochspezialisierten Organ, dem Thymus, statt (Miller, 1961) und beruht auf der regelmäßigen Einwanderung von Vorläuferzellen aus dem Knochenmark. Diese Vorläuferzellen reifen in einem mehrstufigen Entwicklungsprozess heran und durchlaufen schlussendlich Selektionsprozesse. In der frühen Entwicklung exprimieren die heranreifenden Thymozyten weder CD4 noch CD8 und werden daher als doppelt negativ (DN) bezeichnet. Diese frühen Stadien der T-Zellentwicklung lassen sich u.a. anhand der Oberflächenexpression von CD25 und CD44 in die Stadien DN1-4 sowie durch die Verwendung weiterer Marker wie z.B. CD28 in Substadien wie DN3a und DN3b einteilen. Das DN4-Stadium, charakterisiert durch die Abwesenheit von CD25 und CD44, geht final in ein doppelt positives (DP) Stadium über. An diesem Punkt exprimieren die Thymozyten sowohl CD4 als auch CD8 und durchlaufen Selektionsprozesse. Letztere stellen sicher, dass nur T-Zellen heranreifen, die einerseits in der Lage sind, mögliche Pathogene zu erkennen und damit effizient zu bekämpfen (positive Selektion) und andererseits verhindern, dass sich diese Zellen gegen körpereigene Strukturen richten (negative Selektion). Diese hoch komplexen Selektionsprozesse ermöglichen weiterhin, dass ein breites Spektrum an T-Zellen ausgebildet werden kann. Somit kommt es letztlich nicht nur zur Generierung sogenannter konventioneller T-Zellen (CD4 oder CD8 positive T-Zellen), sondern auch zur Entstehung von unkonventionellen T-Zellen mit z.B. regulatorischen Fähigkeiten (Treg). Kommt es jedoch zu Störungen dieses Systems, wird die Entstehung von Immunschwäche- oder Autoimmunerkrankungen begünstigt.

Vorarbeiten unserer Gruppe haben sich besonders auf die Identifizierung und Charakterisierung von Vorläuferzellen spezialisiert (Krueger und Boehmer, 2007; Saran et al., 2010; Saran et al., 2012). Insbesondere konnte dabei gezeigt werden, dass der Eintritt in den Thymus von zwei Chemokinrezeptoren, CCR7 und CCR9, abhängt (Krueger et al., 2010). Quantitative Untersuchungen ergaben, dass CCR7/9-defiziente Mäuse eine etwa 200fache Verringerung an kürzlich eingewanderten Vorläuferzellen im Thymus aufweisen, was in einer reduzierten Frequenz an Zellen in den sehr frühen Entwicklungsstadien resultiert (DN1 und DN2) (Krueger et al., 2010; Ziętara et al., 2015). Dennoch wird diese Beeinträchtigung in den sehr frühen Stadien der T-Zellentwicklung im Verlauf der Thymozytenreifung überwunden, denn spätere Entwicklungsstadien sowie die Gesamtgröße des Thymus sind unbeeinflusst. Ein sehr ähnliches Phänomen zeigte sich auch für das Fehlen von miR-17~92 im Thymus (Regelin et al., 2015). Eine Verminderung an frühen Entwicklungsstadien konnte ebenso beobachtet werden, welche aber auch folgenlos für die Entwicklung späterer T-Zellstadien war. Dies lässt die Vermutung zu, dass die Regulation des Zellzyklus in diesem Stadium der T-Zellentwicklung von fundamentaler Bedeutung ist und kompensatorische Mechanismen vorliegen müssen, die zur physiologischen Entwicklung der späteren Entwicklungsstadien beitragen. Zudem ist ein fehlregulierter Zellzyklus ein Schlüsselereignis in der Entstehung von Leukämien.

Der erste Schwerpunkt der vorliegenden Arbeit war daher die Untersuchung der Zellzyklusdynamik in der Entwicklung von T-Lymphozyten. In einem ersten Schritt erfolgte eine Quantifizierung der Zellzyklusphasen der unterschiedlichen Thymozytenpopulationen auf dem Level der G0-, G1-, S- und G2M-Phase. Hierfür wurde der Zellzyklus basierend auf der *in vivo* Inkorporation des Nukleosidanalogons Bromdesoxyuridin (BrdU) in Verbindung mit einem DNA-interkalierenden Marker sowie der Bestimmung der Expressionslevel von Ki-67 analysiert. Hierbei konnten wir zeigen, dass sich die Mehrheit aller Thymozytensubpopulationen während der T-Zellentwicklung in der G1-Phase befindet. Zudem konnten wir deutliche Unterschiede im Anteil an S-Phase-Zellen in unterschiedlichen Stadien während der T-Zellentwicklung detektieren. Im Einklang mit früheren Studien zeigte sich besonders für die Population der DN2, DN3b und DN4 Thymozyten der größte Anteil an Zellen in der S-Phase (Penit et al., 1988; Baron und Pénit, 1990; Pénit et al., 1995; Vasseur et al., 2001). Im Verlauf dieser Arbeit haben wir anschließend gezielt die individuelle Zellzykluskinetik der Thymozytensubpopulationen während der T-Zellentwicklung

analysiert. Hierbei konnten wir durch den sequentiellen Einbau der Nukleosidanaloga EdU (5-Ethynyl-2'-desoxyuridin) und BrdU eine höhere Auflösung der S-Phase erreichen und u.a. S-Phaseneintritt sowie -austritt bestimmen (Gitlin et al., 2014; Gitlin et al., 2015). Dabei erfolgte in einem ersten Schritt eine EdU-Injektion, der sich exakt eine Stunde später eine BrdU-Injektion anschloss. Nach einer weiteren Stunde folgte der Nachweis der Inkorporationen. Die EdU-positive Fraktion repräsentierte dabei den Anteil an Zellen, die nur während der ersten Injektion in der S-Phase waren und diese damit vor der BrdU-Injektion bereits wieder verlassen hatten. Der Anteil an BrdU-positiven Zellen stellte wiederum die Fraktion dar, die erst kürzlich in die S-Phase eingetreten ist. Die EdU-BrdU-positiven Zellen befanden sich hingegen während der gesamten Dauer (> 2 Std.) in der S-Phase. Die gewonnenen Resultate spiegelten nicht nur die Ergebnisse unserer Zellzykluserstbeschreibung wider, sondern verschafften neue Erkenntnisse über die Dynamik der S-Phase in verschiedenen Stadien während der T-Zellentwicklung. So konnten wir große Unterschiede in Bezug auf den S-Phaseein- und -austritt sowie die Dauer der S-Phase innerhalb der Thymozytensubpopulationen detektieren. In einem weiteren Schritt haben wir die Analyse auf unterschiedliche Zeitpunkte nach Administration der Analoga ausgeweitet (1-6 Std.), sodass wir präzise Quantifizierungen des Wiedereintritts in die G1- und S-Phase sowie schlussendlich eine Berechnung der S- und G1-Phasengeschwindigkeit anbringen konnten. Diese Analysen haben wir in weiteren Versuchen auf CCR7/9-defiziente (Krueger et al., 2010) sowie miR-17~92-defiziente (Regelin et al., 2015) Mäuse ausgeweitet, um neue Erkenntnisse über das Vorliegen kompensatorischer Mechanismen zu erlangen. Hierbei konnten wir feststellen, dass es in Abwesenheit von CCR7/9 zu einer Änderung des Zellzyklusmusters, besonders ausgeprägt für DN2 und DN3a Thymozyten, kommt. Ferner konnten wir zeigen, dass alle untersuchten Thymozytensubpopulationen in CCR7/9-defizienten Mäusen eine verkürzte S-Phasendauer aufweisen. Diese Beobachtungen konnten weiter durch die Ergebnisse eines Einzelzell-RNA-Sequenzierungsexperiments bestätigt werden. Aus diesen Ergebnissen schlussfolgerten wir, dass in CCR7/9-defizienten Thymozyten der Defekt in der frühen T-Zellentwicklung durch eine Verkürzung der Zellzykluslänge kompensiert wird. Dieser kompensatorische Effekt zeigte sich besonders stark ausgeprägt für DN3a, aber auch für DN2, DN3b und DN4 Thymozyten. Für miR-17~92-defiziente Mäuse konnten im Rahmen dieser Arbeit erste Experimente durchgeführt werden, die darauf hindeuteten, dass eine Regulation auf

Zellzyklusebene für DN3b und DN4 Thymozyten besteht. Anhand dieser präliminären Daten lässt sich vermuten, dass nicht nur die Dauer der S-Phase, sondern vermutlich auch die der G1-Phase in Abwesenheit von miR-17~92 verändert ist.

Darüber hinaus wurden in einem weiteren Experiment Zellzyklusveränderungen im Rahmen der Regeneration durch vorangegangene sublethale Bestrahlung untersucht (Kadish und Basch, 1975; Huiskamp und van Ewijk, 1985; Tomooka et al., 1987; Penit und Ezine, 1989; Dudakov et al., 2012). Hierbei konnten wir durch den Vergleich von unbestrahlten und bestrahlten Versuchstieren neue Erkenntnisse über die Anpassung der Zellzykluskinetik gewinnen und insbesondere eine Verlängerung der S-Phase für alle untersuchten Thymozytenpopulationen nach vorangegangener Bestrahlung feststellen. Die Einbettung dieser Daten zur Generierung einer biomathematischen, agentenbasierten Modellierung ist nicht Teil dieser Arbeit, aber Gegenstand einer Publikation, die derzeit angefertigt wird.

Im zweiten Abschnitt der vorliegenden Arbeit wurde die Rolle von miR-21 in der T-Zellentwicklung untersucht. MicroRNAs sind etwa 18-22 Nukleotide lange, nicht-kodierende RNAs, deren Einfluss auf die Entwicklung und Funktion von Lymphozyten bereits seit einigen Jahren beschrieben wird (Baumjohann und Ansel, 2013, 2014). Arbeiten aus unserer Gruppe konnten zur Aufklärung der Funktion etlicher miRNAs beitragen und deutlich aufzeigen, wie mannigfaltig miRNAs Immunzellen beeinflussen (Haas et al., 2011; Surdziel et al., 2011; Ziętara et al., 2013; Regelin et al., 2015; Sandrock et al., 2015; Blume et al., 2016; Lee et al., 2016; Glaesener et al., 2018; Kunze-Schumacher et al., 2018; Blume et al., 2019; Łyszkiewicz et al., 2019; Winter et al., 2019; Winter und Krueger, 2019; Amado et al., 2020; Grewers und Krueger, 2020; Kunze-Schumacher und Krueger, 2020; Meyer et al., 2020; Witkowski et al., 2020). Generell unterscheiden sich miRNAs in ihrem Expressionsprofil während der T-Zellentwicklung stark. Expressionsanalysen von miR-21 zeigten deutlich, dass miR-21 während der intrathymischen T-Zellentwicklung differentiell exprimiert wird (Kirigin et al., 2012). Diese dynamische Expression führte zu der Annahme, dass miR-21 eine fundamentale Rolle in der T-Zellentwicklung innehat. In der vorliegenden Arbeit konnten wir das dynamische Expressionsmuster von miR-21 bestätigen und um Expressionsanalysen in weiteren Thymozytensubpopulationen erweitern. Anhand einer miR-21-defizienten Mauslinie war es uns zudem möglich zu zeigen, dass miR-21 keine deutliche regulatorische Funktion während der T-Zellentwicklung einnimmt. Zudem konnten wir in kompetitiven

Knochenmarkchimären keinen Hinweis auf eine tragende Rolle von miR-21 finden. Auch Überexpressionsstudien untermauerten unsere Ergebnisse und zeigten auf, dass miR-21 für die physiologische T-Zellentwicklung obsolet ist. Funktionelle *in vivo* Studien bestätigten, dass miR-21 die intrathymischen Selektionsprozesse nicht beeinflusst. Ferner konnten wir in der *in vitro* T-Zelldifferenzierung keinen Einfluss durch miR-21 feststellen. Das onkogene Potential von miR-21 ist in der Fachliteratur häufig beschrieben (Chan et al., 2005; Iorio et al., 2005; Si et al., 2007; Schetter et al., 2008; Hatley et al., 2010; Ma et al., 2011). Die Ursache dafür liegt in der tumorsuppressiven Wirkungsweise dieser miRNA. Basierend auf Analysen der Apoptosemarker Annexin V und Caspase-3, konnten wir in der vorliegenden Arbeit nur bedingt Hinweise auf die anti-apoptotische Wirkungsweise dieser miRNA finden. In weiteren Experimenten zeigte sich außerdem, dass miR-21 an der thymischen Geweberegeneration nach Auslösung von zellulärem Stress durch sublethale Bestrahlung (Kadish und Basch, 1975; Tomooka et al., 1987; Penit und Ezine, 1989; Dudakov et al., 2012) nicht maßgeblich beteiligt ist.

Unsere Ergebnisse machten deutlich, dass miR-21 trotz dynamischer Expression während der T-Zellentwicklung kaum Einfluss auf diese hat (Kunze-Schumacher et al., 2018). Weitere Erklärungen für diese Diskrepanz wurden in dieser Arbeit experimentell nicht weiter adressiert. Unsere Ergebnisse lassen den Schluss zu, dass miR-21 vermutlich intrathymische Prozesse vielmehr feinreguliert, anstatt einen spezifischen Aspekt der T-Zellentwicklung zu beeinflussen. Diese Schlussfolgerung konnte auch durch die jüngsten Arbeiten von Fedeli et al. bestätigt werden, die unsere Arbeiten reproduzieren konnten (Fedeli et al., 2021). Eine weitere Studie, die die Rolle von miR-21 in der Leber untersucht, konnte aufzeigen, dass miR-21 ihre Zielgene nur in kanzerösen Zellen effektiv unterdrückt, nicht aber im gesunden Gewebe. Unter physiologischen Bedingungen scheint eine Assoziation der miR-21 mit Polysomen nahezu abwesend zu sein, welche aber wiederum stark ausgeprägt in einer Tumorzelllinie vorliegt (Androsavich et al., 2012). Weitere Studien zeigten zudem eine primäre Häufung von miR-21 in sogenannten ‚low molecular weight RNA-induced-silencing-complex (RISC)s‘. Diese hat wiederum eine verminderte Assoziation mit der Ziel-mRNA zur Folge (La Rocca et al., 2015; Toivakka et al., 2020), da nur eine Bindung an Argonautenproteine besteht, nicht aber mit Komponenten des RISCs. Denkbar wäre auch das Fehlen der endständigen 5‘-Phosphorylierung der miR-21, die für die Inkorporation in den RISC notwendig ist (Salzman et al., 2016).

Weitere Modifizierungen der mRNA durch alternatives Splicen oder Polyadenylierung sowie eine Kürzung der 3’ untranslatierten Region (UTR) (Sandberg et al., 2008) oder aber Adenosinmethylierung (Ke et al., 2015) könnten zudem die Funktion der miR-21 einschränken. Eine Untersuchung dieser Mechanismen könnte Gegenstand weiterer Experimente sein.

Insgesamt wurde in dieser Arbeit eine detaillierte *in vivo* Charakterisierung des Zellzyklus während der murinen T-Zellentwicklung etabliert, mit Hilfe derer regulatorische Mechanismen auf Zellzyklusebene in CCR7/9- und miR17~92-defizienten Mäusen entschlüsselt werden konnten. Ferner konnten neue Erkenntnisse über die Anpassung des Zellzyklus in einem Modell der endogenen thymischen Regeneration gewonnen werden. Darüber hinaus wurde in der vorliegenden Arbeit die Rolle von miR-21 während der T-Zellentwicklung charakterisiert.

1 Introduction

The mammalian immune system established a regulatory network of different cells and mechanisms to protect the body against pathogens but also to hinder transformation of healthy into malignant cells. This highly complex system is divided into two co-existing arms: innate and adaptive immunity. Together, both arms ensure protection throughout the life of an organism by innate rapid recognition as a first line of defense and long-lasting adaptive immunity based on the formation of a specific memory response. Besides B cells, T cells form a central part of adaptive immunity. A special feature of T cells is their unique development in a highly dynamic process embedded in an organ located in front of the heart, the thymus. Many aspects of the sophisticated developmental process of T-cell development in the thymus remain elusive.

1.1 T-cell development: A journey through the thymus

In contrast to all other cells of the immune system that complete their development in the bone marrow (BM), T cells undergo a highly dynamic process of development in a specialized organ, called thymus (Miller, 1961). Bone-marrow derived progenitor cells with the capacity to colonize the thymus were studied intensively over the past years in human and mouse. Interestingly, these so-called thymus seeding progenitors (TSPs) represent a heterogenous mixture of cells with different characteristics including multipotent progenitors (MPPs), common lymphoid progenitors (CLPs) and CLP-like cells as well as T-lineage pre-committed progenitors (Igarashi et al., 2002; Perry et al., 2004; Adolfsson et al., 2005; Rossi et al., 2005; Scimone et al., 2006; Bhandoola et al., 2007; Krueger and Boehmer, 2007; Bell and Bhandoola, 2008; Wada et al., 2008; Serwold et al., 2009; Schlenner et al., 2010; Krueger, 2011; Saran et al., 2012; Luis et al., 2016; Lavaert et al., 2020). These TSPs circulate in the blood and enter the thymus via large venules.

On the molecular level, thymus entry was found to be dependent on the chemokine receptors CCR7 and CCR9. Interestingly, deficiency in one of those chemokine receptors only mildly affected thymus colonization (Uehara et al., 2002; Benz et al., 2004; Misslitz et al., 2004; Liu et al., 2006b; Liu et al., 2006a) whereas the lack of both results in a virtual abrogation of seeding by progenitors (Veerman et al., 2007; Svensson et al., 2008; Krueger et al., 2010; Zlotoff et al., 2010). Thymocyte entry is

located at the corticomedullary junction, the anatomical border between two different thymic architectural structures (Penit and Vasseur, 1988) (Figure 1). Upon entry, early T-lineage progenitors (ETPs, $CD25^{-}CD44^{+}$c-kit^{+}), the most immature detectable thymocytes, migrate towards the subcapsular region in the cortex in response to chemokine gradients and interactions with other cells such as thymic epithelial cells (TECs) and stromal cells (Lind et al., 2001; Prockop et al., 2002). Here, further differentiation into different double-negative (DN, $CD4^{-}CD8^{-}$) stages occurs that can be phenotypically distinguished based on the differential expression of CD44 and the IL-2 receptor alpha chain CD25 (Ceredig et al., 1985; Pearse et al., 1989; Godfrey et al., 1993; Godfrey et al., 1994). Until the DN2 stage, thymocytes still have the ability to adopt alternative lineage fate indicated by B, myeloid, natural killer (NK) and dendritic cell potential (Wu et al., 1991; Matsuzaki et al., 1993; Radtke et al., 1999; Martin et al., 2003; Porritt et al., 2004; Yui et al., 2010). Expression of the transcription factor Bcl11b marks ultimate commitment to the T lineage at the DN2 stage (Ikawa et al., 2010; Li et al., 2010b; Li et al., 2010a; Kueh et al., 2016). Additionally, T-lineage commitment is transcriptionally further supported by Notch signals mediated by the expression of delta-like ligands (DL, mostly DL4) by epithelial cells (Krueger et al., 2006; Besseyrias et al., 2007; Petrie and Zúñiga-Pflücker, 2007; Hozumi et al., 2008; Koch et al., 2008). Moreover, a recent study suggests that Notch signaling is required already in a prethymic setting before the ETP stage (Chen et al., 2019). Additionally, the c-kit ligand stem cell factor (SCF), IL-7, or lymphotoxin β contribute to thymocyte survival and/or proliferation at these early developmental stages (Freeden-Jeffry et al., 1997; Rodewald et al., 1997; Allman et al., 2003; Massa et al., 2006; Lucas et al., 2016; Zhao et al., 2019).

Upon T-lineage commitment at the DN2 stage, somatic recombination of the *Trb, Trg* and *Trd* T-cell receptor (TCR) genes is initiated, proceeding into the DN3 stage. Successful *Trb* rearrangement allows for the formation of the pre-TCR comprising a rearranged TCRβ in conjunction with a generic pTα chain (Groettrup et al., 1993). Signaling through the pre-TCR induces β-selection. The DN3 stage can be phenotypically distinguished by CD28 expression into a DN3a and b stage to discriminate between thymocytes that have successfully passed β selection (Teague et al., 2010). Moreover, thymocytes with productively rearranged TCRγ and δ chain undergo further γδT-lineage maturation (Rodewald and Fehling, 1998; Hayday and Pennington, 2007). DN3b stage thymocytes undergo allelic exclusion as well as

proliferation. In line with this, they lose expression of CD25 and CD44 (DN4 stage) but start to express the CD4 and CD8 co-receptors on their surface (double positive (DP) stage, $CD4^+CD8^+$) coinciding with massive proliferation (Penit, 1988; Pénit et al., 1995; Stritesky et al., 2012). DP thymocytes start rearrangement of their *Tra* locus encoding the TCRα chain to ensure the assembly of a complete αβTCR (Petrie et al., 1995; Schatz and Ji, 2011). V(D)J recombination to generate a diverse repertoire of TCRs is mediated by expression of recombination-activating gene 1 (RAG1) and RAG2 proteins (Turka et al., 1991; Pénit et al., 1995; Schatz, 2004; Schatz and Ji, 2011; Ru et al., 2015; Carmona et al., 2016). This event is accompanied by a pause in proliferation and cells are found to be transcriptionally quiescent (Mingueneau et al., 2013). Subsequently, positive selection of these TCRs is mediated by cortical thymic epithelial cells (cTEC) and ensures the survival of cells capable of recognizing self-peptide:major histocompatibility complex ligands (pMHC). This selection step induces death by neglect of T cells with a non-functional TCR (Huesmann et al., 1991). Negative selection ensures clonal deletion of T cells with high-affinity TCRs to awld-pMHC beginning in the cortex (Nossal, 1994). In a spatio-temporal context, positive and negative selection can proceed (a) in parallel in the cortex or (b) by induction of migration to the medulla upon positive selection, where then negative selection continues (McCaughtry et al., 2008). Additionally, agonist-selection induces the survival of T cells with slightly weaker signals towards self-pMHC than those inducing negative selection (Stritesky et al., 2012). Regulatory T cells as well as TCR-restricted innate-like T cells such as invariant natural killer T cells (iNKT) and mucosal-associated invariant T cells (MAIT) belong to the group of so-called agonist-selected T-cells.

Upon selection, mature CD4 and CD8 single-positive (SP) T cells (SP4 and SP8, respectively) evolve by downregulating a single co-receptor through a developmental progression through an immature $CD4^+CD8^{int}$ stage and finally MHC restriction (Singer et al., 2008). SP4 and SP8 T cells finally egress through post-capillary venules in the medulla to enter the pool of naïve CD4 and CD8 T cells in the periphery.

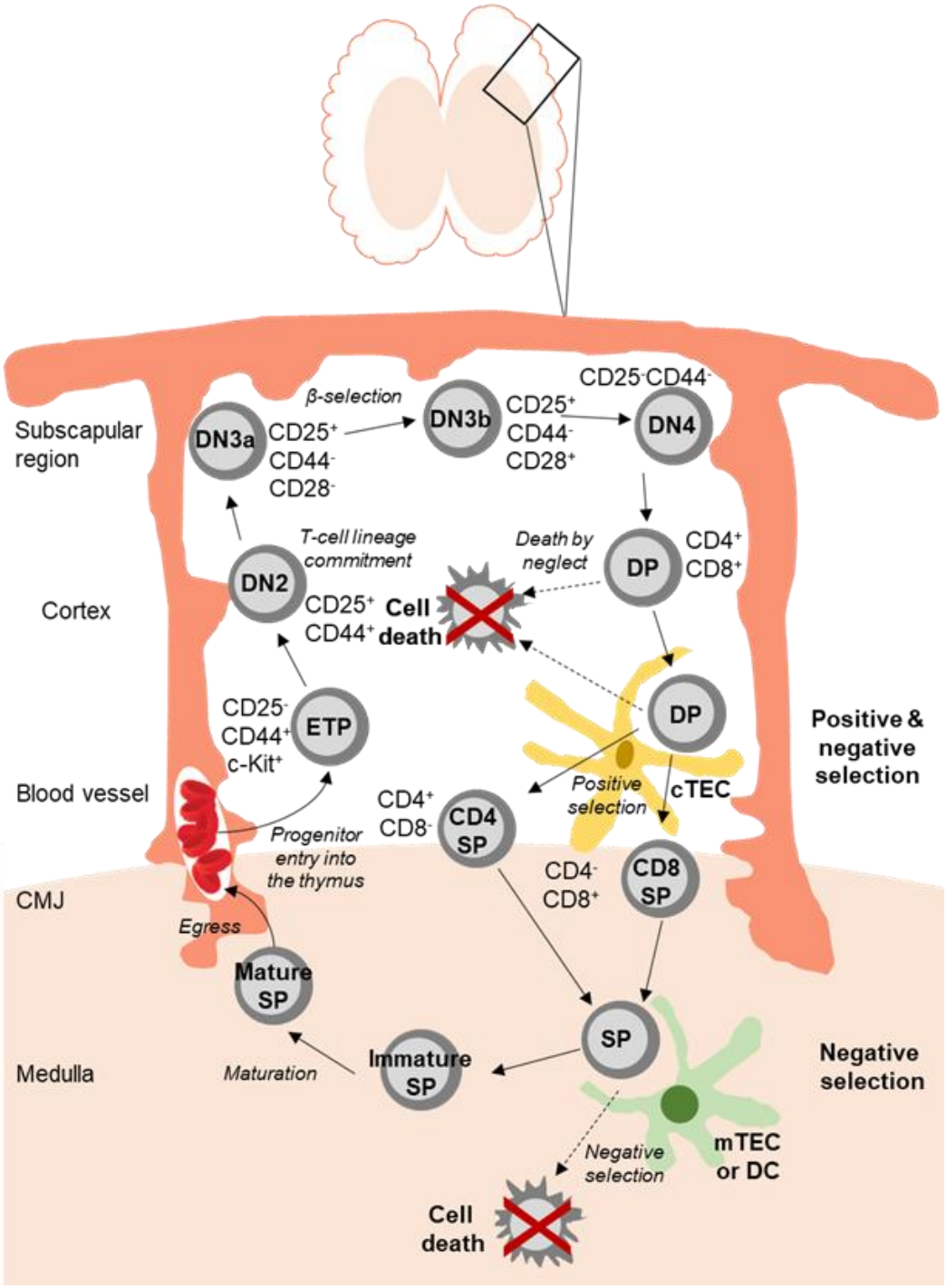

Figure 1: A thymocyte journey in, through and out of the thymus.
The corticomedullary junction is the place of thymus entry. Here, bone marrow (BM)-derived thymus seeding progenitors (TSPs) enter the thymus through afferent blood vessels. TSPs then give rise to early T-lineage progenitors (ETPs), the most immature detectable thymocyte population. Migration towards the outer cortex is initiated through interaction with the thymic microenvironment. ETPs then differentiate through $CD4^-CD8^-$ double negative (DN) stages. The DN2 stage reflects the point of T-lineage commitment followed by β-selection at the DN3 stage. Absence of CD25 and CD44 characterizes the DN4 stage which leads to upregulation of CD4 and CD8, the double positive (DP) stage. Upon completion of TCRα gene rearrangement, these pre-selection DP thymocytes then interact with peptide:MHC (pMHC) presented by cortical thymic epithelial cells (cTECs). Non-responsiveness induces death by neglect of these cells, whereas positive selection leads to the survival of cells with a functional, pMHC-recognizing TCR. Negative selection ensures cell death of thymocytes that interacted strongly with cTECs (clonal deletion). Additionally, negative selection can also happen in the medulla. At the end, surviving cells mature into CD4 or CD8 single-positive (SP) thymocytes and emigrate through post-capillary venules in the medulla. Adapted from (Winter, 2020).

1.2 A quantitative view of T-cell development

Murine blood contains less than 1000 circulating TSPs. To be more precise, approximately 180 MPPs, 180 CLPs and 600 T lineage-committed cells (Schwarz and Bhandoola, 2004; Krueger and Boehmer, 2007; Lai and Kondo, 2007; Umland et al., 2007). First studies that quantitatively addressed thymus colonization were based on irradiation of host mice and subsequent reconstitution with different numbers of syngeneic but chromosomally distinguishable BM cells. Based on this approach, 10-200 thymus-colonizing cells per day were proposed as a first estimate (Wallis et al., 1975; Scollay et al., 1986). Further studies suggested higher cell numbers that initially entered the thymus and interpreted colonization as a periodic, gated event limiting thymic seeding (Mori et al., 2001; Gossens et al., 2009). Studies by our group employed retroviral barcoding and multicongenic fate mapping (Łyszkiewicz et al., 2015; Ziętara et al., 2015) to quantitate thymus colonization and the number of niches available for BM-derived progenitors. This approach revealed that a non-irradiated mouse WT thymus is colonized on average by 10 TSPs at a given time. Taking advantage of the near absence of ETPs while at the same time maintaining normal overall thymic cellularity, CCR7/9-deficient mice were used as recipients. These experiments further highlight that a thymus contains approximately 160 niches available for seeding by TSPs (Figure 2). Additionally, these experiments suggested that niches remain closed for re-occupation by TSPs over a period of 9-12 days. This is consistent with the average lifetime of an ETP before it progresses to the next developmental stage (Porritt et al., 2003; Ziętara et al., 2015). In contrast to ETPs, the DN2 phase as well as the DN3 stage are short (2-3 days), but the transition from DN2 to DN3 cells is characterized by massive proliferation resulting in a 40fold expansion from $2.5x10^4$ DN2 to $1x10^6$ DN3 thymocytes. After 4 days at the DN3 stage, another proliferative burst initiated by successful β-selection leads to the generation of 100 million DP thymocytes. Whereas the pre-selection DP stage lasts for around 60 hrs, post-selection seems to be rather short (16 hrs). Moreover, determination of thymic selection rates unraveled that 5.5-6-times more cells go through negative selection than positive selection (Stritesky et al., 2013). As a consequence of selection, more than 90% of DP thymocytes die (Egerton et al., 1990; Stritesky et al., 2013; Sawicka et al., 2014). Ultimately, $1\text{-}4x10^6$ SP4 and SP8 cells egress which represents approximately 1% of all thymocytes at steady state (Scollay et al., 1980; Scollay and Shortman, 1985).

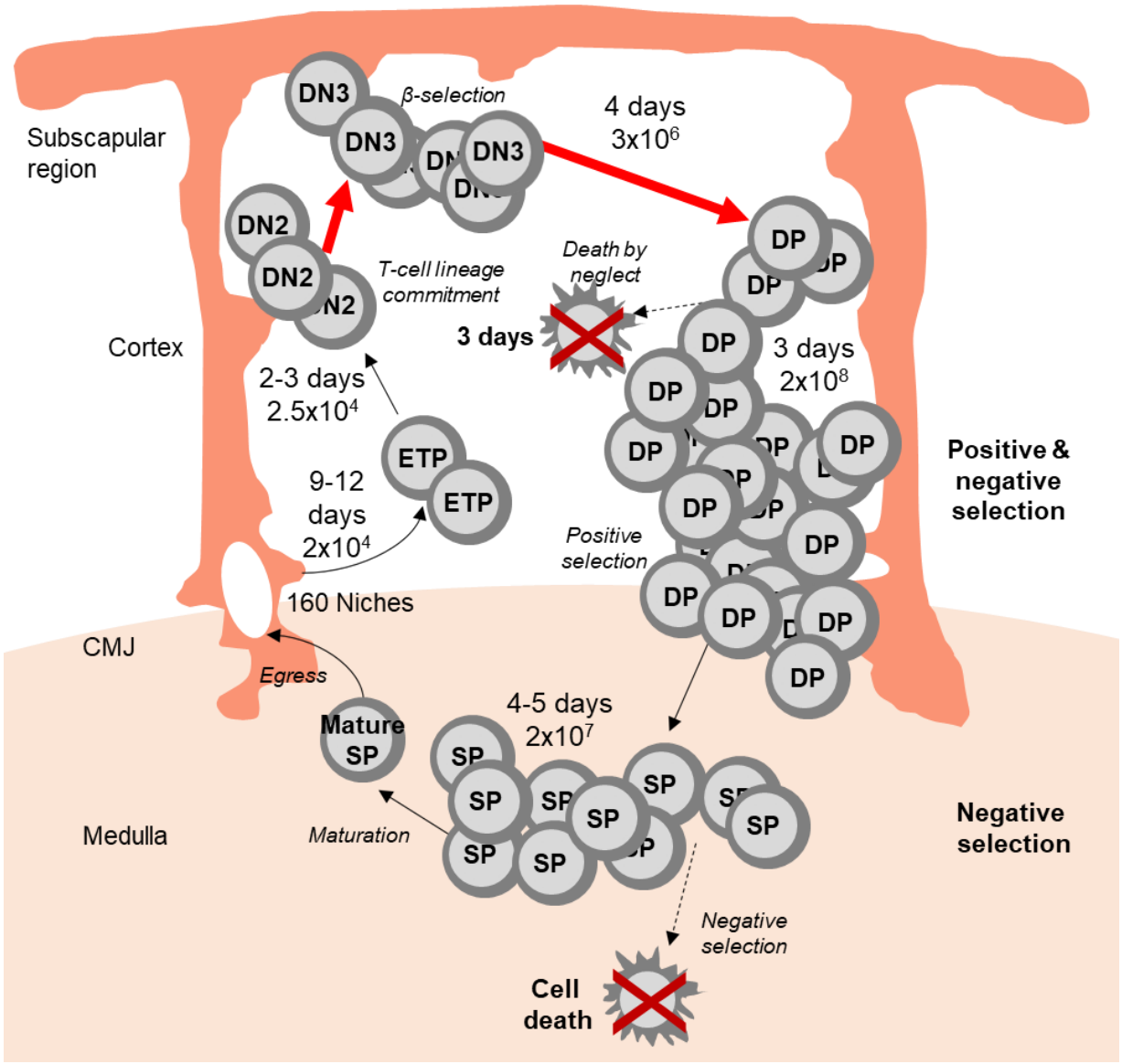

Figure 2: Quantitative T-cell development at a glance.
The thymus contains approximately 160 niches for seeding by TSPs (thymus seeding progenitor) in the cortex. Upon entry, ETPs (early T-lineage progenitor) 'sit and wait' for up to 12 days before differentiation and T-lineage commitment at the DN2 (double negative) stage is completed. Following a first proliferative burst (red arrow), DN3 thymocytes undergo β selection. Upon successful formation of a pre-TCR (T-cell receptor), a second proliferative event (red arrow) occurs that leads to the generation of 100 million of DP (double positive) thymocytes that undergo selection. Ultimately, SP (single positive) thymocytes further mature and leave the thymus. In sum, from entry to egress, the journey through the murine thymus takes approximately 3.5 weeks (Krueger et al., 2017).

Up to now, it remains elusive whether the different cell types comprising the TSP population contribute equally to T-cell development. At least CLPs and MPPs exhibit different kinetics in terms of the developmental progression in the thymus (Schwarz et al., 2007; Serwold et al., 2009; Saran et al., 2010), but the underlying mechanisms are not fully understood: Whereas CLPs seem to differentiate faster into DP thymocytes (within approx. 7 days), they only generate one single wave of T-cells that complete thymic egress latest after 42 days. For MPPs, T-cell development takes longer due to an enhanced lifetime of MPP-derived ETPs. Regarding the fact that TSPs not only consist of CLPs and MPPs, further studies should address the kinetic and proliferative profile of different TSPs (Krueger, 2018).

1.3 Cell cycle

The cell cycle is divided into four distinct phases termed growth/gap 1 (G1, cell growth), S (DNA synthesis), growth/gap 2 (G2) and M (mitosis) (Figure 3). Progression through these phases is tightly controlled to ensure DNA replication of the genome (S phase) and subsequent distribution of the genetic and epigenetic information to both daughter cells during mitosis. Multiple cell cycle checkpoints were described that ensure the power and accuracy of this fundamental process by either inducing or restricting the transition between cell cycle phases (Howard and Pelc, 1986; Hartwell and Weinert, 1989; Jackson, 2008; Pennycook and Barr, 2020; Rubin et al., 2020). Progression through the cell cycle and regulation of the rate of cell division are kinetically flexible in order to meet an organism's demand to ensure tissue homeostasis, stem cell maintenance, wound healing and immunity. The role of cell cycle control during immune system development and function is still not fully understood. For myeloid differentiation, it has been observed that the interdependence of protein production and cell cycle duration determines PU.1 transcription factor levels thus controlling lymphoid and myeloid lineage choice (Kueh et al., 2013). Moreover, modulation of cell cycle duration by shortening of S-phase length was demonstrated during the germinal center reaction (Gitlin et al., 2015). Additionally, studies of cell cycle dynamics and the roles of cell cycle regulation are emerging for the diversification of adaptive immune responses (Heinzel et al., 2018). Cell cycle analyses are mainly based on measurements of the DNA content but also expression of cyclins is dynamically regulated during the different stages and can be employed to discriminate cells in the different phases of the cell cycle (Rowell and Wells, 2006; Vogel et al., 2016).

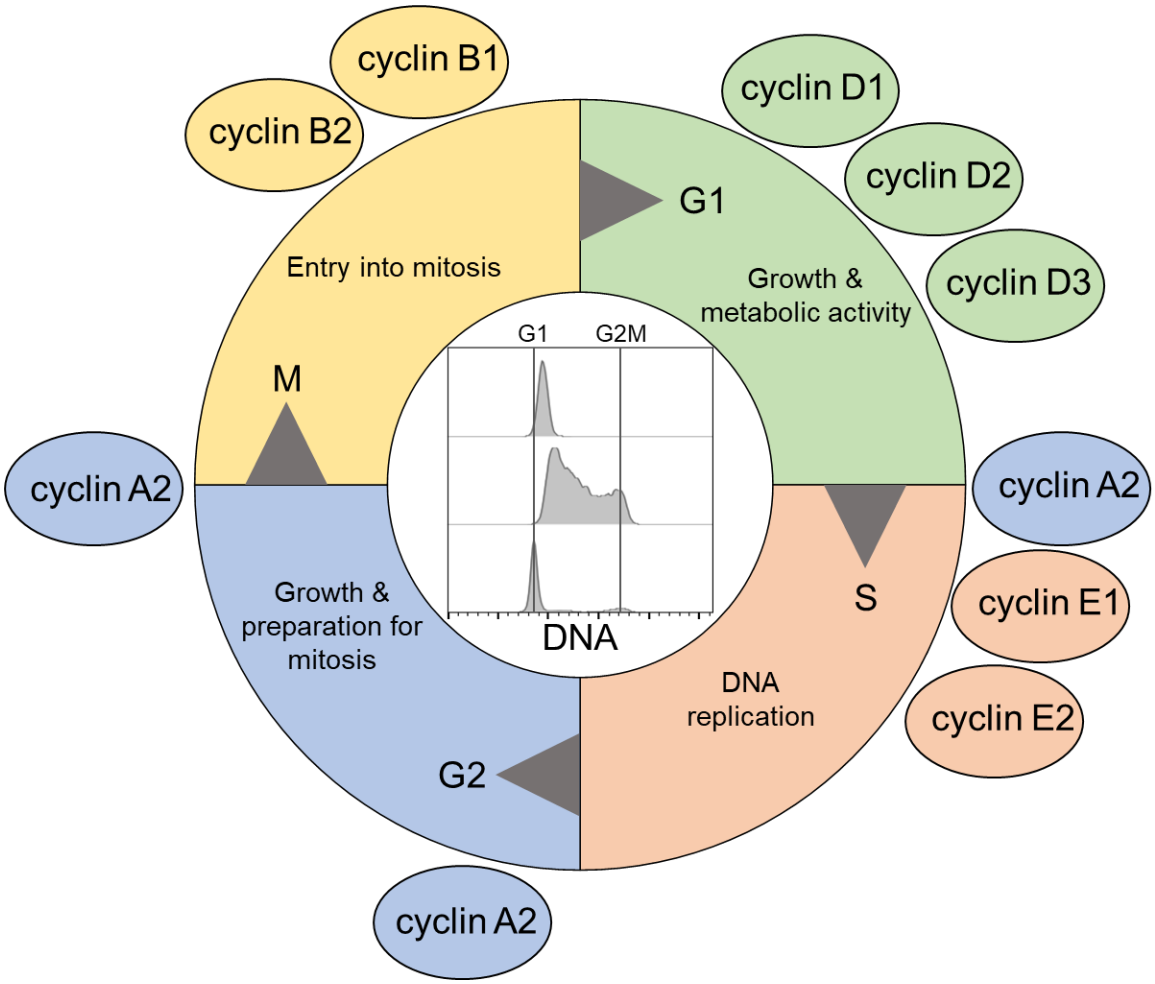

Figure 3: Cell cycle and its regulation by periodic expression and degradation of cyclins.
The cell cycle comprises four major phases. A first growth phase called growth/gap1 (G1, green), synthesis/replication (S, red), a second growth/gap phase, G2 (blue) and finally mitosis (M, yellow). In the center, a histogram represents a staining of thymocytes with a DNA content marker to assess cell cycle phase distribution. Lines represent G1 or G2M peaks. First row: Cells in early S phase; middle row: cells distributed between S and G2M phase; last row: cells in G1 and a minute fraction in G2M phase of the cycle. Outside: Circles represent expression of stage-specific cyclins. The levels of the different cyclins vary considerably across the cell cycle, as shown in the diagram at the right. Cyclin expression corresponds to specific stages making them a suitable tool to study cell cycle phases.

1.3.1 Cell cycle regulators of T-cell development

Molecular mechanisms of thymocyte proliferation and its interdependence with differentiation remain poorly understood. As mentioned before, the first proliferative burst at the DN2 stage can be mainly attributed to signals from the c-kit ligand SCF, IL-7 as well as Notch ligands by the thymic environment (Figure 4) (Massa et al., 2006; Hozumi et al., 2008; Niu and Qin, 2013). Interestingly, two early studies identified the involvement of cyclins A and B, downregulation of p27, cyclin-dependent kinases (CDK2) activity and DNA replication at the DN3 stage (Pénit et al., 1995; Hoffman et al., 1996). Indeed, post-β-selection proliferation of DN3 cells is dependent on c-Myc and cyclin D3 (Sicinska et al., 2003; Kozar et al., 2004; Aifantis et al., 2006; Dose et al., 2006). Although induction of proliferation cannot overrule a developmental block at β-selection, it has been shown that formation of DP thymocytes occurs only in divided cells following β-selection (Kreslavsky et al., 2012). This observation indicates that in this instance proliferation promoting differentiation is rather a separate or opposing event. Moreover, a recent study suggests proliferation upon β-selection to be dependent on the combined activity of two stem cell factor (SCF) ubiquitin ligase complexes (Fbxl1 and 12) targeting a cyclin-dependent kinase inhibitor Cdkn1b. Transcription of Fbxl1 or 12 was Notch signal-mediated or induced by pre-TCR signals, respectively (Zhao et al., 2019).

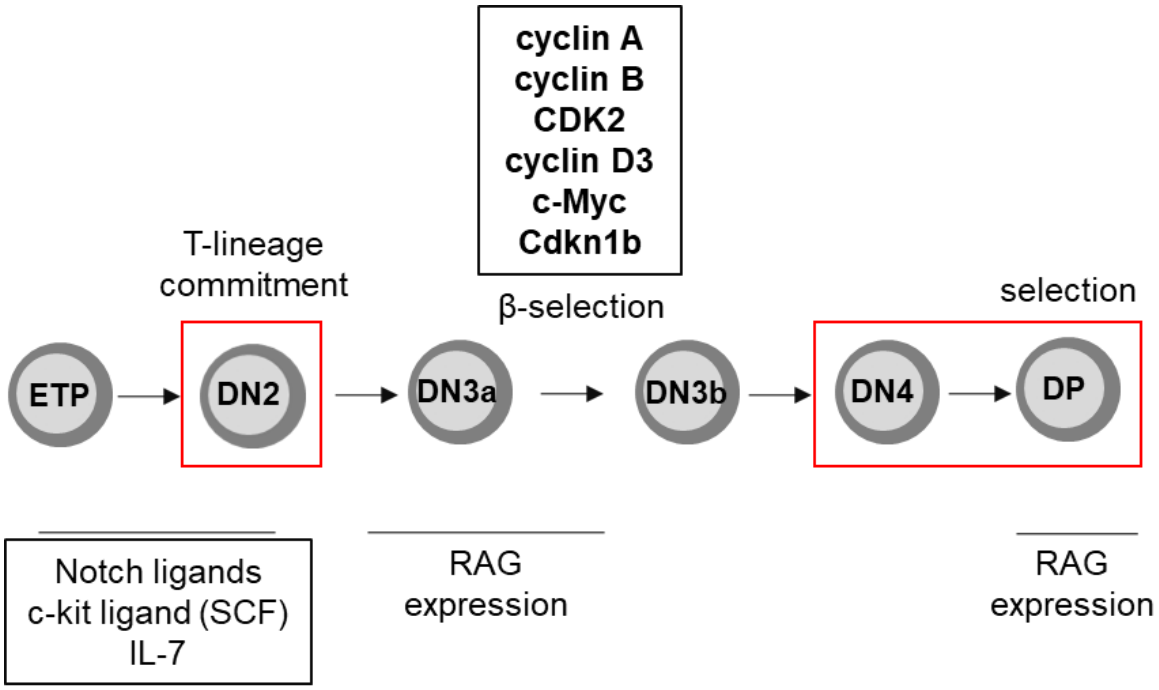

Figure 4: Intrathymic cell cycle regulation.
Schematic depiction of the intrathymic T-cell development. T cells derive from the early thymic progenitor (ETP) and develop through different double negative (DN) 1, DN2, DN3a/b and DN4 stages into mature double positive (DP) cells. In early T-cell development, Notch signaling as well as the cytokines c-kit ligand (SCF) and IL-7 are essential. From a cell cycle perspective, T-cell development is uncompletely understood. Up to now, key cell regulators including cyclin A, B and D3 as well as c-Myc, CDK2 and Cdkn1b (upper black box) are only defined for the DN3 stage of T-cell development. Proliferative events (red box) at the DN2 stage are mainly driven by signals from the thymic microenvironment.

1.3.2 New tools to study cell cycle dynamics

The field of quantitative tools to study biological processes in the immune system *in vivo* is currently expanding due to the availability of lineage fate-tracing techniques, molecular timers, cellular barcoding and other high-end genetic reporters (Schlenner et al., 2010; Tomura et al., 2013; Busch et al., 2015; Buchholz et al., 2016; Pei et al., 2019; Pei et al., 2020; Flommersfeld et al., 2021).

Historically, assessment of proliferation based on the use of 5-(and 6)-carboxyfluorescein diacetate succinimidyl ester (CFSE) helped to quantify cellular turnover, divison and death rates of lymphocytes (León et al., 2004; Ganusov et al., 2005; Boer et al., 2006). Additionally, incorporation of nucleoside analogues such as 5-bromo-2'-deoxyuridine (BrdU) or 5-ethynyl-2'-deoxyuridine (EdU) was established as versatile tool to study actively replicating cells (Leif et al., 2004; Bradford and Clarke, 2011). Moreover, dual nucleoside labeling combined with analysis of DNA content at different time points allowed the precise quantification of cell cycle dynamics (Gitlin et al., 2014; Weber et al., 2014; Gitlin et al., 2015; Akinduro et al., 2018).

However, each approach alone is insufficient to reveal the complete spectrum of cell cycle dynamics. Feeding such data into mathematical models reveals such limitations (Robert et al., 2021).

1.4 Post-transcriptional regulation of T-cell development by microRNAs

MicroRNAs (miRNA/miR) are short RNAs with noncoding function, typically 18-22 nucleotides in length. Their formation commences in the nucleus with the generation of the primary miRNA transcript (pri-miRNA) by RNA polymerase II or III (Figure 5). Subsequently, pri-miRNAs are cleaved by an endonuclease complex containing Drosha and DiGeorge syndrome critical region 8 (DGCR8). This results in the formation of the approximately 65 nucleotide long pre-miRNA, a precursor hairpin that is actively imported into the cytoplasm by Exportin-5-RAN-GTP for further processing. Upon arrival, the pre-miRNA is cleaved by a complex composed of the endonuclease Dicer with the double-stranded RNA-binding protein transactivation response element RNA-binding protein (TRBP). This leads to cleavage of the pre-miRNA hairpin into its mature double-stranded form. The two single strands then undergo different fates: The more thermodynamically stable strand of the mature miRNA is incorporated into the RNA-induced silencing complex (RISC) consisting of Argonaute (Ago2) proteins and various cofactors, whereas the passenger strand (Figure 5, black) is degraded. Ultimately, enabled by complementarity of the nucleotides 2-7 of the miRNA (seed region) to miRNA recognition elements (MREs), RISC is silencing target mRNAs by cleavage, translational repression or deadenylation (Guo et al., 2010). Additionally, multiple factors contribute to efficient targeting, such as extended complementarity around the seed region to a MRE, additional complementary regions to the 3’ end of the miRNA, structural accessibility of an MRE as well as multiplicity of MREs, proximity of multiple MREs and sequence context (such as AU content) (Grimson et al., 2007; Kertesz et al., 2007). Given the possibility of individual miRNAs to target hundreds of mRNAs, repression of a single mRNA target is generally rather low. This led to the hypothesis that miRNAs function in a broader network by affecting pathways rather than individual molecular components (Tsang et al., 2010; Mukherji et al., 2011).

T-cell development is tightly controlled by miRNAs (Koenecke and Krueger, 2018; Winter and Krueger, 2019; Grewers and Krueger, 2020; Kunze-Schumacher and Krueger, 2020). Indeed, analyses of miRNA expression levels unraveled dynamic expression of over 600 different miRNAs with individual expression profiles during T-cell development (Neilson et al., 2007; Kuchen et al., 2010; Kirigin et al., 2012).

Moreover, loss of all miRNAs due to deletion of Dicer results in profound defects in T-cell development (Cobb et al., 2005).

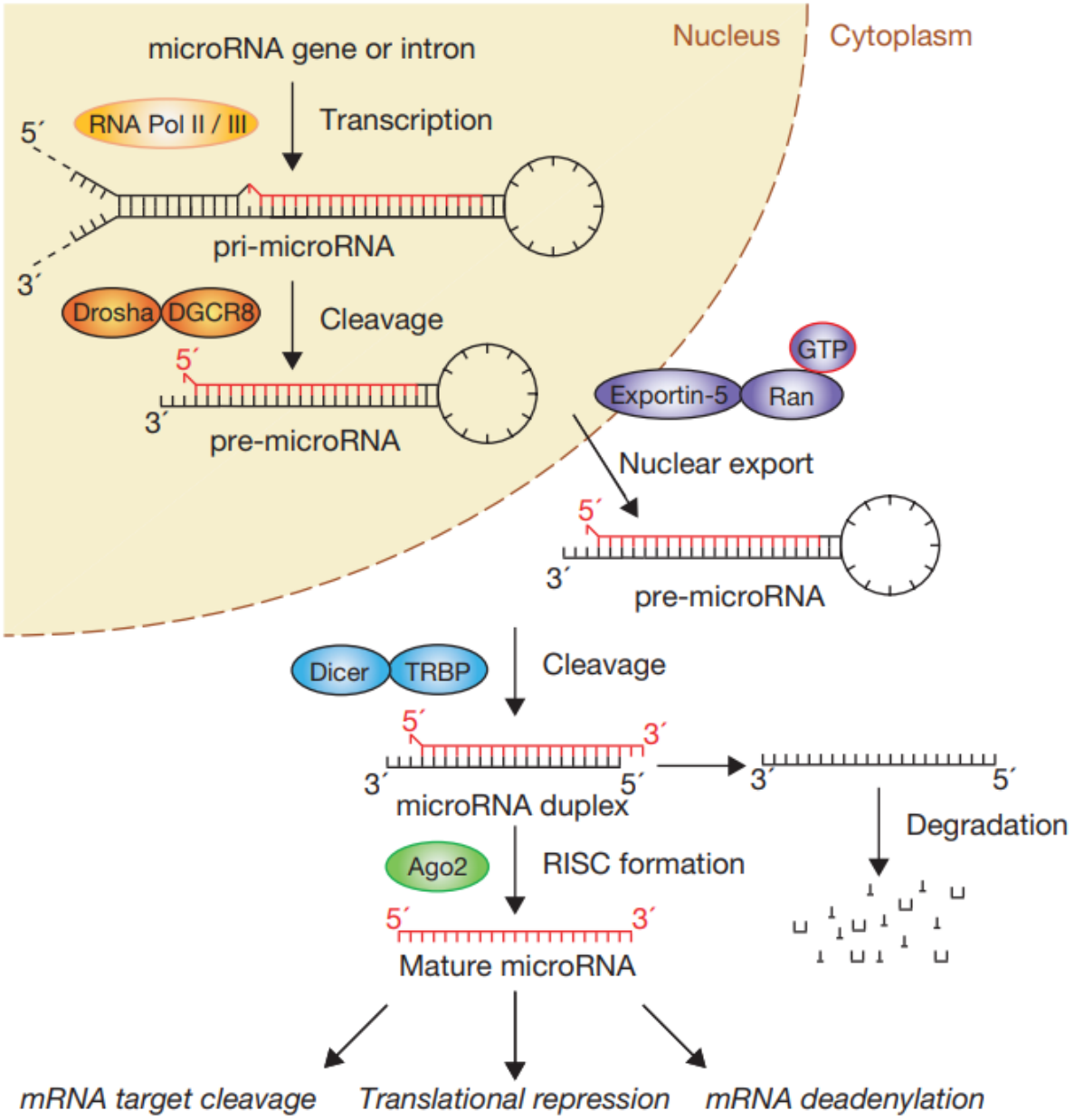

Figure 5: The canonical pathway of miRNA processing.
Processing of miRNAs starts in the nucleus where transcription via RNA polymerase II or III induces the formation of a pri-miRNA containing a stem-loop structure. Cleavage by the microprocessor complex (Drosha/DGCR8) results in a pre-miRNA that is exported into the cytoplasm where it is further cleaved by Dicer and its cofactor transactivation response element RNA-binding protein (TRBP). The resulting miRNA duplex is separated into two strands, one of which is loaded onto Ago2 to form the RNA-induced silencing complex (RISC) that targets the mRNA of interest. Extracted from (Winter et al., 2009).

1.4.1 miR-21

In case of miR-21, expression is distributed among various different mammalian tissues especially liver, heart, lung, breast and kidney (Landgraf et al., 2007; Kumarswamy et al., 2011). Moreover, this miRNA is highly expressed and reported in all major classes of transformed cells derived from epithelial, connective tissues, hematopoietic cells, germ cells or neuronal cells. For this reason, miR-21 is classified as 'oncomiR', a cancer-related miRNA with strong ubiquitous oncogenic potential (Asangani et al., 2008; Frankel et al., 2008; Lu et al., 2008; Medina et al., 2010). Furthermore, studies verified that most of miR-21's targets are direct or indirect tumor suppressors which in turn explain the anti-apoptotic nature of miR-21 (Buscaglia and Li, 2011).

Interestingly, miR-21 turned out to be located in the 3' untranslated region (UTR) of transmembrane protein/vacuole membrane protein (TMEM49/VMP1). However, miR-21 seems to be independently regulated through long, non-spliced and non-coding pri-miR-21 transcripts (Cai et al., 2004; Löffler et al., 2007).

Based on miRNA-sequencing, a highly dynamic expression of miR-21 during T-cell development was verified (Kirigin et al., 2012) (Figure 6). Highest levels of miR-21 are expressed in immature double negative DN1 thymocytes which is accompanied by a substantial downregulation to basal levels until the double positive stage. In single positive CD4 and CD8 T cells, a slight re-expression is observed but does not reach the initial expression level. Additionally, the role of miR-21 in the thymus remains elusive. For T cells, previous *in vitro* studies observed substantial expression of miR-21 upon activation in naïve and memory T cells in line with expression of CCR7 and described large tumor suppressor kinase 1 as a miR-21 target (Smigielska-Czepiel et al., 2013; Teteloshvili et al., 2017).

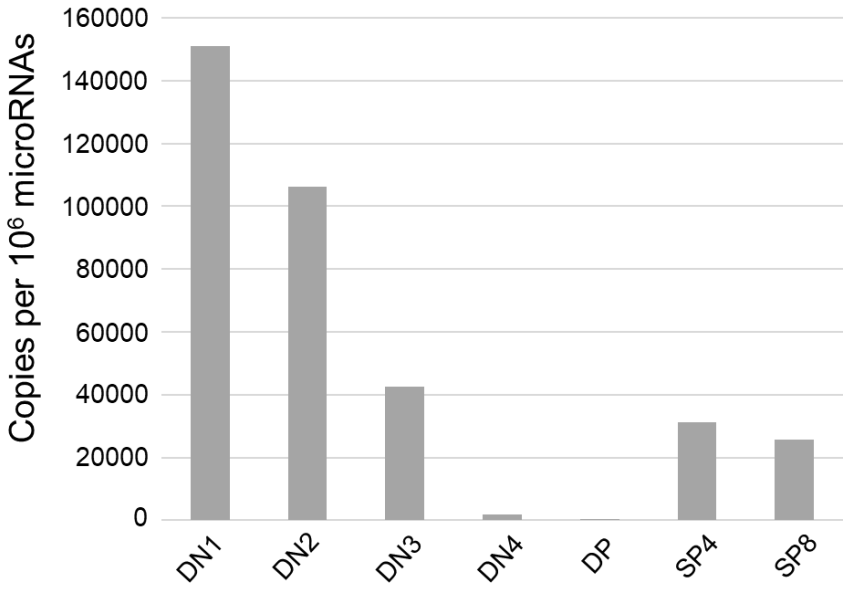

Figure 6: Substantial downregulation of miR-21 in developing thymocytes.
miR-21 expression was assessed in the indicated populations by miRNA-seq. Data extracted from (Kirigin et al., 2012). DN: double negative, DP: double positive, SP: single positive.

1.4.2 miR-17~92

The miR-17~92 cluster consists of six miRNAs (miR-17, miR-18a, miR-19a, miR-20a, miR-19b-1, and miR-92-1), which are all together processed from a single primary transcript. As described for miR-21, miR-17~92 is classified as oncomiR (He et al., 2005). Especially miR-19 was identified to promote B- and T-cell malignancies via interaction with c-Myc and Notch (Mu et al., 2009; Olive et al., 2009; Mavrakis et al., 2010).

Our group has recently shown that miR-17~92 serves as an interface between transcriptional programs and cytokine signaling. Accordingly, mice deficient in these miRNAs have a profound defect at the earliest stages of T-cell development due to limited responsiveness to IL-7 signals accompanied by a virtually complete recovery of thymocyte numbers from DN3 stage on (Regelin et al., 2015).

2 Aim

Intrathymic T-cell development ensures the continuous production of a functional pool of naïve T cells in a highly specialized environment. The underlying stepwise program includes commitment of BM-derived progenitor cells to the T-lineage, generation of a diverse TCR repertoire and selection of functional yet non-autoreactive T-cell clones. The different steps of this developmental process are interspersed by waves of proliferation. Proliferation is fundamental to maintain tissue homeostasis and continuous T-cell output. Moreover, an altered cell cycle regulation is a hallmark of multiple types of cancer, such as leukemia. However, analysis of cell cycle dynamics at high-resolution during T-cell development *in vivo* has not been performed.

For this reason, the first aim of the thesis is to understand T-cell population dynamics during T-cell development on the cell cycle level. To this end, a high-resolution cell cycle map based on complementary *in vivo* labeling approaches is generated. To test, how perturbation of tissue homeostasis affects cell cycle dynamics, three genetic and treatment models of altered T-cell development are investigated.

Short non-coding, single-stranded RNAs regulate target gene expression post-transcriptionally either via suppressing translation or enhancing degradation. Evidence is emerging that these miRNAs are key regulators of developmental processes including numerous aspects of T-cell development.

The second aim of this work is to study the role of miR-21. This miRNA was found to be prominently expressed in distinct thymocyte populations and to be dynamically regulated during T-cell development. The regulatory function of miR-21 in the thymus is explored using genetic loss-of-function and gain-of-function models in combination with analysis of T-cell development at steady-state, during differentiation *in vitro* as well as in a model of irradiation-induced perturbation.

3 Materials and methods

3.1 Antibody list

Table 1: Antibodies used for flow cytometry

Antibody target	Clone	Company
BrdU	3D4	BioLegend
CCR7	4B12	BioLegend
CD3e	145-2C11	Thermo Fisher Scientific
CD3	17A2	BioLegend
CD4	GK1.5	BioLegend
CD4	RL1.72	Krueger laboratory
CD5	53-7.3	Thermo Fisher Scientific
CD8α	53-6.7	BioLegend
CD8	M31	Krueger laboratory
CD24	M1/69	BioLegend
CD25	PC61.5	Thermo Fisher Scientific
CD28	E18	BioLegend
CD44	IM7	BioLegend
CD45.1	A20	Thermo Fisher Scientific
CD45.2	104	BioLegend
CD45R (B220)	RA3-6B2	BioLegend
CD62L	MEL-14	Thermo Fisher Scientific
CD69	H1.2F3	BioLegend
CD117	2B8	BioLegend
CD127	SB/199	BioLegend
CD135	A2F10	BioLegend
Cleaved caspase-3	Asp175	Cell Signaling Technology
Foxp3	MF-14	BioLegend
Ki-67	16A8	BioLegend
NK1.1	PK136	BioLegend
Phospho-histone H3 (Ser10)	D2C8	Cell Signaling Technology
TCRβ	H57-597	BioLegend
TCRγδ	GL3	BioLegend
Sca-1	D7	BioLegend

3.2 Molecular biology

3.2.1 Retroviral constructs

The empty vector MDH1-PGK-GFP_2.0 was a kind gift from Chang-Zheng Chen (Chen et al., 2004) (Addgene plasmid # 11375). In this construct, eGFP is encoded as a reporter gene under control of the PGK promoter and was used to determine transduction efficiency. This construct also served as a backbone to generate the MDH1-PGK-GFP_2.0-miR-21 construct to achieve stable overexpression of miR-21. This was done by a previous member of the group by amplification of the 273-bp miRNA gene segment containing the miR-21 hairpin following introduction via *Xho*I and *EcoR*I (both NEB) in the 3'LTR under control of the human H1 promoter.

3.2.2 Plasmid purification

In general, plasmids were purified using the PureYield Plasmid Miniprep kit (Promega) or the NucleoBond PC kit (Macherey-Nagel) according to the manufacturer's recommendations.

3.2.3 Quantitative Real-Time PCR (qRT-PCR)

In this thesis, total RNA extraction was generally performed using the miRNeasy kit (Qiagen) as per manufacturer's instructions. In case of miR-21 expression in different sorted murine T cells, quantitative qRT-PCR using miRNA specific looped reverse transcriptase primers and corresponding TaqMan probes for hsa-miR-21 (Applied Biosystems, Taqman miRNA Assay ID 00397) were used (compatible with murine miR-21).

As sequence alignment of murine and human (mmu vs hsa) miR-21 sequences revealed sequence identity apart from three minor mismatches, well-established mmu-miR-21 was used for all further experiments. Relative expression was calculated as % expression of house-keeping gene using the Δ cycle threshold method. SnoRNA412 (Applied Biosystems, ID 001243) served as house-keeping gene.

Expression of Bcl11b was assessed by reverse transcription using M-MLV Reverse Transcriptase (Promega) and random hexamer primers (Promega) according to the manufacturer's recommendations. For quantitative RT-PCR analysis of Bcl11b expression, the respective Bcl11b TaqMan probe (Applied Biosystems,

Mm01332818_m1) was used. Fold differences were determined using the Δ cycle threshold method normalized to Hprt, serving as housekeeping gene (Applied Biosystems, Mm00446968_m1).

In general, all reactions were performed as triplicates on a Quantstudio 3 (Applied Biosystems).

3.2.4 Single-cell RNA-sequencing (scRNA-seq)

ScRNA-seq was done on a collaborative basis with the laboratory of Dr. Mir-Farzin Mashreghi (Therapeutic Gene Regulation) at the Deutsches Rheuma-Forschungszentrum (DRFZ) in Berlin. In order to sort c-kit positive or c-kit negative DN thymocytes, cells were harvested and enriched as described before. Subsequently, cells were sorted by myself using a BD FACS Aria II. All steps upon successful sorting of the populations were done by Dr. Gitta Heinz (DRFZ) using the 10x Genomics workflow for cell capturing and scRNA gene expression (GEX). 5' gene expression library preparation was performed using the Chromium™ Single Cell 5' Library & Gel Bead Kit (10x Genomics) according to the manufacturer's protocol. The quality and quantity of the final sequencing libraries was assessed using the Fragment Analyzer with the HS NGS Fragment Kit (Agilent) (1-6000 bp) and the Qubit Fluorometer with the dsDNA HS Assay Kit (ThermoFisher Scientific). Sequencing with the recommended sequencing conditions for 5' GEX libraries (read1: 26nt, read2: 98nt, index1: 8nt, index2: n.a.) was performed on a NextSeq 500 device (Illumina) with High Output v2 Kits (150 cycles).

Bioinformatic analyses were done in consultation and applied by Dr. Pawel Durek and Dr. Frederik Heinrich (DRFZ). Raw sequence reads were processed using cellranger-3.1.0, including the default detection of intact cells. Mkfastq and count were used in default parameter settings for demultiplexing and quantifying the gene expression. Refdata-cellranger-mm10-1.2.0 was used as reference. The number of expected cells was set to 3000. The cellranger output was further analyzed in R using the Seurat package (version 3.1.1) (Butler et al., 2018). In particular, transcriptome profiles were merged, normalized, variable genes were detected and a Uniform Manifold Approximation and Projection (UMAP) was performed in default parameter settings using FindVariableGenes, RunPCA and RunUMAP with 30 principal components. Expression values are represented as ln (10,000 * UMIsGene) /UMIsTotal +1). Transcriptionally similar clusters were identified using shared nearest

neighbor (SNN) modularity optimization, SNN resolutions ranging from 0.1 to 1.0 in 0.1 increments were computed, or gating was performed manually using the Loupe Browser (10x Genomics). Cell cycle scores were determined as described in (Fischer et al., 2019).

3.3 Cell biology

3.3.1 Mammalian cell lines

HEK293T (human embryonic kidney) cells were used for production of retroviral particles and cultured in DMEM (Gibco) containing 10% FCS (GE Healthcare), 1% L-glutamine (Sigma-Aldrich) and 1% P/S (Sigma-Aldrich). Murine fibroblast 3T3 cells were primarily used for viral titration and cultured in DMEM supplemented with 10% FCS, 1% L-glutamine, 1% P/S, 1% non-essential amino acids (Thermo Fisher Scientific) and 0.1% β-Mercaptoethanol (50 µM, Sigma-Aldrich). BM-derived stroma cell lines OP9-GFP and OP9-DL1 (Schmitt and Zúñiga-Pflücker, 2002) were used for *in vitro* T-cell differentiation and maintained in α-MEM (Gibco) supplemented with 20% FCS and 1% P/S. All cells were cultured at 37°C and 5% CO_2.

3.3.2 Retrovirus production

For all retroviral constructs used in this thesis, $5x10^6$ HEK293T cells were transfected with 6.5 µg of the ecotropic packaging plasmid pCL-Eco (co-expressing gag, pol and env) and 6.5 µg of the retroviral vector of interest using the CalPhosTM Mammalian Transfection kit according to the manufacturer (Takara Bio). The virus containing supernatant was collected on three consecutive days in mornings and in evenings.

3.3.3 Virus titration

In order to determine the titer of the produced virus, $1x10^5$ 3T3 cells/well were seeded in a 6-well plate the day before transduction. The next day, 50 µL or 20 µL of virus supernatant were used for subsequent transduction of the cells in the presence of 8 µg/mL polybrene (Sigma-Aldrich). After four hours, the medium was exchanged and transduction efficiency was evaluated via flow cytometry 48 hrs later.

3.3.4 Flow cytometry

Monoclonal antibodies specific for B220 (RA3-6B2), CCR7 (4B12), CD3 (145-2C11), CD4 (GK1.5), CD5 (53-7.3), CD8α (53-6.7), CD24 (M1/69), CD25 (PC61.5), CD28 (E18), CD44 (IM7), CD45.1 (A20), CD45.2 (104), CD62L (MEL-14),

CD69 (H1.2F3), CD117 (2B8), CD127 (SB/199), CD135 (A2F10), Foxp3 (MF-14), NK1.1 (PK136), TCRβ (H57-597), TCRγδ (GL3) and Sca-1 (D7) labelled with either of the fluorophores AmCyan, Brilliant Violet (BV) 510, BV421, Pacific Blue (PB), eFluor450, fluorescein isothiocyanate (FITC), Alexa Fluor 488, Alexa Fluor 647, phycoerythrin (PE), peridinin chlorophyll protein-Cy5.5 (PerCP-Cy5.5), PE-Cy7, Allophycocyanin (APC) or APC-Cy7 were used and purchased from Thermo Fisher Scientific or BioLegend. APC-conjugated CD1d/PBS-57 loaded and unloaded tetramers as described (Liu et al., 2006b) were provided by the NIH Tetramer Core Facility. Cells were acquired using a BD FACSCanto II (BD Biosciences) and data was processed using FlowJo software (BD Biosciences). For data analyses, doublets and cells in sub-G0/G1 phase were excluded. For all panels, thymocytes were defined as follows:

ETPs ($CD4^-$, $CD8^-$, $TCR\beta^-$, $CD117^{hi}CD25^-CD44^+$),
DN1 ($CD4^-$, $CD8^-$, $TCR\beta^-$, $CD25^-CD44^+$),
DN2 ($CD4^-$, $CD8^-$, $TCR\beta^-$, $CD25^+CD44^+$),
DN2a ($CD4^-$, $CD8^-$, $TCR\beta^-$, $CD117^{hi}CD25^+CD44^+$),
DN2b ($CD4^-$, $CD8^-$, $TCR\beta^-$, $CD117^{lo}CD25^+CD44^+$),
DN3 ($CD4^-$, $CD8^-$, $TCR\beta^-$, $CD25^+CD44^-$),
DN3a ($CD4^-$, $CD8^-$, $TCR\beta^-$, $CD25^+CD44^-CD28^-$),
DN3b ($CD4^-$, $CD8^-$, $TCR\beta^-$, $CD25^+CD44^-CD28^+$),
DN4 ($CD4^-$, $CD8^-$, $TCR\beta^-$, $CD25^-CD44^-CD28^+$),
pre-selection DP ($CD4^+CD8^+CD69^-TCR\beta^-$),
post-selection DP ($CD4^+CD8^+CD69^+TCR\beta^+$),
SP4 ($TCR\beta^+$, $CD4^+$) and
SP8 ($TCR\beta^+$, $CD8^+$).

3.3.5 Cell preparations

Thymus, spleen and inguinal lymph nodes were meshed through a 70 µm cell strainer to obtain single-cell suspensions. For splenic samples, red blood cells (RBCs) were depleted using Qiagen RBC Lysis Solution according to manufacturer's instructions. Cell numbers were determined using a CASY Cell Counter and Analyzer Model TT (Innovatis).

3.3.6 Cell sorting

Cells were sorted using a FACS Aria III cell sorter. In the first step, cells of interest were stained with indicated antibodies, filtered to obtain a single-cell suspension and sorted into tubes containing sterile PBS/3% FCS or medium as required.

3.3.7 Enrichment of DN thymocytes

To enrich for DN thymocytes, total thymocytes were stained with anti-CD4 (RL1.72) (Ceredig et al., 1985) and anti-CD8 (M31) non-purified hybridoma supernatants (Sarmiento et al., 1980), followed by lysis with Low-Tox®-M Rabbit Complement (Cedarlane) and subsequent density gradient centrifugation with Lympholyte-M (Cedarlane).

3.3.8 Isolation of lin^- BM cells

Murine BM cells were isolated from the femur and tibia and stained with a lineage-specific antibody cocktail followed by magnetic bead depletion using the Lineage Cell Depletion Kit (antibody cocktail against CD5, CD45R (B220), CD11b, Gr-1 (Ly-6G/C), 7-4, and Ter-119) as per the manufacturer's instructions (Miltenyi Biotec).

3.3.9 Transduction of lin^- BM cells

First, BM was isolated and lineage-committed cells depleted as described before. Cells were then cultured overnight at a density of 0.5-1x10^6 cells/well in a 24-well plate in α-MEM (Gibco) containing 20% FCS (GE Healthcare) supplemented with mouse SCF (50 ng/mL), IL-7 (25 ng/mL), Flt3-L (25 ng/mL), and IL-6 (20 ng/mL) (all obtained from Peprotech). On two subsequent days, lin^- BM cells were transduced with respective viruses in the presence of 8 µg/mL polybrene (Sigma-Aldrich) using spin infection (700 *g*, 1.5 hours, RT) and subsequent incubation for four hours in a 37°C incubator before replacing with fresh medium supplemented with cytokines as described before. On day 4, transduction efficiency was determined via flow cytometry. Afterwards, cells were washed twice in sterile PBS, resuspended in sterile PBS and injected intravenously into lethally irradiated (9 Gy) recipients 4-5 hrs after irradiation.

Mice were given antibiotics in the drinking water for two weeks and were checked daily. Analyses were performed after eight weeks.

3.3.10 Magnetic bead-enrichment

For some cell populations, such as iNKT cells or c-kit positive DN thymocytes, well-established magnetic-bead enrichment was performed after staining with indicated tetramers or antibodies (Cossarizza et al., 2019; Cossarizza et al., 2021) using Miltenyi Biotec anti-APC or anti-PE microbeads according to the manufacturer's instructions.

3.3.11 Cell viability staining

Discrimination of live/dead cells was performed using Zombie Aqua dye (BioLegend) or 7-AAD (BioLegend) according to the manufacturer's instructions.

3.3.12 Tetramer staining

To identify iNKT cells, thymocytes or splenocytes were stained with Fc block for 10 min on ice prior to staining with APC-conjugated CD1d/PBS-57 loaded and unloaded tetramers for 30 min at RT in the dark. In a following step, cells were stained with surface antibodies to further characterize iNKT cells (Cossarizza et al., 2019; Cossarizza et al., 2021).

3.3.13 Intracellular staining

To detect expression of the transcription factor Foxp3, thymocytes were harvested and live/dead cell staining using Zombie Aqua dye (BioLegend) as well as staining for surface markers was performed. Fixation and subsequent permeabilization was achieved using the eBioscience™ Foxp3/transcription factor staining buffer set (Thermo Fisher Scientific). In the first step, thymocytes were incubated in Fix/Perm buffer for 30 min at RT or fixed with 2% paraformaldehyde for 10 min at RT (to preserve GFP staining) and washed twice in Permeabilization buffer afterwards. Staining for Foxp3 expression was performed overnight at 4°C with the indicated antibody diluted in Permeabilization buffer.

3.3.14 OP9 cocultures

In order to differentiate primary thymocytes or BM-derived precursors *in vitro*, OP9-DL1/OP9-GFP coculture assays were performed (Schmitt and Zúñiga-Pflücker, 2002). One day prior to the start of the coculture assay, OP9-DL1 and OP9-GFP cells were seeded in a 24-well plate ($2x10^4$ cells/well). Sorted cells (either primary thymocytes of different developmental stages or BM-derived precursors) were plated onto the subconfluent OP9 BM stromal cells the next day. In general, cocultures were maintained in the presence of 10 ng/mL SCF, 5 ng/mL Flt3-L and 1 ng/mL IL-7 for OP9-DL1 T-cell differentiation and 5 ng/mL IL-7 for OP9-GFP cultures (all obtained from Peprotech).

After four days, the first analyses via flow cytometry were performed. For this, half of one wells' coculture medium was replaced with fresh medium supplemented with cytokines as described before and differentiated cells were separated from contaminating OP9 cells by filtering the supernatant through a 50 µm filter prior to staining with antibodies. On day 7, the total culture medium was replaced and differentiated thymocytes were plated on fresh OP9 monolayers and analyzed via flow cytometry to monitor ongoing *in vitro* T-cell differentiation. Lineage differentiation was investigated for up to five weeks.

3.3.15 Apoptosis detection assay

Thymi from WT and miR-$21^{-/-}$ mice were harvested and isolated as described before. Single-cell suspensions were resuspended in α-MEM (Gibco) supplemented with 20% FCS and incubated at 37°C for up to 48 hours. In order to quantify apoptotic cells, thymocytes were stained with monoclonal antibodies against surface markers followed by Annexin V detection and staining with PI according to manufacturer's recommendations (BioLegend) after 0, 24 and 48 hours.

3.3.16 Measurement of intracellular Ca^{2+}-flux in thymocytes

To study Ca^{2+}-flux upon TCR stimulation, $5x10^6$ thymocytes from CD45.1 WT mice were mixed in a 1:1 ratio with thymocytes from miR-$21^{-/-}$ mice and incubated for 1 hr in 1 mL Ca^{2+}- and Mg^{2+}-free Hanks' PBS (HBSS, pH 7.4) (Sigma-Aldrich) at RT. Subsequently, thymocytes were washed and loaded with Fluo-4 (3 µM) and FuraRed (6 µM) dyes (both Thermo Fisher Scientific) and incubated at 37°C in Ca^{2+}- and

Mg^{2+}-sufficient HBSS (Gibco). After 45 min, thymocytes were simultaneously stained for CD45.1, CD45.2, CD4 and CD8α and stimulated with 100 µg purified anti-mouse CD3 (17A2, BioLegend) for 30 min on ice. Samples were rested at 37°C for 30 min. Flow cytometric analyses were performed and started with recording of a baseline for 30 seconds prior to addition of 12 µg goat anti-rat antibody (Jackson ImmunoResearch). Data acquisition was conducted for additional 210 seconds. In a last step, 2 µg ionomycin (Sigma-Aldrich) were added and served as positive control. For data analyses, median peak height resulting from anti-CD3-stimulation was assessed.

3.4 *In vivo* experiments

3.4.1 Mice

C57BL/6N (WT) mice (CD45.2) were purchased from Janvier Labs. miR-21 knockout mice (B6;129S6-Mir21a^{tm1Yoli}/J; termed miR-21$^{-/-}$ mice throughout this thesis) were purchased from The Jackson Laboratory (#016856). CCR7$^{-/-}$CCR9$^{-/-}$ (DKO) mice (Krueger et al., 2010), B6.SJL-PtprcaPepcb/BoyJ mice (CD45.1), C57BL/6N x B6.SJL-PtprcaPepcb/BoyJ F1 mice (CD45.1/CD45.2 heterozygous), Mirc1$^{tm1.1Tyj}$/J and B6.Cg-Tg(Vav1-icre)^{A2Kio}Mirc1$^{tm1.1Tyj}$/J (termed miR-17~92$^{fl/fl}$ and miR-17~92$^{\Delta/\Delta}$ respectively) were bred at the ZFE, Goethe University Frankfurt and maintained under specific pathogen-free conditions. Male and female mice were used between 4-20 weeks of age. All animal experiments were performed in accordance with local and institutional guidelines and have been approved by the Regierungspräsidium Darmstadt, Abteilung Veterinärwesen.

3.4.2 Dual pulse labeling using EdU and BrdU

First, mice were intravenously injected with 1 mg EdU (Thermo Fisher Scientific) following an injection of 2 mg BrdU (BioLegend, Germany) 60 min later. Subsequently, mice were sacrificed after 1 h, 2, 4 or 6 hrs and thymi were harvested. Single-cell suspensions were obtained as described before and 1x10^7 cells were stained with monoclonal antibodies followed by EdU and BrdU staining procedure according to the manufacturer's instructions using the Click-iT™ Plus EdU Alexa Fluor™ 647 Flow Cytometry Assay Kit (Thermo Fisher Scientific), Fixation/Permeabilization Solution Kit (BD Biosciences), Permeabilization Buffer Plus (BD Biosciences) and treatment with DNase I from bovine pancreas (Sigma-Aldrich). In more detail, cells were resuspended in 1 mL Fixation/Permeabilization solution and incubated for 22.5 min at RT in the dark. Cells were washed once with 10 mL 1x BD Perm/Wash™ Buffer per sample and then incubated with 100 µL Permeabilization Buffer Plus for 10 min on ice. Afterwards, cells were washed with 5 mL 1x BD Perm/Wash™ Buffer, again fixed with 1 mL Fixation/Permeabilization solution for 5 min on ice and washed with 10 mL 1x BD Perm/Wash™ Buffer per sample. After washing, cells were resuspended in 1 mL DNase I (300 µg/mL) and incubated for 60 min at 37°C. Subsequently, cells were resuspended in 100 µL 1x Click-iT™ permeabilization and wash reagent and 500 µL Click-iT™ Plus reaction cocktail prepared according to the manufacturer's instruction

were added and samples were incubated for 30 min in the dark. To avoid any potential interference of remaining Click-iT™ Plus reaction cocktail components, samples were washed four times (2x 10 mL, 1x 5 mL and 1x 3 mL) with 1x Click-iT™ permeabilization and wash reagent. To detect BrdU, samples were stained with FITC-conjugated anti-BrdU antibody (3D4, BioLegend) and incubated for 20 min at RT. After staining, cells were washed once with 5 mL BD Perm/Wash™ Buffer and two times with 5 mL PBS/3% FCS. In the last step, cells were stained with DAPI (BioLegend) to perform DNA content analysis. All centrifugation steps were performed at 300 *g* for 5 min. For DN subsets, the following surface antibodies were used: CD4-PE-Cy-7, CD8-PE-Cy7, TCRβ-PE-Cy7, CD25-PerCP-Cy5.5 and CD44-APC-Cy7. For pre- and post-selection DP subsets as well as SP4 and SP8 subsets CD4-PerCP-Cy5.5, CD8-PE-Cy7, CD69-PE and TCRβ-APC-Cy7 were used.

3.4.3 Quantification of quiescent and mitotic cell frequencies

For analysis of quiescent or mitotic cells, mice were injected with 2 mg BrdU intravenously. After one hour, thymi were collected and staining for incorporated BrdU was performed as described before. Afterwards, cells were either stained for 60 min at RT with Ki-67-APC (16A8, BioLegend) to quantify the frequency of quiescent cells or in order to distinguish cells in G2 and M phase, cells were stained with phospho-histone H3 (Ser10) (D2C8)-Alexa 647 (Cell Signaling Technology). In both cases, DAPI staining for DNA content analyes was performed afterwards.

3.4.4 Thymus regeneration

As a model to evaluate cell cycle dynamics after endogenous regeneration, WT mice were sublethally irradiated (5.5 Gy). Six days after irradiation, dual pulse labeling using EdU and BrdU was performed as described before.

In order to assess an involvement of miR-21 in stress responses and T-cell regeneration, the described approach was applied correspondingly. For this reason, WT or miR-21$^{-/-}$ mice were sublethally irradiated (5.5 Gy). Immediately after irradiation as well as on day 3, 7 and 14 after irradiation, thymi were harvested and flow cytometric analyses were performed.

3.4.5 Competitive BM chimeras

Donor BM cells from WT (CD45.1, competitor), WT (CD45.2, test/control) and miR-21$^{-/-}$ (CD45.2, test) mice were isolated as described above. Lethally irradiated (9 Gy) CD45.1/CD45.2 mice (serving as recipients) were reconstituted intravenously with mixtures of competitor and test cells resuspended in sterile PBS in a 1:1 ratio four hours after irradiation (2x10^6 cells per mouse). Mice were given antibiotics in the drinking water for two weeks, checked daily and analyzed after eight weeks.

3.4.6 *In vivo* T-cell receptor stimulation

200 µg purified anti-mouse CD3 (17A2, BioLegend) was injected into WT or miR-21$^{-/-}$ mice. Two days later, thymocytes were isolated and stained with monoclonal antibodies followed by live/dead staining to exclude dead cells as described before. Afterwards, samples were fixed using paraformaldehyde (4%) and permeabilized prior to anti-active-caspase-3 staining (Asp175, Cell Signaling Technology) followed by staining with secondary donkey anti-rabbit-Alexa647 antibodies (Poly4064, BioLegend) and subsequent analyses via flow cytometry. In order to assess proliferation in this assay, a single BrdU pulse was performed. For this, mice were injected intravenously with 2 mg BrdU (BioLegend) 3 hrs before harvesting the thymocytes and the subsequent staining for BrdU was performed as described before using a FITC anti-BrdU antibody (BioLegend, clone: 3D4).

3.5 Statistical analyses

All statistical analyses were performed using GraphPad Prism software (version 7 and 8). Detailed information about number of mice being used and number of replicates are described in the figure legends. In general, data are represented as mean ± SEM unless otherwise mentioned in the figure legends. Analysis of significance between two groups of mice was performed using unpaired t-tests unless otherwise specified in the figure legends. For comparison between three or more groups, ordinary one-way analysis of variance (ANOVA) followed by Tukey's test was used unless otherwise specified in the figure legends. In all figures, *P<0.05; **P<0.01; ***P<0.001; ****P<0.0001 was considered as significant. When no p-value is indicated, samples were not significant.

4 Results

4.1 Cell cycle dynamics during T-cell development

4.1.1 Steady-state analysis of thymocyte cell cycle dynamics

Classically, cell cycle phases can be quantified by flow cytometric analyses using DNA content markers. This allows to distinguish between cells in the G0/G1 (2N), S (>2N) and G2/M phase (4N). Cells in S phase can be further identified by their capability to incorporate nucleoside analogues such as BrdU. Here, we made use of a single pulse of BrdU combined with analyses of DNA content to assess the steady-state proportions of thymocytes at distinct cell cycle states (Figure 7). In addition, we included Ki-67 staining to discriminate between cells in G1 phase and quiescent cells in G0 phase. Ki-67 accumulates from the beginning of the S phase onwards until mitosis and is degraded continuously in G0 and G1 cells (Schwarting et al., 1986; Miller et al., 2018). Since Ki-67 protein is absent from G0 phase cells, it can be used to identify quiescent cells (Vignon et al., 2013).

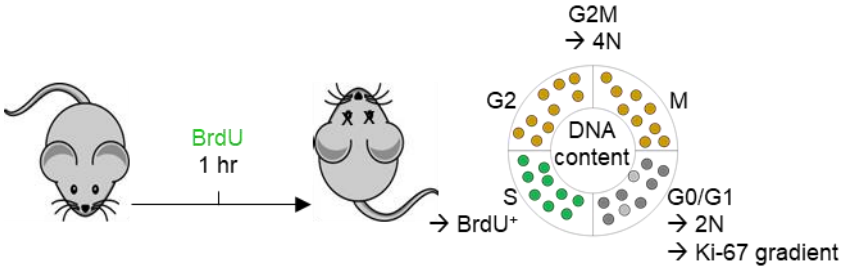

Figure 7: Schematic depiction of the performed experiments using *in vivo* BrdU single-pulse-labeling.
Mice were injected with BrdU and sacrificed after one hour prior to identification of actively replicating cells. In addition, DNA content analyses were performed to determine frequencies of cells in G0/G1, S and G2M phase. To assess the frequency of quiescent cells, Ki-67 staining was performed.

Flow cytometric analyses of thymocytes derived from a WT mouse injected once with BrdU and stained with Ki-67 and DAPI as DNA content marker revealed distinct populations (Figure 8). We found WT thymocytes in the G0/G1 phase of the cell cycle ($BrdU^-$, 2N DNA), S-phase cells ($BrdU^+$, 2N < DNA < 4N) and a small fraction of cells in G2/M phase ($BrdU^-$, 4N DNA). In addition, we identified a minute fraction of $Ki\text{-}67^-$ cells when comparing Ki-67 expression levels of $BrdU^-$ and $BrdU^+$ cells (green).

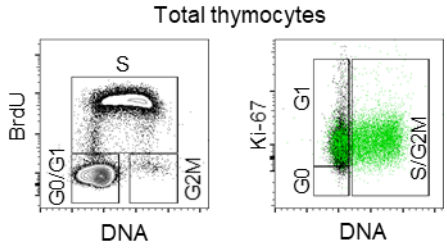

Figure 8: Flow cytometric gating strategy to identify cells in G0, G1, S or G2M phase.
Representative flow cytometric analyses of WT thymocytes of BrdU-injected mice. BrdU labeling was performed prior to DNA staining to discriminate cells in the G0/G1, S and G2/M phase. To further distinguish cells in the G0 (quiescent) and G1 phase, Ki-67 staining was performed. Quiescent cells were defined by lower levels of Ki-67 in $BrdU^-$ (black) cells in comparison to Ki-67 levels in $BrdU^+$ (green) cells.

In a next step, we assessed the steady-state cell cycle states of different WT thymocyte subsets by flow cytometric analyses of BrdU incorporation and DNA content starting with the earliest thymocyte subset DN1 to fully mature SP cells. In all subsets the majority of cells were in the G0/G1 phase of the cell cycle ($BrdU^-$, 2N DNA) (58.4% - 98.5%) (Figure 9a). We identified a large proportion of DNA replicating cells in the DN2, DN3b and DN4 subsets (incorporation of BrdU and 2N < DNA < 4N) (25.2% - 40.9%), whereas the earliest thymocyte subset (DN1) as well as the DN3a subset showed less than 4.5% S-phase cells. We also detected a lower proportion of S-phase cells (1.37 - 8.77 %) among thymocytes either before or after selection steps as well as upon full maturation. A minute proportion of cells in G2/M phase ($BrdU^-$, 4N DNA) was detectable in all subsets with highest levels in DN1 cells (1.17%).
To quantify the proportion of quiescent cells, we then assessed Ki-67 levels (Figure 9b) and observed highest frequencies of quiescent G0 cells following selection (up to 12.27%). In line with our S phase analyses, we found lowest proportions of G0 cells in the DN2 and DN3b subset (1.65% and 1.09%, respectively).

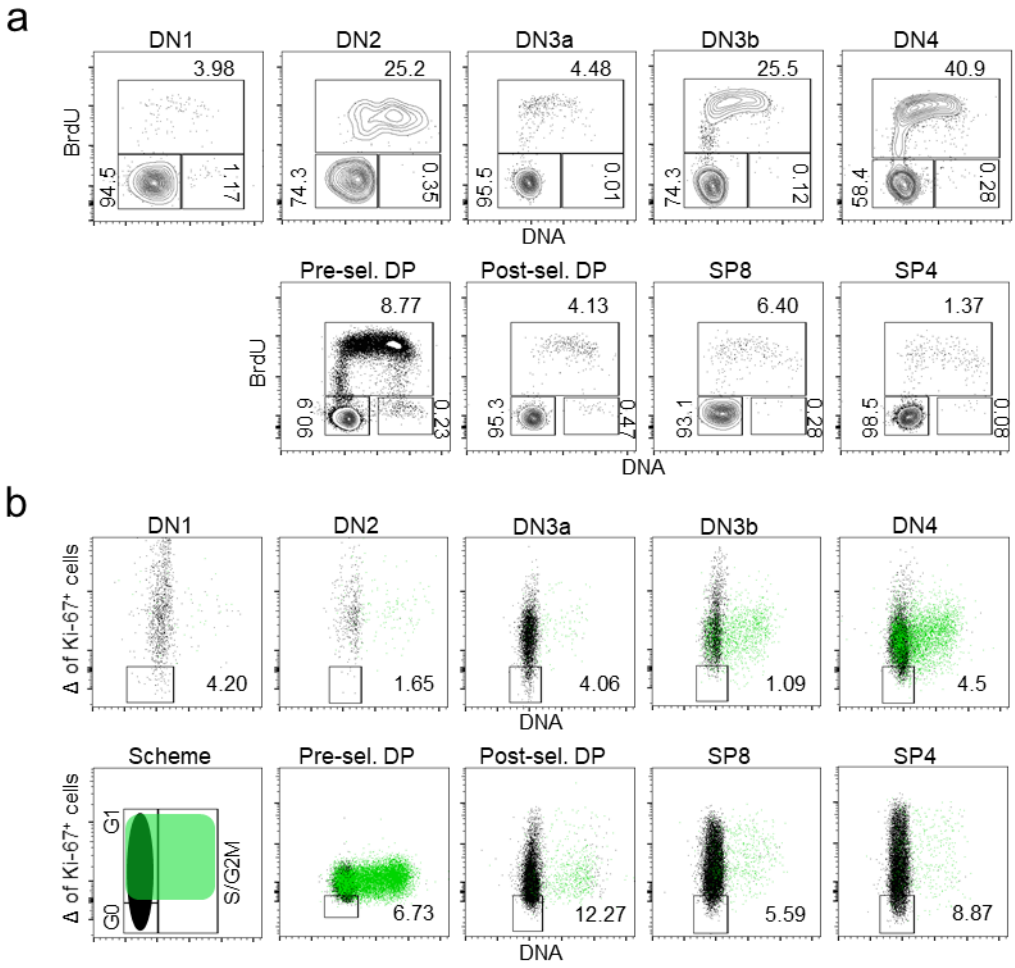

Figure 9: Thymocyte subsets are characterized by different cell cycle dynamics.
(a) Representative flow cytometric analyses of *in vivo* BrdU single pulse labeling in combination with DNA content analyses to quantify cells in the G0/G1 ($BrdU^-$, 2N DNA), S ($BrdU^+$, 2N < DNA content < 4N) and G2/M phase ($BrdU^-$, 4N DNA) among different thymocyte subsets. Numbers adjacent to or in gates indicate frequencies. (b) Representative flow cytometric analyses and scheme of *in vivo* labeling in combination with DNA content analyses and Ki-67 staining to discriminate G0 and G1 cells of different thymocyte subsets. For this, an overlay of Ki-67 levels in $BrdU^+$ (green) and $BrdU^-$ cells (black) was applied to determine the frequency of quiescent cells. Numbers adjacent to gates represent the differences in Ki-67 levels, considering this as frequency of quiescent cells.

Based on this, we were able to compile a detailed picture about the individual cell cycle state distribution of different WT thymocyte subsets at steady-state (Figure 10). Consistent with earlier studies (Penit et al., 1988; Baron and Pénit, 1990; Pénit et al., 1995; Vasseur et al., 2001) it can be concluded that T-cell development is marked by periodic changes between cycling and non-cycling phases corresponding to stage-specific developmental events, e.g. TCR gene rearrangement at the DN3a stage.

a

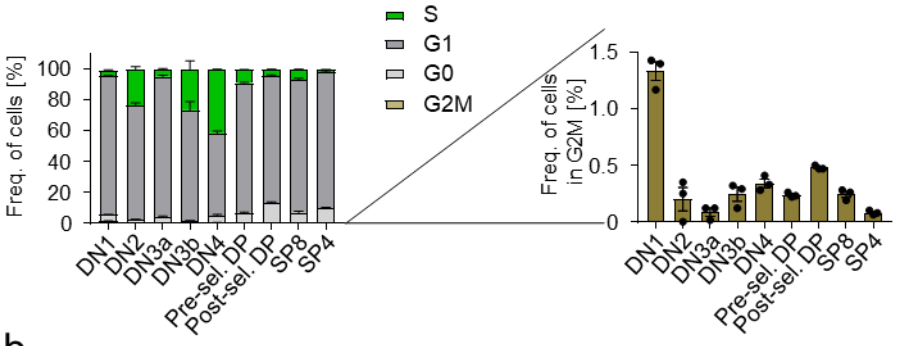

b

	G0	G1	S	G2M
DN1	3.96 ± 0.59	90.51 ± 0.35	3.83 ± 0.39	1.33 ± 0.14
DN2	1.87 ± 0.82	74.53 ± 2.78	23.33 ± 3.32	0.2 ± 0.18
DN3a	4.14 ± 0.53	91.09 ± 1.57	4.68 ± 1.13	0.08 ± 0.06
DN3b	0.94 ± 0.85	72.26 ± 10.10	26.4 ± 10.28	0.24 ± 0.11
DN4	4.21 ± 1.87	53.99 ± 2.56	41.17 ± 0.74	0.34 ± 0.07
pre-sel. DP	6.51 ± 0.83	84.49 ± 0.62	8.67 ± 0.29	0.24 ± 0.02
post-sel. DP	12.4 ± 1.55	86.04 ± 1.20	3.99 ± 0.59	0.48 ± 0.02
SP8	6.54 ± 1.68	86.43 ± 2.18	6.65 ± 0.49	0.24 ± 0.05
SP4	9.49 ± 1.33	88.84 ± 1.46	1.53 ± 0.14	0.08 ± 0.02

Figure 10: Different stages of T-cell development are marked by alternating cycling and non-cycling phases.
(a) Frequencies of cells in G0, G1, S or G2M phase of murine WT thymocyte subpopulations, n = 3 mice.
(b) Summary of subpopulations shown in (a), numbers indicate mean frequencies ± SD.

4.1.2 High-resolution cell cycle stage analysis

Single-pulse experiments using nucleoside analogues represent a fundamental tool to measure DNA synthesis. However, they cannot provide detailed information about cell cycle kinetics. For this reason, we increased the temporal resolution of steady-state cell cycle analysis of thymocytes by using a dual-pulse labeling approach (Figure 11). We adopted an experimental system of sequential nucleoside labeling with EdU and BrdU at 1 hr apart in conjunction with analyses of DNA content which allows for high-resolution cell cycle evaluation *in vivo* (Gitlin et al., 2014; Gitlin et al., 2015). Due to the short half-life of the nucleoside analogues, sequential labeling enabled a virtual synchronization of thymocytes *in situ* (Hagan, 1984; Matiašová et al., 2014).

Cells positive for both labels (EdU^+BrdU^+) represent the frequency of cells that have been in S phase during both pulses corresponding to a time window of less than 2 hrs. EdU^+ cells have ceased DNA replication within 1 hr and can therefore be stated as post S phase at the time of analysis. This population allowed for quantification of S-phase exit whereas the cells positive for BrdU represent the fraction of cells newly entered S phase within less than 1 hr because those cells have initiated DNA replication during this time window.

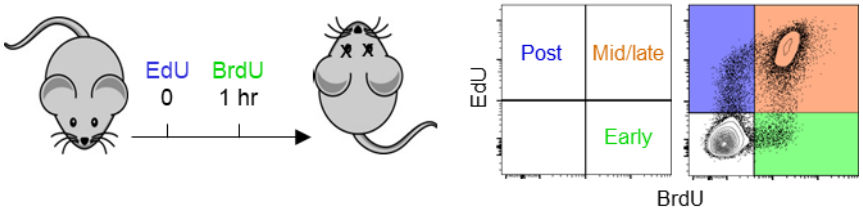

Figure 11: *In vivo* dual-pulse labeling approach.
Schematic depiction and representative flow cytometric gating strategy of *in vivo* dual-pulse labeling. Mice were administered EdU and BrdU 1 hr apart followed by analysis 1 hr after the second pulse. After thymus harvest and staining, four populations can be distinguished: Cells negative for both labels (EdU^-BrdU^-) represented a population that has not undergone DNA replication within the last 2 hrs. BrdU single positive thymocytes ($BrdU^+$, green, early S phase) were classified as the frequency of cells that newly entered S phase during the last 60 min, because these cells did exclusively incorporate the second nucleoside analogue. In comparison, EdU single positive cells represent a population which has ceased DNA replication and left S phase (EdU^+, blue, post S phase) prior to the second pulse. Thymocytes that actively replicated their DNA during both pulses appeared as double positive stained cells, EdU^+BrdU^+ (orange, mid/late S phase).

We then performed dual-pulse labeling experiments for different WT thymocyte populations, starting at DN1 thymocytes to fully mature SP cells (Figure 12). Frequencies of double-labeled thymocytes (EdU^+BrdU^+) reflecting the proportion of cells that actively replicated their DNA during both pulses corresponding to a time window of less than 2 hrs were highest for DN2, DN3b and DN4 thymocyte populations

(29.8%, 44.3% and 26.5%, respectively) corroborating our previous results obtained from single BrdU pulse experiments (Figure 10). In those populations, we also found highest levels of S-phase entry ($BrdU^+$) and S-phase exit (EdU^+). DN1, DN3a and pre-selection DP had rates of S-phase entry of around 2% whereas those of post-selection DP and SP thymocytes were even lower (less than 1%).

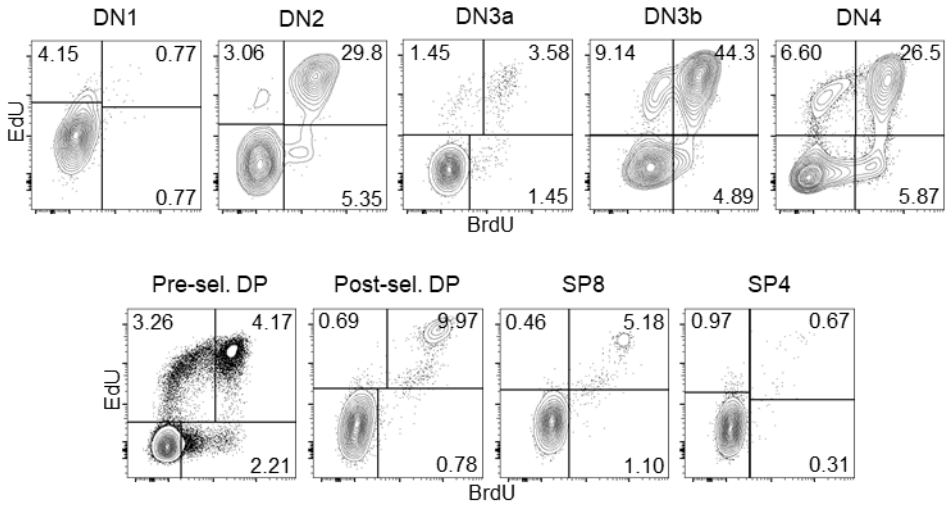

Figure 12: High resolution S-phase profiling of thymocyte subsets.
Representative flow cytometric analyses of *in vivo* dual-pulse labeling among early and late staged thymocyte subpopulations. Mice were administered EdU and BrdU as described before and subsequently prepared for flow cytometric analyses. Numbers in gates indicate frequencies.

Figure 13 provides a detailed summary of our findings: As also observed in the single-pulse experiments, DN2, DN3b and DN4 subsets showed the largest proportion of DNA replicating cells. In addition, this was true for the fraction of EdU^+BrdU^+ cells (in S phase during a time window of less than 2 hrs) (Figure 13a) as well as for $BrdU^+$ (Figure 13b) and EdU^+ (Figure 13c) cells reflecting the rates of S-phase entry and exit, respectively. The proportion of unlabeled cells (Figure 13d) reflecting thymocytes that have not been in S phase of the cycle during administration of EdU and BrdU is therefore lowest in those populations. Especially DN3b thymocytes showed the highest S-phase cycling activity. In contrast, DN3a thymocytes, cells in a developmental stage between the aforementioned DN2 and DN3b subsets, had high rates of unlabeled cells (EdU^-BrdU^-) (Figure 13d) and low levels of S-phase entry and exit (Figure 13a and b, respectively). We also found pre- and post-selection DPs to be characterized by different S-phase kinetics: Whereas less EdU^+BrdU^+ cells (Figure 13a) were found in the pre-selection DP subpopulation, this subset was characterized by more S-phase entry (Figure 13b) and exit (Figure 13c) in comparison to post-selection DP thymocytes. At this particular stage of development, S-phase cells were mostly found

in the fraction of double-labeled cells (Figure 13a) and we detected only a minute proportion of cells entering or leaving S phase (less than 1%). As an additional read-out, we compared the frequencies of cells in S phase in relation to entry or exit of those cells for pre- and post-selection DP thymocytes (Figure 13e and f). We detected an increase in those ratios for post-selection thymocytes which led us to hypothesize that these cells might stall or arrest in the S phase of the cell cycle. Statistical analyses can be found in the appendix (Figure 48).

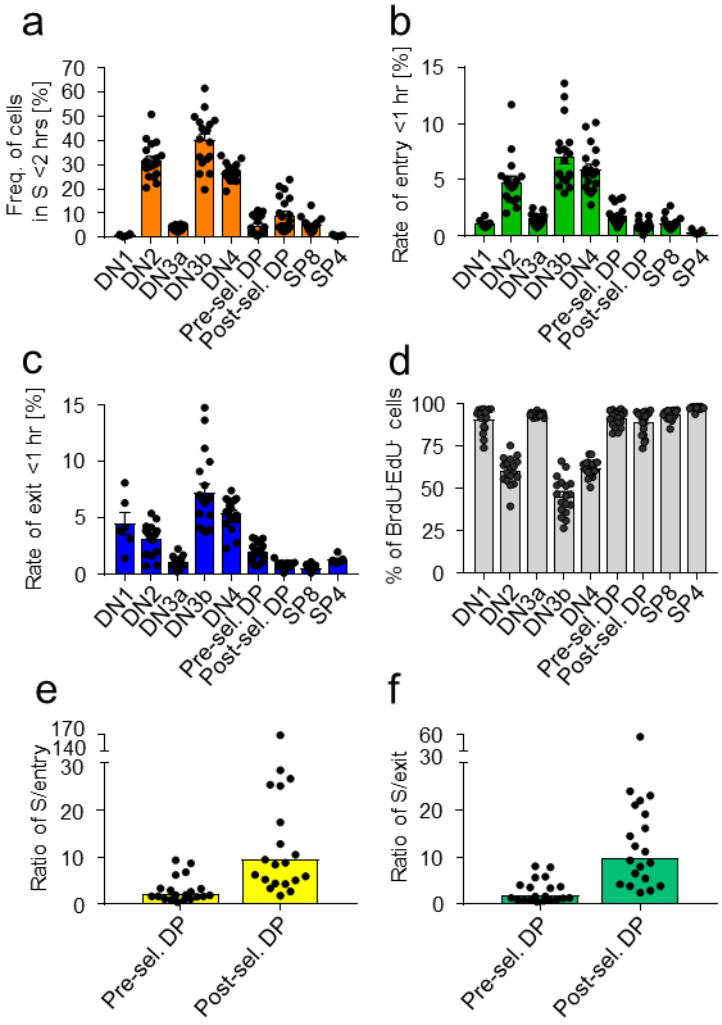

Figure 13: Steady-state cell cycle dynamics among murine WT thymocytes.
Flow cytometric analyses of *in vivo* dual pulse labeling. Graphs show frequencies of EdU^+BrdU^+ cells (a), $BrdU^+$ cells (b), EdU^+ cells (c), EdU^-BrdU^- cells (d), ratio of $EdU^+BrdU^+/BrdU^+$ cells (e) and EdU^+BrdU^+/EdU^+ cells ($p = 0.0004$) (f) of different murine WT thymocyte subpopulations, n = 6-20 mice of two independent experiments.

We further observed rates of S-phase entry and exit to be largely similar for each subset except for DN1 and SP4 cells that showed higher exit than entry rates (Figure 13c). Presumably, this was due to low numbers in the EdU^+ fraction.

In a next step, we combined *in vivo* dual-nucleoside pulse labeling with analysis of DNA content. Determination of DNA content at different time points enabled to assess rates of DNA replication and thus, duration of S phase and total cell cycle length. To do so, we gated on the fraction of $BrdU^+$, EdU^+BrdU^+ and EdU^+ cells in different thymocyte subsets and quantified DNA content 1 hr, 2, 4 or 6 hrs post dual-nucleoside administration (Figure 14). This approach allowed for fate mapping of thymocytes that were initially labeled during their early S phase ($BrdU^+$), mid/late S phase ($BrdU^+EdU^+$) or post S phase (EdU^+) and enabled quantitative determination of the individual cycling behaviour.

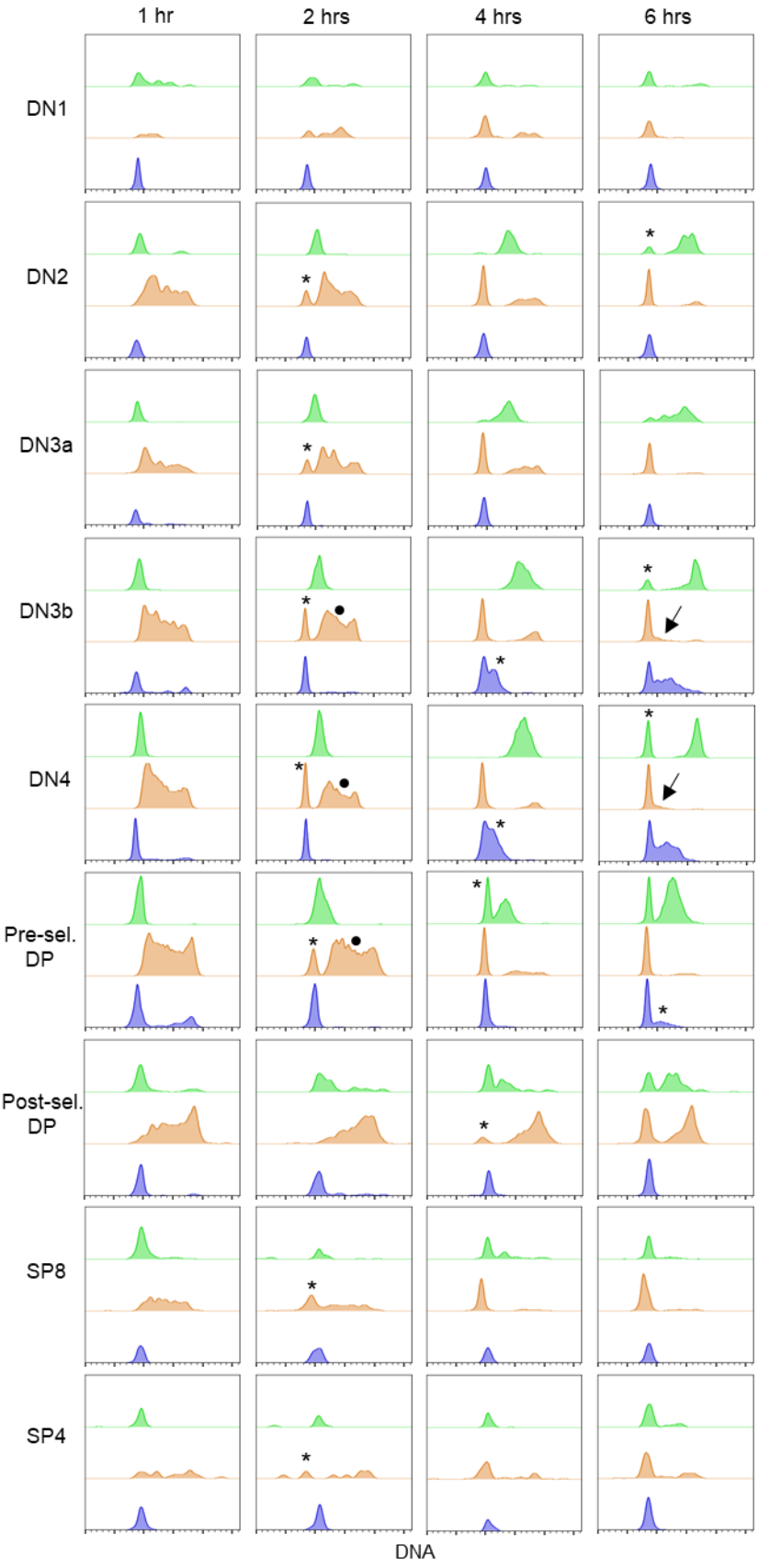

Figure 14: Dynamic analysis at cell cycle stage resolution.
Representative flow cytometric histograms visualizing the DNA content of DN1 until SP4 thymocytes of WT mice over time. Each plot depicts an overlay of the DNA content of $BrdU^+$ (top, green), EdU^+BrdU^+ (middle, orange) and EdU^+ (bottom, blue) cells. Asterisks, dots and arrows points out highlights.

Based on these DNA content analyses, we unraveled clear differences in cell cycle kinetics of slow and fast proliferating populations. As a read-out for S-phase cell cycle length, $BrdU^+$ cells which were originally labeled during early S phase (Figure 14, green) were analyzed regarding their DNA content. In light of this, $BrdU^+$ cells of DN2, DN3b and DN4 subpopulations were found to be back in the G1 phase after 6 hrs (asterisk). $BrdU^+$ cells of pre-selection DP thymocytes were found to be back in G1 phase already after 4 hrs indicating a shortened S phase cell cycle length before selection in comparison to early developmental stages. These findings were further supported by analyses of the EdU^+BrdU^+ (orange) cells. Here, for nearly all thymocyte subpopulations we detected cells back in the G1 phase already after approximately 2 hrs with one exception for the EdU^+BrdU^+ post-selection cells (asterisk). This time window was interpreted as the time for finalizing DNA replication, undergoing mitosis and re-entry into G1. For post-selection thymocytes, the EdU^+BrdU^+ cell fraction re-entered G1 phase after 4 hrs indicating a prolonged S phase in this subset (asterisk). Among the EdU^+BrdU^+ fraction of cells in the DN3b and DN4 stage, we also identified a slight proportion of cells potentially re-entering S phase after 6 hrs (black arrow). This assumption was verified by analyses of the EdU^+ data (Figure 14, blue). Here, we detected S-phase cells for DN3b and DN4 thymocytes after 4 hrs and in pre-selection DP thymocytes after 6 hrs (asterisk). For nearly all subsets, EdU^+ cells mostly reached G1 phase already at the 1 hr time point of analysis, corresponding to approximately 1-1.5 hrs G2/M duration.

We also observed heterogeneity in DNA replication as exemplarily highlighted in the EdU^+BrdU^+ population (orange) of DN3b, DN4 and pre-selection DP thymocytes after 2 hrs (black dots) which was mostly recovered after 4 hrs when cells were found to be back in the G1 phase of the cycle.

For DN1 and SP subsets, low cell numbers and very low numbers of nucleoside incorporated cells provided too little information to draw a reliable conclusion. For this reason, we omitted these subsets from the following analyses.

A quantitative analysis of this experiment which supports the aforementioned findings and provides first estimations of the duration of individual cell cycle phase length is shown in Figure 15. Notably, duration of G1 phase re-entry of EdU^+BrdU^+ cells (Figure 10a) was similar for all developmental stages, except for post-selection DP thymocytes which showed reduced percentages of cells back in the G1 phase of

the cycle at all time points analyzed. This argues for a prolonged S-phase length in this particular subpopulation. S-phase re-entry of EdU$^+$ cells (Figure 15b) was mostly observed in DN3b, DN4 and pre-selection DP thymocytes after 4 and 6 hrs, respectively indicating a G1-phase duration of approximately 5 to 6 hrs. From this data, we also estimated G2/M duration to be in a range of 1 to 1.5 hrs and similar for all thymocyte populations. Additionally, statistical analyses are shown in the appendix (Figure 49).

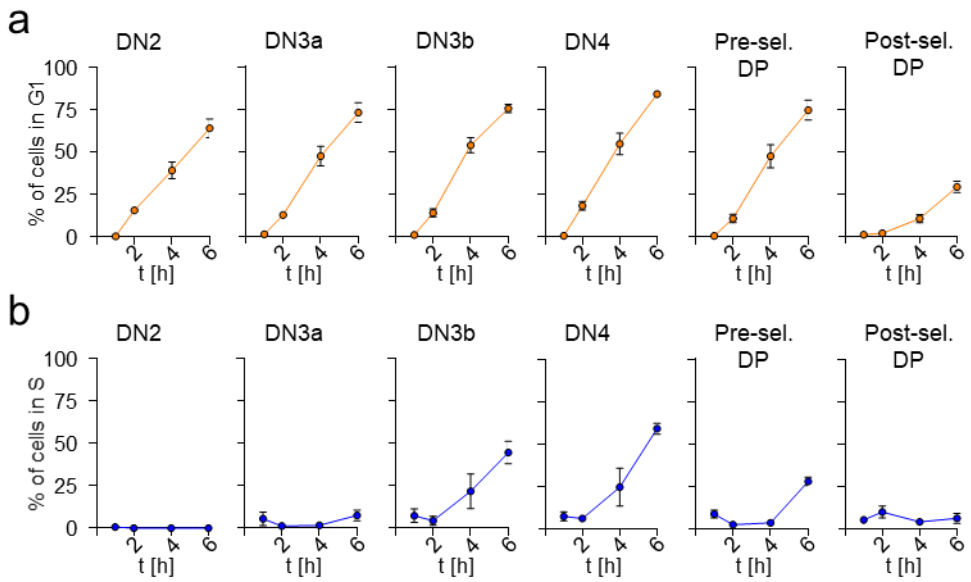

Figure 15: Re-entry of EdU$^+$BrdU$^+$ thymocytes in G1-phase and EdU$^+$ thymocytes in S-phase.
(a) Quantification of G1-phase re-entry of EdU$^+$BrdU$^+$ (orange) WT thymocyte subpopulations over time. (b) Quantification of S-phase re-entry of EdU$^+$ (blue) WT thymocyte subpopulations over time. (a, b) n = 4-5 for each point in time, data from two independent experiments.

Next, we applied linear regression analysis of DNA content towards 4N as direct read-out for the duration of S phase. We therefore applied an approach to quantify the relative movement (RM) of nucleoside-incorporated cells through the S phase relative to that of G1 and G2M cells by measuring their mean fluorescence intensity (Begg et al., 1985; Baron and Pénit, 1990) (Figure 16). This calculation revealed S-phase duration of WT thymocytes in a range of 6.43 to 11.1 hrs. Our results further supported our findings of short S-phase lengths of 6-7 hrs for DN3b as well as DN4 thymocytes and prolonged S-phase durations for DN2, DN3a and pre-selection DP cells. Post-selection DP thymocytes remained in S phase for 11.1 hrs consistent with our previous observations. For post-selection DP thymocytes, RM values were of a high level already at early timepoints but did not change as much over time as detected in the other thymocyte subsets. The underlying reasons are currently unknown but point

towards a pause in DNA replication and further support our aforementioned hypothesis that these cells might stall or arrest in the S phase of the cell cycle. Statistical analyses are shown in the appendix (Figure 50).

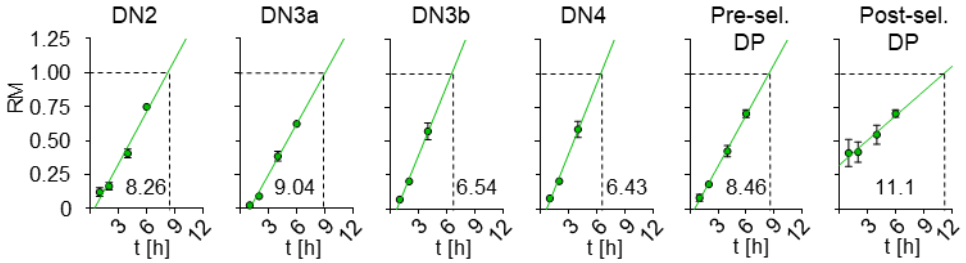

Figure 16: S-phase duration of WT thymocyte subsets based on RM values of BrdU$^+$ cells.
Statistical analyses of WT thymocyte subpopulations to assess S-phase time duration based on the relative movement (RM) values of BrdU$^+$ cells (early S phase) over time (green dots). Green lines represent linear regression and numbers indicate estimated S-phase times in hours, n = 3-5 mice for each point in time, data from two independent experiments.

Finally, we analyzed whether label-negative cells (EdU$^-$BrdU$^-$, grey) entered S phase at some point (Figure 17). Consistent with our estimations for G1-phase duration, we found cell cycle entry in at least some label-negative cells already after 2 hrs and more pronounced after 4 hrs in fast cycling popuations such as DN3b and DN4 thymocytes. On the other hand, no S-phase entry was detected in pre-selection DP cells.

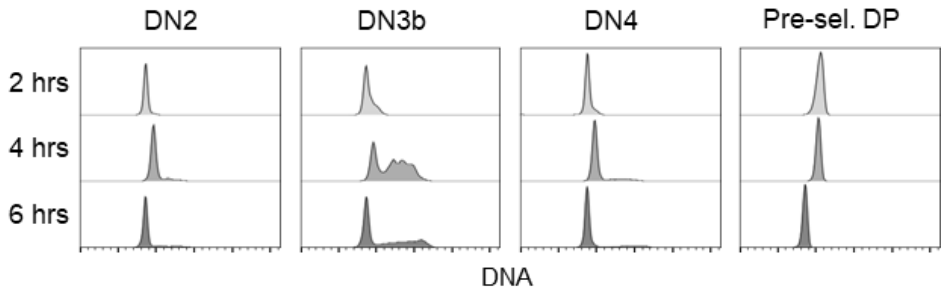

Figure 17: BrdU$^-$EdU$^-$ cells show distinct characteristics over time.
Representative flow cytometric histograms show DNA content of EdU$^-$BrdU$^-$ DN2, DN3b, DN4 and pre-selection WT thymocytes over time. Each plot represents an overlay of the DNA content at 2, 4 and 6 hrs.

In summary, we defined cell cycle kinetics in different WT thymocyte subsets based on high-resolution *in vivo* cell cycle analysis and provided accurate information on the duration of individual cell cycle phases.

4.1.3 Models of altered T-cell development - population recovery via adaptive cell cycle regulation

We next utilized these aforementioned tools to better understand alterations in cell cycle regulation to maintain population homeostasis. We employed two representative mouse models with defects in the earliest thymocyte populations (DN1 and DN2) but an almost complete recovery of thymocyte numbers at later stages: We first analyzed CCR7/CCR9-deficient (DKO) mice which are characterized by a defect in thymus colonization, but show near normal DN3 cellularity (Krueger et al., 2010). Similarly, miR-17~92-deficient mice display a failure of prethymic IL-7 signaling but still exhibit a nearly physiological DN3 compartment (Regelin et al., 2015).

4.1.3.1 Thymic CCR7/9-deficiency results in shortening of S-phase duration of thymocytes to overcome developmental defects

In a first experiment, we performed steady-state cell cycle analyses of thymocytes of CCR7/9-deficient mice (Figure 18). We observed a decrease in the frequencies of quiescent cells in all thymocyte subsets in the absence of CCR7/9 (Figure 18a). The frequencies of cells in G1 phase (Figure 18b) were comparable to the WT thymocyte counterparts. Nevertheless, we found lower levels of cells in the G1 phase in the DN2 compartment of DKO mice consistent with elevated frequencies of S-phase cells in this subset (Figure 18c). In addition, we detected an increase in the frequencies of cells in S phase especially in the DN3a compartment, but also for pre- and post-selection DP thymocytes. We also observed differences in the frequencies of cells in the G2M phase but considering the low frequencies of G2M cells in WT thymocyte subsets (Figure 10), differences in this cell cycle phase in DKO mice were mostly negligible (Figure 18d).

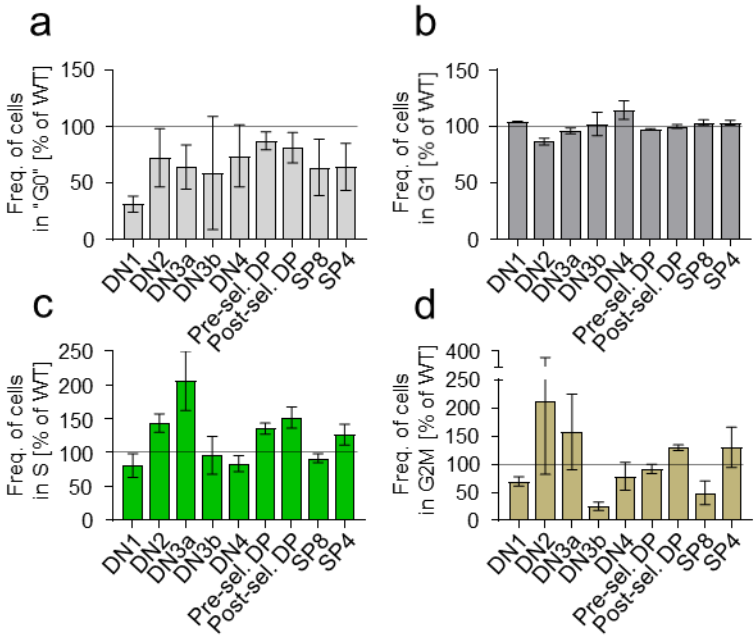

Figure 18: Steady-state cell cycle analyses of CCR7/9-deficient mice.
(a-d) Statistical analyses of cells among thymocyte subpopulations in (a) G0, (b) G1, (c) S and (d) G2M phase in CCR7/9-deficient (DKO) mice. Data is presented as % of WT, error bars indicate SE of ratios calculated as $SE\left(\frac{x}{y}\right) = \left(\frac{x}{y}\right)\sqrt{\left(\frac{SE(x)}{x}\right)^2 + \left(\frac{SE(y)}{y}\right)^2}$ with n = 3 mice for each genotype.

We further performed dual-pulse labeling in DKO mice to obtain more information about cell cycle kinetics of thymocytes in the absence of CCR7/9 (Figure 19). Consistent with our WT data (Figure 13), high proportions of DNA replicating cells were found in the DN2, DN3b and DN4 subsets, whereas frequencies among DN3a and pre-selection DP thymocytes as well as post-selection DP and SP cells were low. When we compared S-phase entry and exit of DKO DN3a cells with the WT counterparts, we found elevated levels of $BrdU^+$ (green) and EdU^+ (blue) cells in this subset. This was also true for DN3a cells that were in S phase during both pulses (EdU^+BrdU^+, orange). For DN2 cells from DKO mice, we observed no difference in rate of entry ($BrdU^+$, green), but higher rates of S-phase exit (EdU^+, blue). In the absence of CCR7/9, we also observed higher rates of S-phase exit (EdU^+, blue) for SP8 thymocytes in line with lower rates of S-phase entry and frequencies of cells in S phase during both pulses (EdU^+BrdU^+, orange). In general, we detected small differences in all thymocyte subsets which indicates changes in cell cycle lengths of thymocytes in DKO mice in comparison to WT thymocytes. Additionally, statistical analyses are shown in the appendix (Figure 51). Taken together, the bulk of compensatory cell cycle related events occurs at or immediately prior to the DN3a stage rather than the DN3b stage. Thus, compensation seems to occur in a slow cycling compartment.

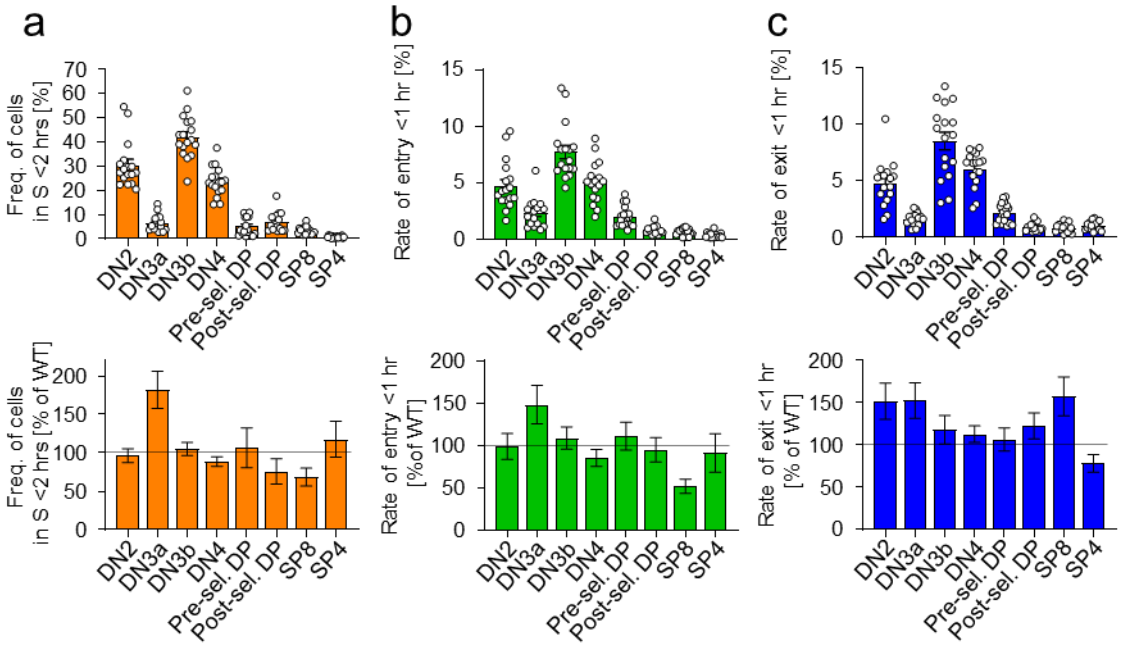

Figure 19: In-depth analysis reveals changes in S-phase distribution of CCR7/9-deficient (DKO) thymocyte subsets.
Flow cytometric analyses of *in vivo* dual pulse labeling of WT and DKO mice. Graphs show frequencies of (a) EdU⁺BrdU⁺ cells (orange), (b) BrdU⁺ cells (green) and (c) EdU⁺ cells (green) of murine DKO thymocyte subpopulations, n = 17-19 mice of two independent experiments. Additionally, data is presented as % of WT (bottom row), error bars indicate SE of ratios calculated as

$$SE\left(\frac{x}{y}\right) = \left(\frac{x}{y}\right)\sqrt{\left(\frac{SE(x)}{x}\right)^2 + \left(\frac{SE(y)}{y}\right)^2}$$

, with n = 7-20 mice for WT and n = 17-19 mice for DKO.

To further characterize cell cycle dynamics in the absence of CCR7/9, we quantified G1- and S-phase re-entry of different EdU⁺ thymocyte subsets in comparison to their WT counterparts (Figure 20). For DN2 DKO thymocytes, we detected a faster re-start in S phase after 6 hrs pointing towards a shortened length of the G1 phase. Interestingly, for EdU⁺ DKO DN3a thymocytes we found no significant differences in S-phase or G1-phase re-entry, whereas differences for DN3b DKO thymocytes were more pronounced. CCR7/9-deficient DN3b thymocytes showed a faster S-phase re-entry which is in line with a steeper decline in G1-phase re-entry over time and points towards a shortened duration of the cell cycle.

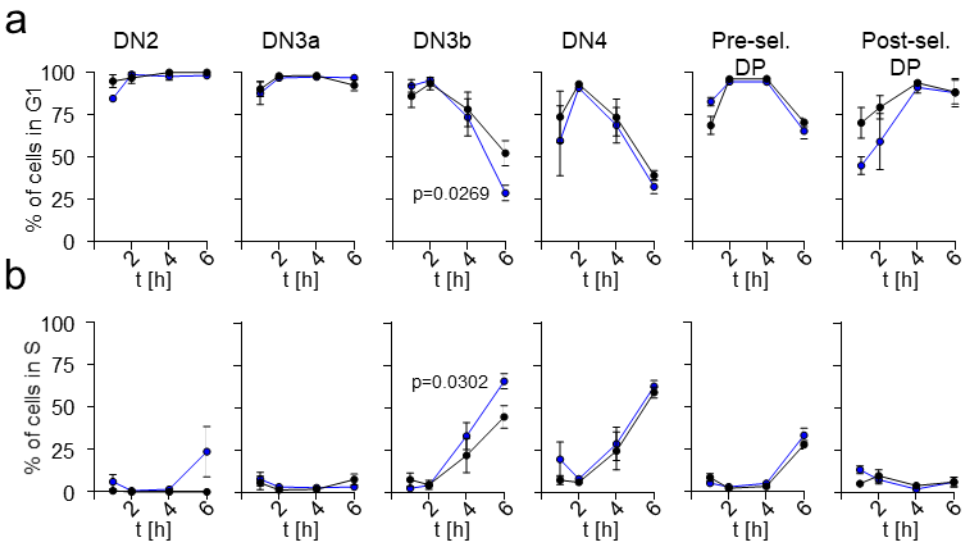

Figure 20: CCR7/9-deficient (DKO) DN3b thymocytes show faster cell cycle dynamics than WT counterparts.
Quantification of (a) G1- and (b) S-phase re-entry of EdU⁺ WT (black dots) and DKO (blue dots) thymocyte subpopulations over time, n = 3-5 mice for each point in time and each genotype (except for DKO DN2 thymocytes G1-phase re-entry, 1 h time point, n = 1 mouse), data from two independent experiments. Analysis of significance between WT and DKO was performed using unpaired t-test for the 6 hrs time point.

We then repeated linear regression analysis of DNA content towards 4N of BrdU⁺ thymocytes of DKO mice and detected shorter duration of the S phase for all DN subsets in a range of 0.73 to 1.16 hrs (Figure 21).

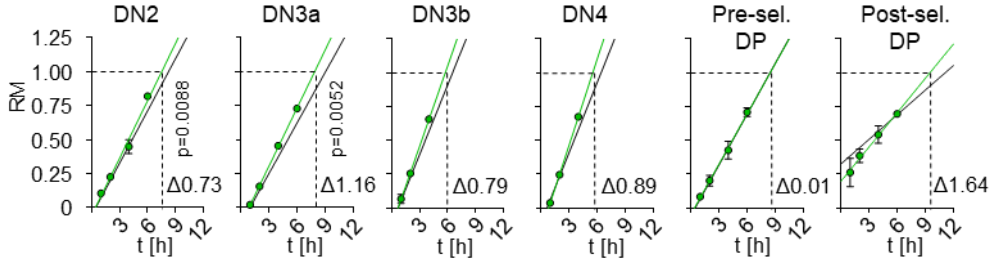

Figure 21: Shortening of S-phase duration in all thymocyte subsets in DKO mice.
Statistical analysis of DKO thymocyte subpopulations to assess S-phase duration based on RM values of BrdU⁺ cells (early S phase) over time (green dots). Green lines represent linear regression of DKO thymocyte analyses and black lines show linear regression of WT thymocytes as determined and shown in Figure 16. Numbers adjacent to linear regression show S-phase time in hours calculated based on the linear regression, n = 3-5 mice for each point in time, data from two independent experiments. Analysis of significance between WT and DKO was performed using an unpaired t-test for the latest time point.

In order to unravel potential alterations in G1-phase length, we performed linear regression analysis as described before for EdU⁺ thymocytes derived from WT and DKO mice and estimated the G1-phase duration for DN3a, DN3b, DN4 and pre-selection DP (Figure 22). Due to the low cell numbers within the EdU⁺ subsets,

analyses were restricted to the aforementioned populations. However, we observed similar lengths for the G1 phase.

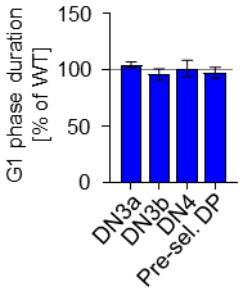

Figure 22: G1-phase duration is unaltered in the absence of thymic CCR7/9.
G1-phase duration of DKO thymocyte subpopulations presented as % of WT based on EdU⁺ cell population, error bars indicate SE of ratios calculated as $SE\left(\frac{x}{y}\right) = \left(\frac{x}{y}\right)\sqrt{\left(\frac{SE(x)}{x}\right)^2 + \left(\frac{SE(y)}{y}\right)^2}$ with n = 2-5 mice for WT and n = 2-4 mice for DKO.

In conclusion, we observed subtle alterations in cell cycle phase contribution most prominently for DN3a thymocytes of DKO mice consistent with earlier studies (Krueger et al., 2010). Additionally, we detected a moderate acceleration in S phase of various thymocyte subsets in the absence of CCR7/9.

In addition to quantitative analyses of the duration of individual cell cycle phases in the absence of CCR7/9, we also performed scRNA-sequencing to reveal differences in cell cycle regulation. For this purpose, we FACS-sorted c-kit positive (DN1/DN2) or c-kit negative DN thymocytes (DN3/DN4) of WT and DKO mice in order to enrich for c-kit positive subsets, which in normal thymus and even more in DKO thymus are underrepresented when compared to more mature DN3 and DN4 cells. ScRNA-sequencing was then performed in the laboratory of Dr. Mir-Farzin Mashreghi (Therapeutic Gene Regulation) at the Deutsches Rheuma-Forschungszentrum (DRFZ) (Figure 23a).
Based on the expression profiles of subset-specific marker genes (Figure 52, appendix) we manually curate data sets to separate seven well-defined thymocyte populations corresponding to ETP, ETP2, DN2a, DN2b, DN3a, DN3b and DN4 thymocytes (Figure 23).

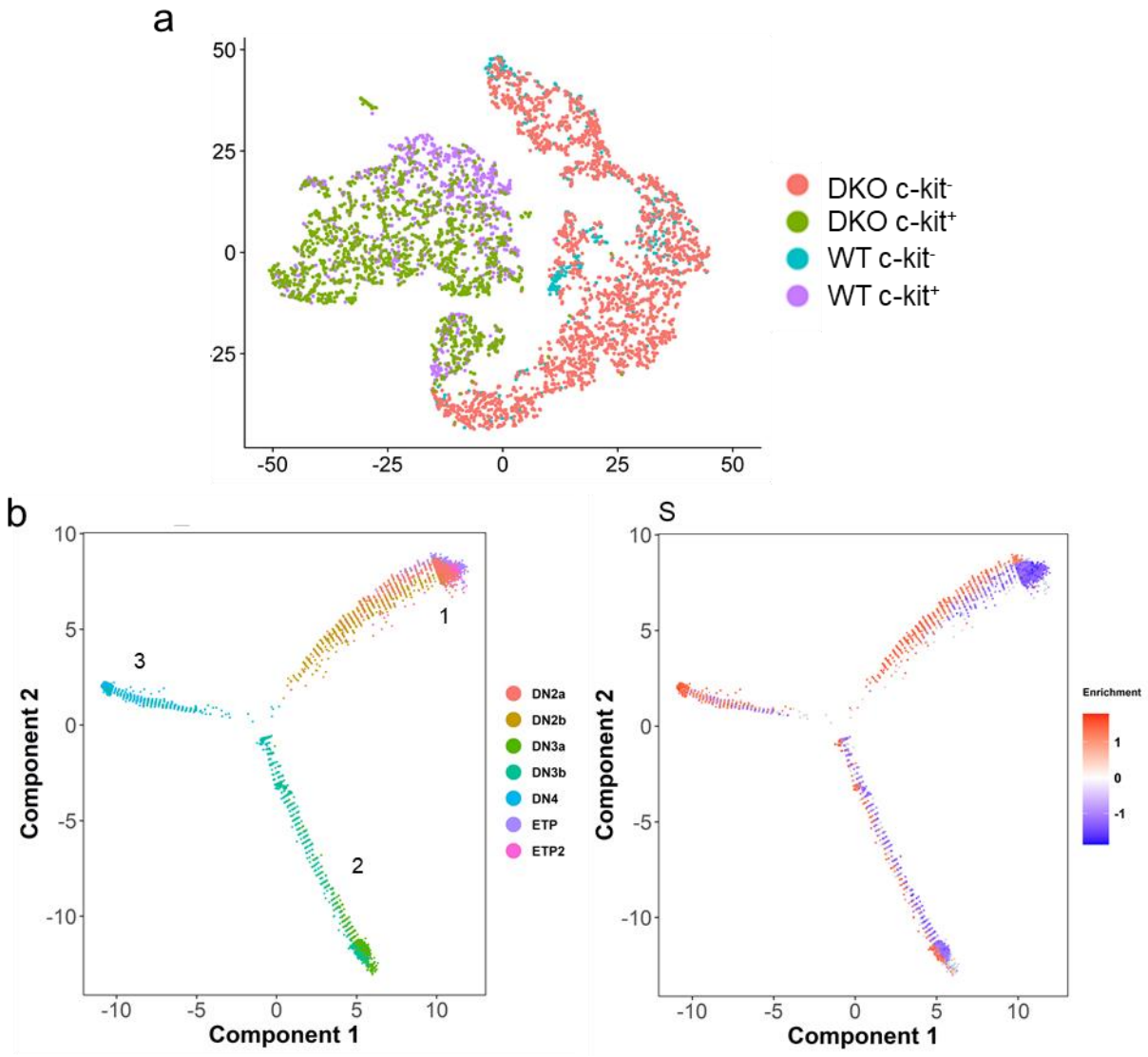

Figure 23: scRNA-seq of WT and CCR7/9 DKO thymocytes.
(a) Clustering of sorted c-kit positive (DN1/DN2) or c-kit negative DN thymocytes (DN3/DN4) of WT and DKO mice visualized by t-distributed stochastic neighbor-embedding (t-SNE) map. Black circle indicates absence of cells. (b) Pseudotime trajectories of the individual clusters (for definition of cluster see: Figure 52) (left) and S phase transcriptomes (right).

To investigate whether the absence of CCR7/9 introduces changes in the dynamics of T-cell differentiation, we used monocle pseudotime trajectory analysis (Qiu et al., 2017), which connects related clusters to construct differentiation trajectories (Figure 23b). We validated ETP cells as the root of the progression trajectory (Figure 23b, left panel, upper right). Consistent with the well-defined developmental progression of thymocyte populations, the pseudotime trajectory proceeded linearly towards the DN3a stage with a certain contribution of DN3b cells (Figure 23b, left panel, lower right). Surprisingly, some DN3b cells and DN4 thymocytes were assigned a distinct trajectory (Figure 23b, left panel, left), which may be due to a certain heterogeneity of this subset and/or a major contribution of cell-cycle associated genes, masking

developmental trajectories. An overlay of expression of S-phase related gene sets revealed that DN2b, in contrast to DN2a, go through a proliferative state, which becomes apparent in close proximity to the DN3a subset in pseudotime analysis (comparison with S-phase trajectory, Figure 23b, right panel). Thus, our data indicate that developmental trajectories as predicted in the pseudotime model are tightly associated with alterations in cell-cycle state.

To investigate this association further, we applied cell cycle scoring based on gene sets previously selected to separate cell cycle stages in transcriptomics data (Fischer et al., 2019) and detected a similar distribution of the clusters (Figure 24). This gene set based model essentially reflects steady-state cell cycle distributions as detectable by single nucleoside-analog labeling. However, the selection of gene sets provides limitations for comparisons across methods. Furthermore, this analysis does not reflect cell-cycle dynamics. We conclude that more refined analyses based on a combination of cell-cycle and pseudotime approaches are likely to provide information on cell cycle pseudodynamics, as has been recently demonstrated using RNA velocity as additional parameter (Rappez et al., 2020).

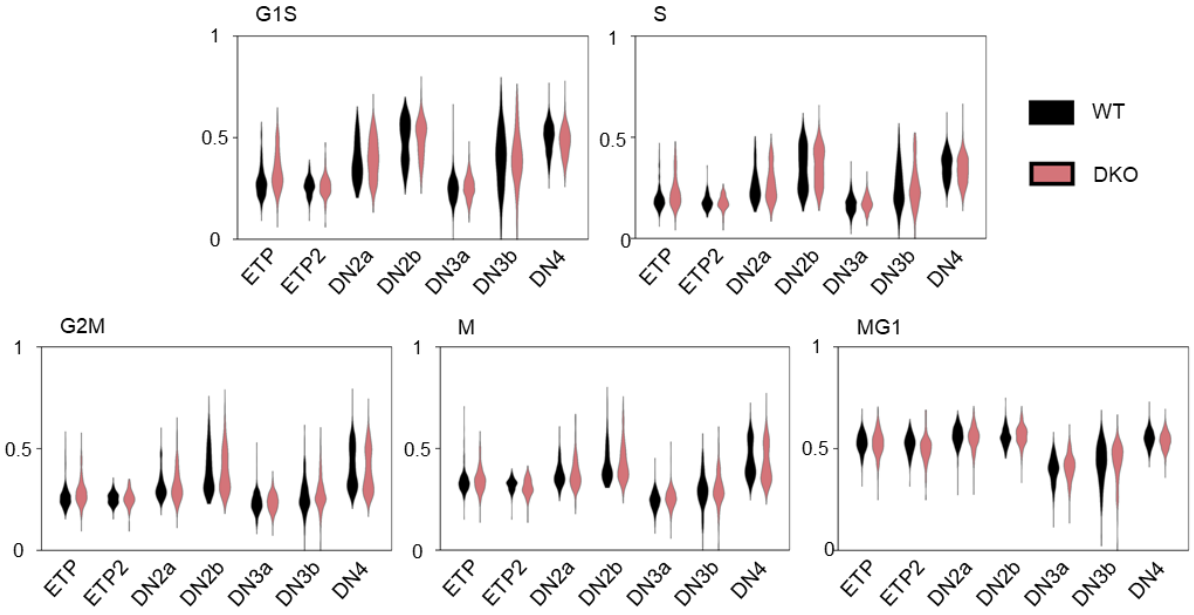

Figure 24: Cell cycle scoring.
Transcriptome-based cell cycle scores of defined clusters of WT (black) and CCR7/9-deficient thymocytes (pink) among different cell cycle phases as described in (Fischer et al., 2019).

In a last step, we analyzed transcript levels of *Mki67* (cycling), *Ccne2* (S phase) and *Ccnb2* (M phase) (Figure 25). Overall, expression levels were considered low. Nevertheless, distinct clusters of cycling cells were identified. Consistent with our

previous conclusions on population heterogeneity in cell cycle dynamics, it will be of interest to further concentrate in-depth dynamic analysis on these subsets. Moreover, we did not detect any differences between c-kit positive (DN1/DN2) or c-kit negative DN thymocytes (DN3/DN4) of WT and DKO mice.

In summary, our data unraveled altered cell cycle dynamics in thymi of CCR7/9 deficient mice that were mostly attributed to accelerations in cell cycle speed. ScRNA sequencing analysis essentially recapitulated differences in cell cycle state between thymocyte subsets. Currently existing analysis tools are of insufficient resolution to validate previously established differences in cell cycle regulation in the absence of CCR7/9. Our data sets provide an excellent basis for the development of novel pseudotime based analysis approaches.

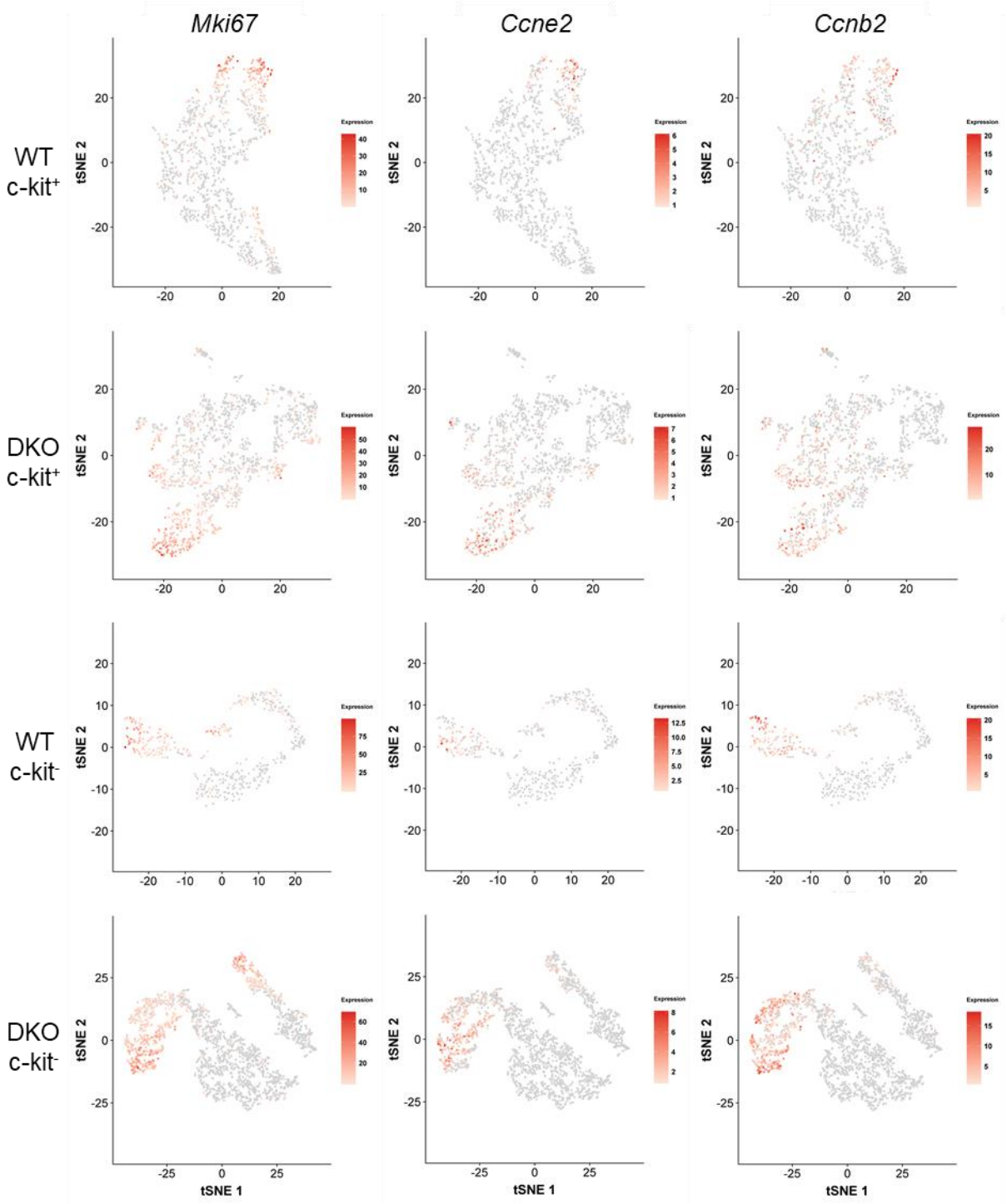

Figure 25: Similar transcript levels for *Mki67*, *Ccne2* and *Ccnb2* of WT and CCR7/9-deficient thymocytes.
Distribution of transcription levels for representative genes visualized by t-distributed stochastic neighbor-embedding (t-SNE) among c-kit positive (DN1/DN2) or c-kit negative DN thymocytes (DN3/DN4) of WT and DKO thymi.

4.1.3.2 Compensatory mechanisms to overcome developmental defects in the absence of miR-17~92

Mice deficient of miR-17~92 have a profound defect at the earliest stages of T-cell development, but nevertheless show a near normal DN3 compartment (Regelin et al., 2015). Data from the following experiments are preliminary and provide restricted information about the underlying mechanism of population recovery in the absence of miR-17~92. However, we were able to draw first conclusions from our experiments encouraging the inclusion of the data in this part of the thesis.

In a first experiment, we performed dual-pulse labeling of miR-17~92-sufficient (fl/fl) and -deficient mice (Δ/Δ) (Figure 26) and detected elevated frequencies of EdU^+BrdU^+ cells (Figure 26a, orange), prominently in DN3b and DN4 thymocytes in Δ/Δ mice. In addition, we observed alterations in the ability of S-phase entry (Figure 26b, green) and -exit (Figure 26c, blue) of thymocytes in the absence of miR-17~92. Indeed, DN4 thymocytes of miR-17~92-deficient mice exhibited increased rates of S-phase entry and exit. Enhanced S-phase exit was also pronounced for DN3b thymocytes of Δ/Δ mice. These findings are in contrast to the observed cell cycle kinetics in the absence of CCR7/9 which mainly affected the DN3a compartment (Figure 18 and Figure 19). Here, the lack of miR-17~92 leads to S-phase alterations rather on the level of DN3b and DN4 thymocytes than DN3a cells.

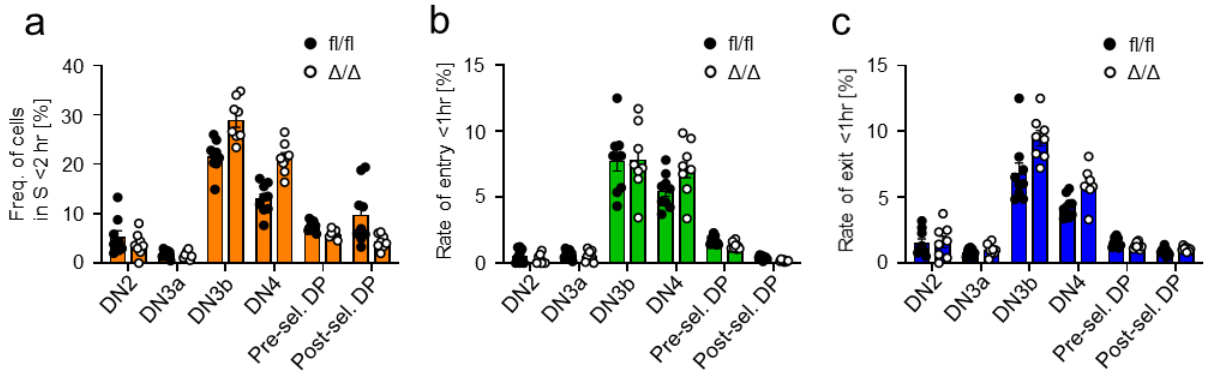

Figure 26: Influence of thymic miR-17~92 on S-phase kinetics.
Flow cytometric analyses of *in vivo* dual pulse labeling of miR-17~92$^{fl/fl}$ (black dots) or miR-17~92$^{Δ/Δ}$ mice (white dots). Graphs show frequencies of (a) EdU^+BrdU^+ cells (orange), (b) $BrdU^+$ cells (green) and (c) EdU^+ cells (blue) among thymocyte subsets of miR-17~92$^{fl/fl}$ (black dots) or miR-17~92$^{Δ/Δ}$ mice (white dots), with n = 9 miR-17~92$^{fl/fl}$ and n = 8 miR-17~92$^{Δ/Δ}$ mice.

In addition, we quantified G1-phase re-entry based on DNA content analyses of EdU^+BrdU^+ DN3a, DN3b and DN4 thymocytes (Figure 27a and b) at two different time points and detected a trend towards a faster progression back into G1 phase of DN3a

and DN3b thymocytes in Δ/Δ mice. However, when we determined S-phase length in those populations, we could not detect any differences (Figure 27c) except for DN3a thymocytes of miR-17~92-deficient mice which exhibited a prolonged S-phase duration. Given the low frequencies of this population in general and even lower cell numbers within the EdU$^+$BrdU$^+$ subset, definitive conclusions need further investigation. From these preliminary results, we speculate that in the absence of miR-17~92 population recovery is not exclusively regulated on the level of S-phase cell cycle length as observed for CCR7/9-deficient mice (Figure 21). We rather assume differences on the level of G1-phase duration in conjunction with altered S-phase kinetics.

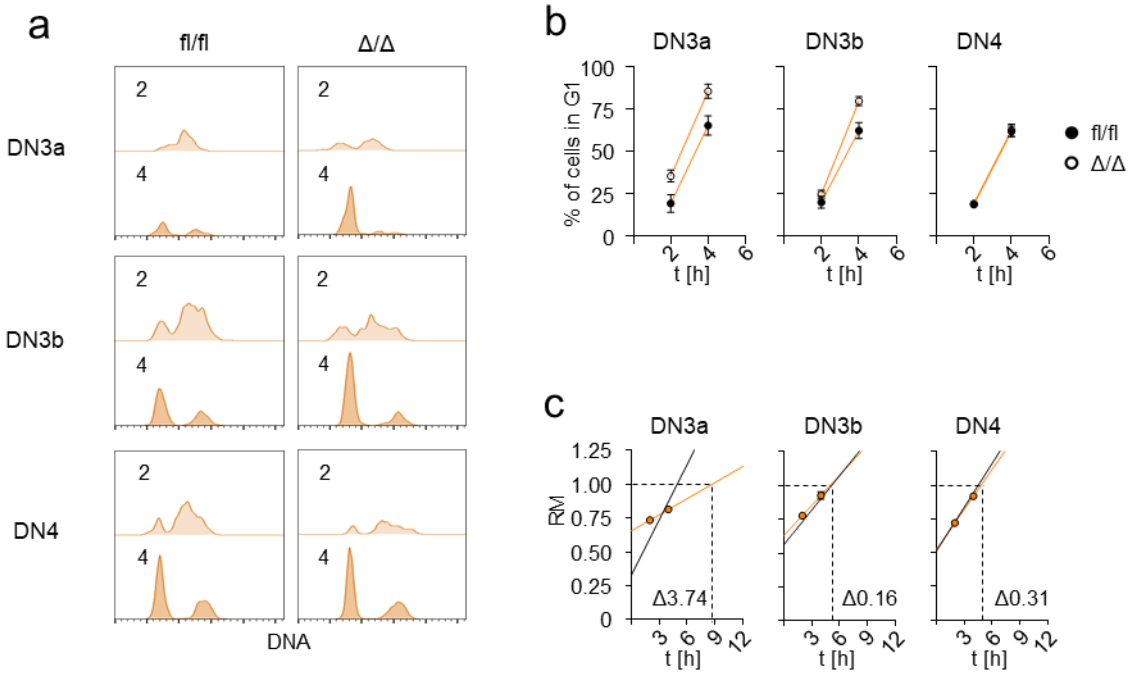

Figure 27: miR-17~92 affects cell cycle speed of DN3a thymocytes.
(a) Representative flow cytometric histograms visualizing the DNA content of DN3a, DN3b and DN4 thymocytes of miR-17~92$^{fl/fl}$ (left) or miR-17~92$^{\Delta/\Delta}$ mice (right) at 2 and 4 hrs. Each plot depicts an overlay of the DNA content of EdU$^+$BrdU$^+$ cells at 2 (light orange) and 4 hrs (dark orange). (b) Quantification of G1-phase re-entry of EdU$^+$BrdU$^+$ thymocyte subpopulations of miR-17~92$^{fl/fl}$ (black dots) or miR-17~92$^{\Delta/\Delta}$ (white dots) mice over time. (c) Statistical analysis of miR-17~92$^{fl/fl}$ (black line) or miR-17~92$^{\Delta/\Delta}$ (orange dots) thymocyte subpopulations to assess S-phase time duration based on RM values of EdU$^+$BrdU$^+$ cells over time. The orange line represents the resulting linear regression. The black line shows the linear regression of analyses of thymocytes derived from miR-17~92$^{fl/fl}$ mice. Numbers adjacent to linear regression show resulting S-phase time in hours. (b, c) n = 3-5 mice for each point in time and genotype.

4.1.4 Cell cycle adaptation upon endogenous thymic regeneration

We further investigated the role of cell cycle regulation in a model of endogenous thymic repair upon sublethal total body irradiation (Kadish and Basch, 1975; Huiskamp and van Ewijk, 1985; Tomooka et al., 1987; Penit and Ezine, 1989; Dudakov et al., 2012). We performed dual-pulse labeling experiments of irradiated WT (5.5 Gy) and control mice six days after irradiation. As shown in Figure 28, frequencies of thymocyte subsets were significantly altered upon irradiation. We found decreased levels of DN2, DN4 and post-selection DP cells, whereas DN3a frequencies were elevated. In addition, for DN3b thymocytes we detected a tendency towards increased cell frequencies six days after irradiation, whereas frequencies of pre-selection DP thymocytes were mostly recovered.

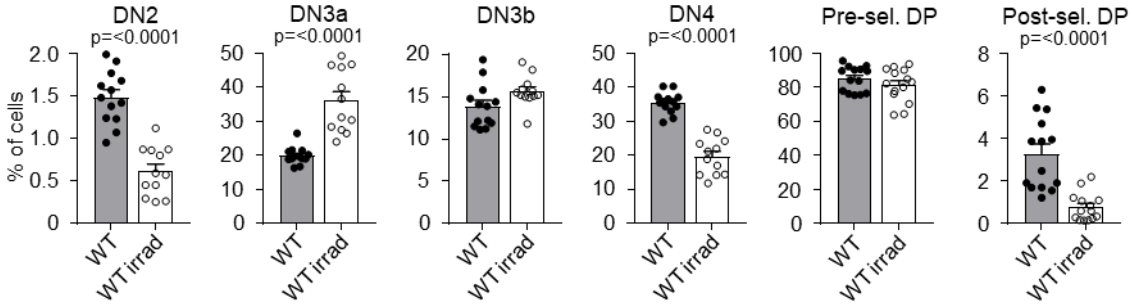

Figure 28: Population size is altered upon irradiation.
Statistical analyses of flow cytometric results of different thymocyte subsets from WT (grey, black dots) and irradiated WT (white, white dots) mice indicated as frequencies with n = 13-14 WT mice and n = 12-14 irradiated WT mice.

Next, we analyzed cell cycle kinetics of WT and irradiated WT mice (Figure 29). Due to low frequencies of $BrdU^+$ and EdU^+ post-selection DP thymocytes upon irradiation, we omitted these populations from our analyses (Figure 29). Representative flow cytometric analyses of dual-pulse labeling of WT and irradiated WT mice are shown in the appendix (Figure 53). Upon irradiation, we detected more DN2 cells in S phase during both pulses (orange) and decreased S-phase exit (blue) pointing towards a prolonged S-phase duration. On the other hand, we found more DN3a cells that had recently entered S phase (green) in irradiated mice suggesting the presence of compensatory mechanisms for cell cycle regulation. Consistent with unaltered frequencies of DN3b thymocytes upon irradiation (Figure 28), S-phase kinetics of this subset were also mostly unaffected. In addition, we found enhanced S-phase entry (green) for DN4 thymocytes in irradiated mice. Most strikingly, although frequencies of pre-selection DP thymocytes were constant, S-phase kinetics were strongly affected.

In light of this, we found more cells in S phase during both pulses (orange) as well as more cells that had entered or left S phase (green, blue). Additionally, statistical analyses are shown in the appendix (Figure 54).

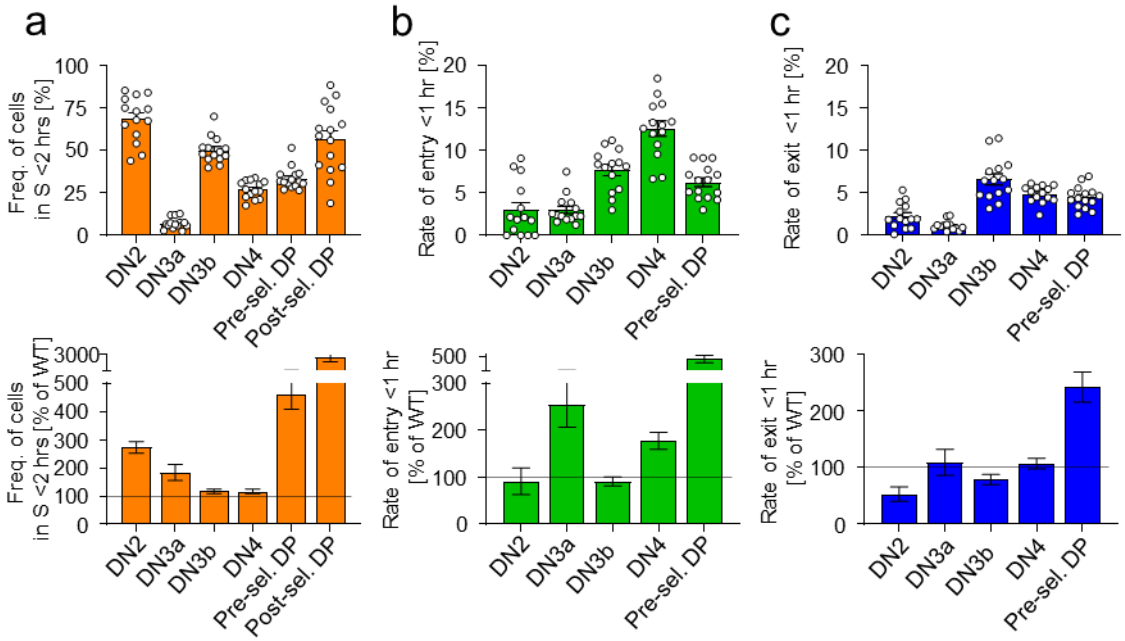

Figure 29: Endogenous thymic repair influences S-phase kinetics of WT thymocyte subsets. Flow cytometric analyses of *in vivo* dual pulse labeling of WT and irradiated WT mice. Graphs show frequencies of (a) EdU⁺BrdU⁺ cells (orange), (b) BrdU⁺ cells (green) and (c) EdU⁺ cells (blue) of thymocyte subpopulations of irradiated WT mice, n = 14-15. Additionally, data is presented as % of WT (bottom row), error bars indicate SE of ratios calculated as $SE\left(\frac{x}{y}\right) = \left(\frac{x}{y}\right)\sqrt{\left(\frac{SE(x)}{x}\right)^2 + \left(\frac{SE(y)}{y}\right)^2}$, with n = 16 mice for WT and n = 14-15 mice for irradiated WT mice.

To address whether S-phase duration of thymocyte subsets per se was affected upon irradiation, we performed DNA content analyses of EdU⁺BrdU⁺ cells at different time points (Figure 30). In addition, we quantified G1-phase re-entry of EdU⁺BrdU⁺ thymocytes (Figure 30b) and observed less re-entry for all thymocyte subsets upon irradiation pointing towards prolonged S-phase lengths. Indeed, our linear regression analyses verified this assumption. We revealed consistently longer S-phase duration for all subsets from irradiated WT thymi in a range of 0.06 to 1.20 hrs (Figure 30c).

To sum this up, this model of endogenous thymic repair provided insight into intrathymic cell cycle regulation as an adjustable system to re-establish normal thymus cellularity.

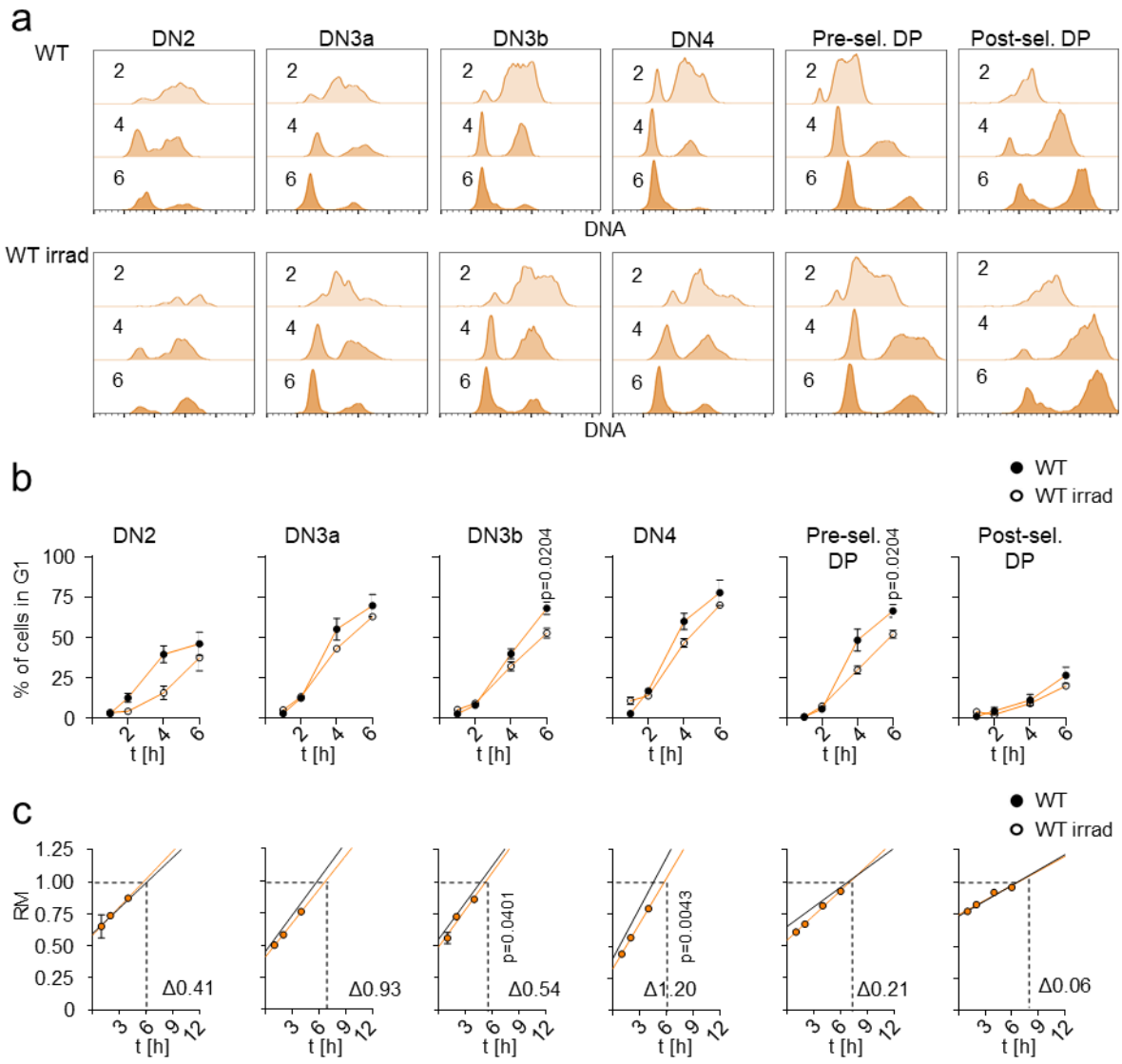

Figure 30: Cell cycle dynamics during regeneration.
Flow cytometric analyses of *in vivo* dual pulse labeling of WT and irradiated WT mice. (a) Representative flow cytometric histograms visualize the DNA content of different thymocyte subsets of WT and irradiated WT mice over time of EdU$^+$BrdU$^+$ (orange) cells. Each individual plot represents an overlay of the DNA content at 2, 4 and 6 hrs. (b) Quantification of G1-phase re-entry of EdU$^+$BrdU$^+$ WT (black dots) and irradiated WT (white dots) thymocyte subpopulations over time, n = 3-4 WT mice and n = 2-4 irradiated WT mice for each time point. Analysis of significance between WT and irradiated WT mice was performed using unpaired t-test for the 6 hrs time point. (c) Statistical analysis of irradiated WT thymocyte subpopulations to assess S-phase time duration based on RM values of EdU$^+$BrdU$^+$ cells over time (orange dots). The orange line represents the resulting linear regression. The black line displays the corresponding linear regression of analyses in control WT mice. Numbers adjacent to linear regression show difference in S-phase time in hours between WT and irradiated WT mice, with n = 2-4 WT mice and n = 2-4 irradiated WT mice for each point in time. Analysis of significance between WT and irradiated WT mice was performed using unpaired t-test for the latest time point.

4.2 miRNA-21: Dynamic expression, but enigmatic function

4.2.1 Expression pattern of miR-21 during T-cell development

Expression levels of miR-21 are highly dynamic in certain T-cell subsets (Figure 6). In order to validate and further extend this current view, we sorted different thymocyte subsets of wildtype (WT) mice and determined relative expression of miR-21 (Figure 31). We started our analysis within the most immature detectable thymocyte population (ETPs, $CD117^{hi}CD25^{-}CD44^{+}$) and found high miR-21 expression at this particular stage. Interestingly, at the DN2a ($CD25^{+}CD44^{+}CD117^{hi}$) stage, we detected a decrease as compared to the ETP level, whereas the highest levels of miR-21 were found at the following DN2b ($CD25^{+}CD44^{+}CD117^{lo}$) stage. As stated in the introduction, the DN2a and the DN2b stages differ in their expression of CD117. In addition, DN2a thymocytes still have alternative lineage fate options such as the ability to enter the B- or NK-cell lineage, whereas thymocytes at the DN2b stage have fully undergone T-lineage fate determination. Consistent with the previous data from (Kirigin et al., 2012), we showed that highest levels of miR-21 can be detected in DN thymocytes and lowest levels were observed in pre- and post-selection DP thymocytes. Furthermore, we demonstrated that miR-21 is again slightly upregulated in SP8 T cells.

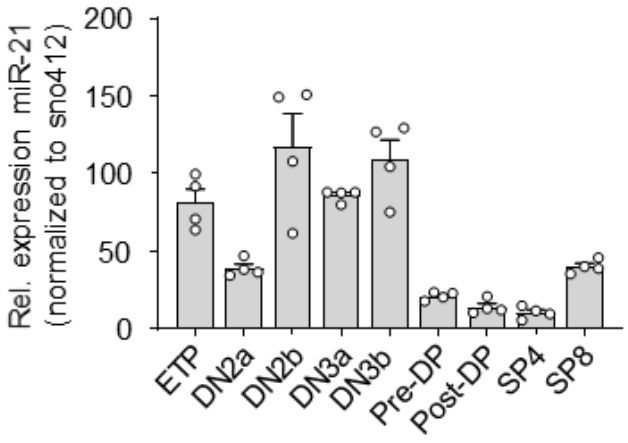

Figure 31: Dynamic expression of miR-21 during T-cell development.
miR-21 expression determined via quantitative RT-PCR in different sorted thymic subsets from WT mice. Relative expression levels were normalized to snoRNA412. Each dot represents one mouse, n = 4 mice.

In summary, we validated previously published data and provided a more detailed analysis of miR-21 expression at key stages of T-cell development in the thymus.

The dynamic expression pattern of miR-21 in thymocyte subsets prompted us to hypothesize that this miRNA has a fundamental role in the thymus.

4.2.2 Characterization of T-lineage progenitors in BM of miR-21-deficient mice

To understand the role of miR-21 in the thymus, we adopted a commercially available miR-21 knockout mouse model (Jackson, B6;129S6-Mir21a^{tm1Yoli}/J). This mouse strain was generated by Yong Li (University of Louisville) using a targeting vector replacing the 93 bp precursor sequence (pre-miR-21) with a neomycin resistance cassette via homologous recombination. These miR-21 knockout mice are viable, fertile and no immune defects were observed as long as the mice were not fed a high-fat diet (Ma et al., 2011). Interestingly, an increase in apoptotic cells among keratinocytes, elevated expression of target proteins (including Spry1, Pten, and Pdcd4) as well as dampened Ras signaling of Ras effector pathways were observed. We validated the absence of miR-21 expression in total thymocytes of miR-21 knockout mice via quantitative RT-PCR.

With regard to the high expression levels of miR-21 in hematopoietic progenitors (Kirigin et al., 2012), we first investigated whether the frequencies of pre-thymic progenitors in the BM were influenced by the absence of miR-21. We observed similar frequencies of hematopoietic stem cells (HSCs, lin$^-$Sca-1$^+$CD117^{hi}CD135$^-$), multipotent progenitors (MPPs, lin$^-$Sca-1$^+$CD117^{hi}CD135$^+$), and common lymphoid progenitors (CLPs, lin$^-$Sca-1$^-$CD135$^+$CD127^{int}) in miR-21$^{-/-}$ mice as compared to WT mice (Figure 32).

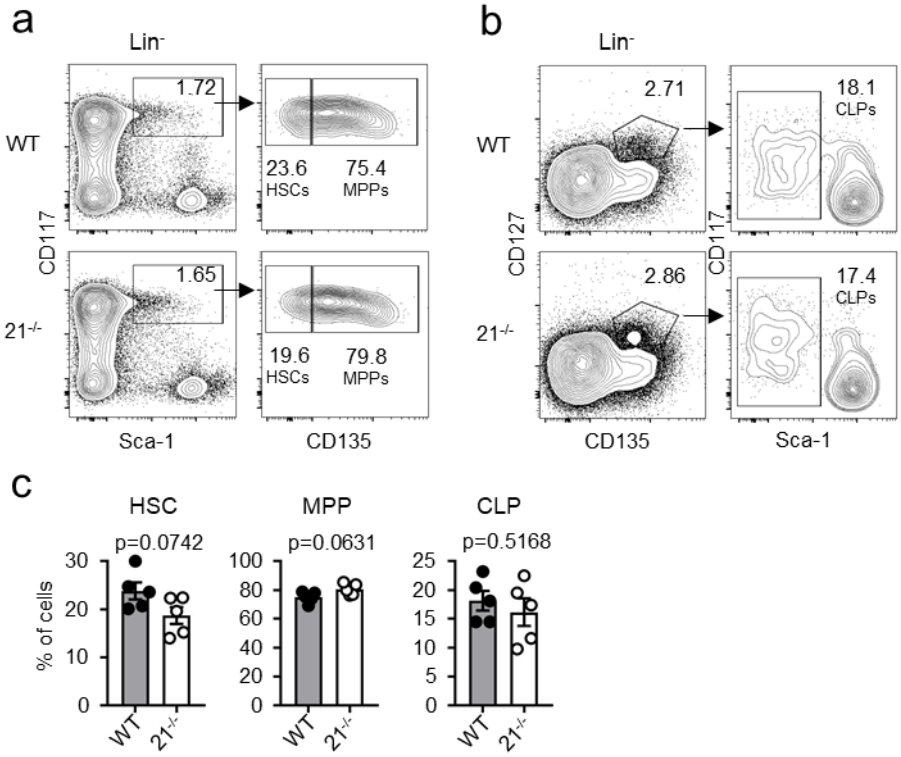

Figure 32: Development of BM-derived T-lineage progenitors is not affected by loss of miR-21. (a) Representative flow cytometric analysis of lineage-depleted BM from WT and miR-21$^{-/-}$ mice stained with antibodies against Sca-1, CD117 and CD135 to identify HSCs (lin^{-}Sca-1^{+}CD117^{hi}CD135^{-}) and MPPs (lin^{-}Sca-1^{+}CD117^{hi}CD135^{+}). (b) Representative flow cytometric analysis of lineage-depleted BM from WT and miR-21$^{-/-}$ mice stained with antibodies against CD135, CD127, Sca-1 and CD117 to identify CLPs (lin^{-}Sca-1^{-}CD135^{+}CD127^{int}). (a) and (b) Numbers adjacent to gates represent frequencies relative to parent gate. (c) Statistical analysis of flow cytometric results shown in (a) and (b). Each dot represents one mouse, n = 5 mice for each genotype. Data is represented as mean ± SEM. Statistical analyses were performed using unpaired t-test.

In summary, despite its high expression in hematopoietic progenitors, miR-21 does not contribute to the generation of pre-thymic progenitors that will ultimately colonize the thymus.

4.2.3 Early T-cell development is largely unaffected by loss of miR-21

To understand the role of miR-21 in the thymus, we characterized miR-21-deficient mice phenotypically to assess the role of miR-21 in T-cell development at steady-state as a starting point. We found absolute total thymocyte numbers to be unaltered in the absence of miR-21 (Figure 33a). Given the high expression levels of miR-21 detected at the earliest stages of T-cell development, we subsequently focused on analyzing different DN subsets in thymi of miR-21$^{-/-}$ mice (Figure 33b and c).

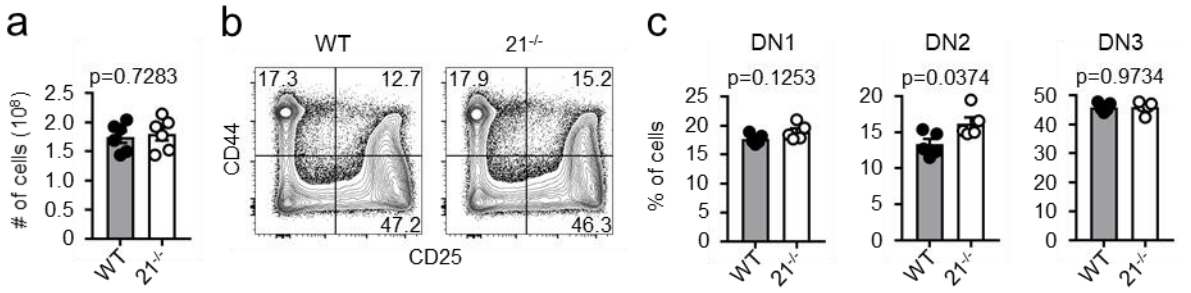

Figure 33: Thymus cellularity and early thymocyte subsets are largely unchanged in miR-21$^{-/-}$ mice.
(a) Total cellularity of thymi from WT and miR-21$^{-/-}$ mice, n = 6 mice for each genotype. (b) Representative flow cytometric analyses of thymocytes (lineage-depleted) from WT and miR-21$^{-/-}$ mice stained with antibodies against CD25 and CD44 to identify DN1 (CD25^{-}CD44^{+}), DN2 (CD25^{+}CD44^{+}) and DN3 (CD25^{+}CD44^{-}) thymocyte subsets. Numbers in quadrants represent frequencies. (c) Statistical analyses of flow cytometric results shown in (b), n = 5 mice for each genotype. Data is represented as mean ± SEM. Statistical analyses were performed using unpaired t-test.

While frequencies of DN1 (CD25^{-}CD44^{+}) and DN3 (CD25^{+}CD44^{-}) thymocytes were unaffected by loss of miR-21, we observed a significant increase in the frequency of DN2 (CD25^{+}CD44^{+}) thymocytes in miR-21$^{-/-}$ mice (Figure 33c). However, the observed difference between miR-21$^{-/-}$ and WT was very slight and thus does not suggest an essential function of miR-21 for the earliest stages of T-cell development.

4.2.4 miR-21 is redundant for late T-cell development

Regarding the steep decline of miR-21 expression at the transition from DN3 cells to pre-selected DP cells and the modest re-expression in SP thymocytes (Figure 31), we next investigated whether miR-21 is critical for selection processes or the generation of mature SP cells. For this reason, we analyzed the frequencies of DP, SP4 and SP8 (Figure 34) in miR-21-sufficient and -deficient mice.

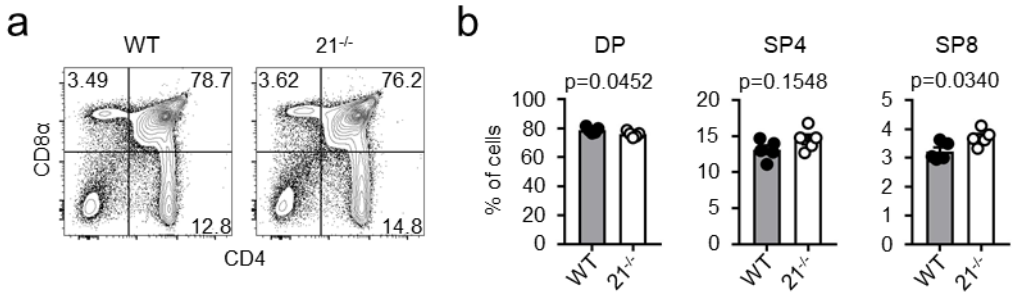

Figure 34: Minor alterations in late thymocyte subsets upon loss of miR-21.
(a) Representative flow cytometric analysis of thymocytes from WT and miR-21$^{-/-}$ mice stained with antibodies against CD4 and CD8α. Numbers in quadrants represent frequencies. (b) Statistical analysis of flow cytometric results shown in (a), n = 5 mice for each genotype. Data is represented as mean ± SEM. Statistical analyses were performed using unpaired t-test.

In the absence of miR-21 we detected a small, but significant decrease in the frequency of DP thymocytes accompanied by increased frequencies of SP T cells. In case of SP8 T cells, these differences were again significant, but small. Thus, our data suggest that miR-21 might be critical for selection steps in the thymus.

4.2.5 Absence of miR-21 does not affect negative selection

To validate a potential role of miR-21 in the control of selection processes (Figure 34), we characterized this key stage in T-cell development more precisely. For this, we first analyzed the frequencies of pre- and post-selected DP thymocytes based on the expression of CD69 and CD62L and found those to be unaffected by the absence of miR-21 (Figure 35a and b). To identify a potential involvement of miR-21 during selection steps, we first made use of surface expression of CD5 as a surrogate marker of TCR signal strength in DP, SP4 and SP8 thymocytes (Figure 35c). In this light, T cells are marked by high levels of CD5 surface expression when they have received strong TCR signals (Azzam et al., 1998).

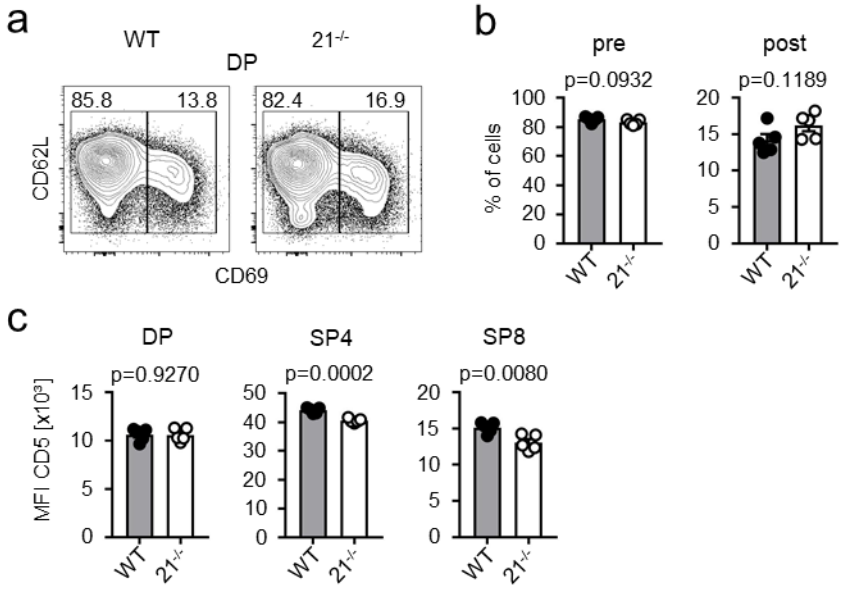

Figure 35: miR-21 is mainly dispensable for T-cell selection processes.
(a) Representative flow cytometric analyses of thymocytes from WT and miR-21$^{-/-}$ mice stained with antibodies against CD4, CD8α, CD62L and CD69. Numbers in left and right corners represent frequencies of pre- and post-selection DP thymocytes, respectively. (b) Statistical analysis of flow cytometric results shown in (a), n = 5 mice for each genotype. (c) Statistical analysis of mean fluorescence intensity of CD5 on DP, SP4 and SP8, n = 5 mice for each genotype. Data is represented as mean ± SEM. Statistical analyses were performed using unpaired t-test.

Upon loss of miR-21, we found similar levels of CD5 on all DP thymocytes, whereas for both, SP4 and SP8 T cells we detected significantly reduced levels indicative of an altered TCR signaling process in miR-21$^{-/-}$ mice. To delve further into these analyses, we next performed Ca^{2+}-flux experiments. For this, we stimulated thymocytes with anti-CD3 antibodies and measured the resulting calcium-response over time (Figure 36). To circumvent a potential misinterpretation of the data resulting from slight differences in handling or staining of the cells, we mixed equal amounts of WT (CD45.1) and miR-21$^{-/-}$ (CD45.2) thymocytes in the same tube. Due to their different congenic backgrounds, samples were distinguishable in the subsequent flow cytometric analyses.

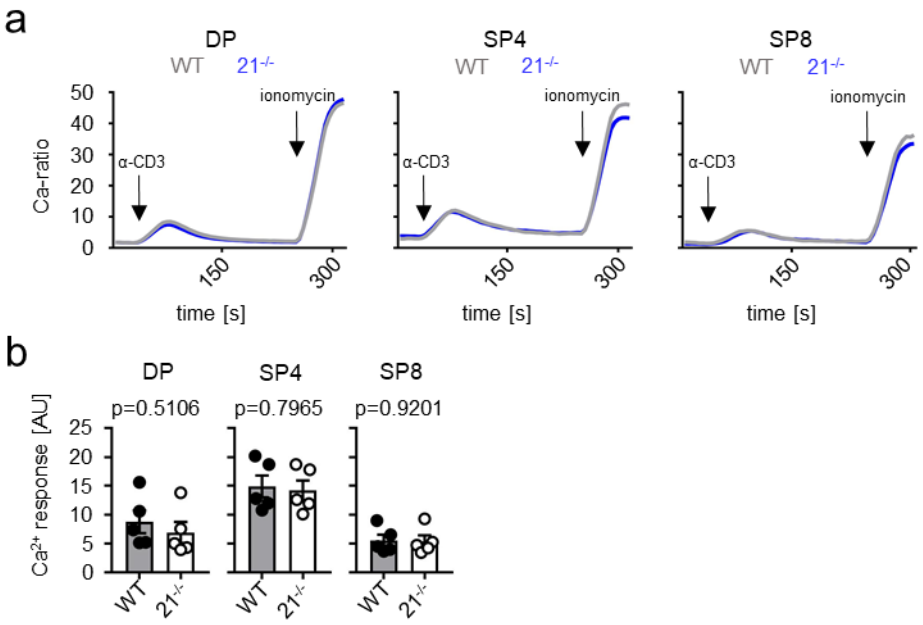

Figure 36: miR-21-deficiency has no effect on Ca^{2+}-flux upon stimulation with anti-CD3 antibodies.
(a) Representative flow cytometric analyses of Ca-ratio over time of DP, SP4 and SP8 thymocytes stimulated with anti-CD3 and ionomycin as a control (WT grey, miR-$21^{-/-}$ blue). (b) Statistical analysis of resulting Ca^{2+}-response upon stimulation in DP, SP4 and SP8 thymocytes, n = 5 mice for each genotype. Data is represented as mean ± SEM. Statistical analyses were performed using unpaired t-test.

We observed no significant differences in the ability of miR-$21^{-/-}$ DP, SP4 or SP8 thymocytes to generate a Ca^{2+} signal upon TCR triggering, not supporting a role of miR-21 in modulation of TCR signal strength.

To fully exclude a pivotal role of miR-21 in negative selection, we next moved on to adapt an *in vivo* TCR stimulation approach (Davalos-Misslitz et al., 2007). For this, miR-21-sufficient and deficient mice were injected with a single dose of anti-CD3 antibodies (or PBS as control) to activate TCR signaling. After 48 hrs, frequencies of DP, SP4 and SP8 thymocytes as well as their levels of activated caspase-3 as indicator of apoptosis were analyzed. In general, caspase-3 is cleaved and thus activated upon initiation of apoptosis. Absolute total thymocyte numbers were not significantly altered within the anti-CD3 or PBS treated groups (Figure 37a). However, we found a small, but statistically significant decrease in the frequencies of DP thymocytes derived from anti-CD3-treated miR-$21^{-/-}$ mice (Figure 37b and d). This finding led us to the hypothesis that the absence of miR-21 renders DP thymocytes more prone to apoptosis in comparison to their WT counterparts (Medina et al., 2010). Yet, we could not detect any changes in the cleaved caspase-3 staining of DP thymocytes of WT or

miR-21$^{-/-}$ mice arguing against this hypothesis (Figure 37c and d). To further analyze whether a defect in proliferation of miR-21$^{-/-}$ thymocytes may account for the decreased frequencies of DP thymocytes detected in anti-CD3-treated mice, we included a single BrdU administration in this assay to monitor proliferation (Figure 37e). Again, we could not detect any significant differences within the treated groups excluding a role of miR-21 in the modulation of negative selection.

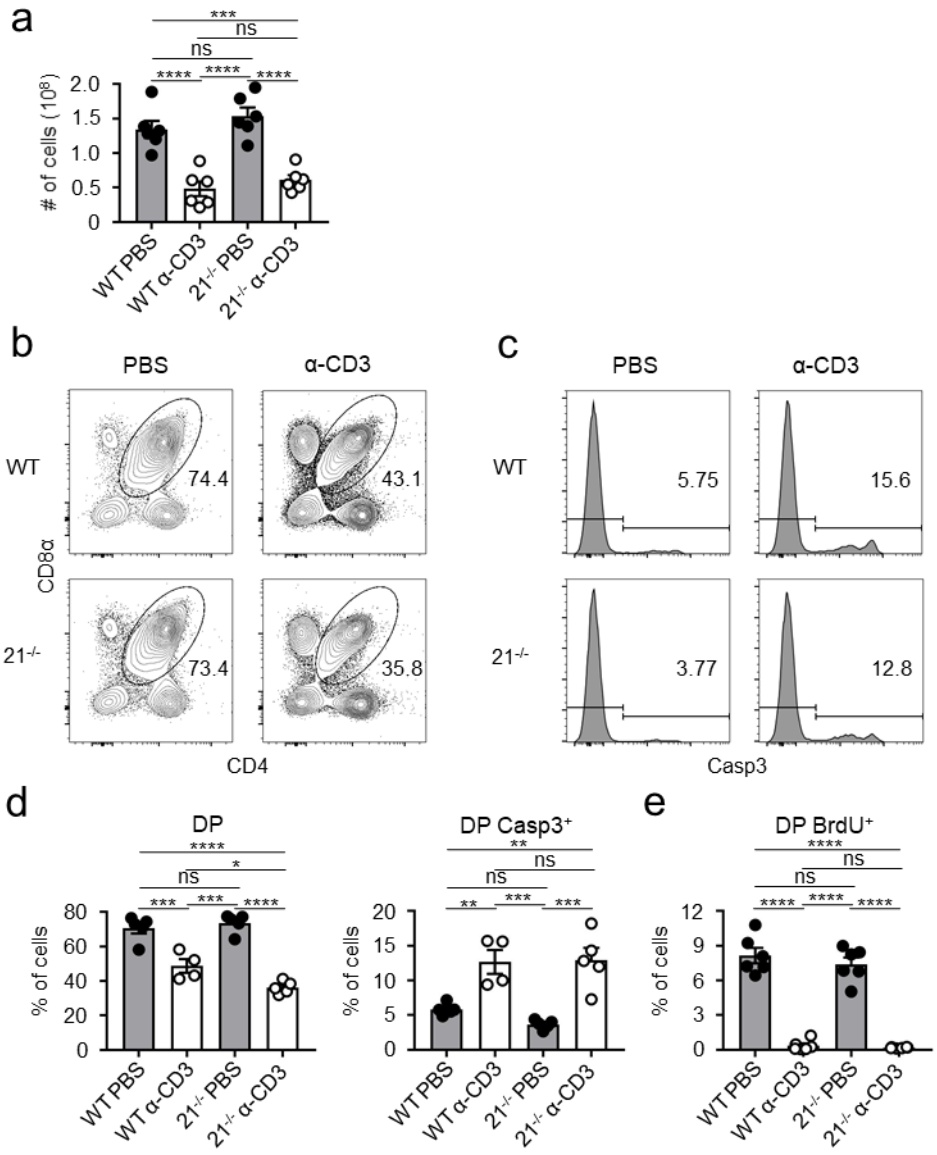

Figure 37: *In vivo* TCR stimulation identifies miR-21 as mostly redundant for negative selection. (a) Total cellularity of thymi from WT and miR-21$^{-/-}$ mice, 48 hours post injection with either PBS or anti-CD3 antibodies (α-CD3), n = 6 mice for each genotype. Pooled data of two independent experiments. (b) Representative flow cytometric analysis of thymocytes from WT and miR-21$^{-/-}$ mice, 48 hrs post injection with either PBS or α-CD3, stained with antibodies against CD4 and CD8α. Numbers adjacent to gates represent frequencies. (c) Histograms display expression of cleaved caspase-3 (Casp3) in DP thymocytes from WT and miR-21$^{-/-}$ mice, 48 hrs post injection with either PBS or α-CD3, n = 4-5 mice per group. Numbers adjacent to gates indicate frequencies. (d) Statistical analysis of flow cytometric results shown in (c). Data is represented as mean ± SEM. Analyses of significance were performed using one-way ANOVA followed by Tukey's post hoc test (ns, not significant; *P<0.05; **P<0.01; ***P<0.001; ****P<0.0001).

4.2.6 Intrathymic development of γδ T cells and agonist-selected T cells are largely unperturbed in miR-21$^{-/-}$ mice.

To extend our studies about the role of miR-21 in the thymus, we next investigated whether the development of γδ T cells as well as agonist-selected T cells is influenced

by miR-21. For the latter populations, we could show that miR-181 is fundamental in the development of iNKT, MAIT and Treg cells (Ziętara et al., 2013; Blume et al., 2016; Łyszkiewicz et al., 2019; Winter et al., 2019). For miR-21, an influence on Foxp3 transcription factor levels as well as on frequencies of circulating Treg cells has been described (Rouas et al., 2009; Dong et al., 2014; Hackett and Sheedy, 2017). Additionally, miR-21 was found to be preferentially expressed in iNKT and Treg cells as compared to naïve T cells (Fedeli et al., 2009).

In case of thymic γδ T cells, we saw no difference in frequencies when mice were deficient for miR-21 (Figure 38a). In thymi of miR-21$^{-/-}$ mice, we also analyzed frequencies of iNKT cells and found those to be largely unaffected (Figure 38b). This underlined our hypothesis that despite high expression levels in this subset, miR-21 is largely dispensable for the development of iNKT cells. For MAIT cells, we also observed no changes in frequency in the absence of miR-21 (unpublished observation). Consistent with the previous reports about miR-21 affecting Treg frequency, we detected a small, but statistically significant increase of Treg frequencies in thymi of miR-21$^{-/-}$ mice (Figure 38c).

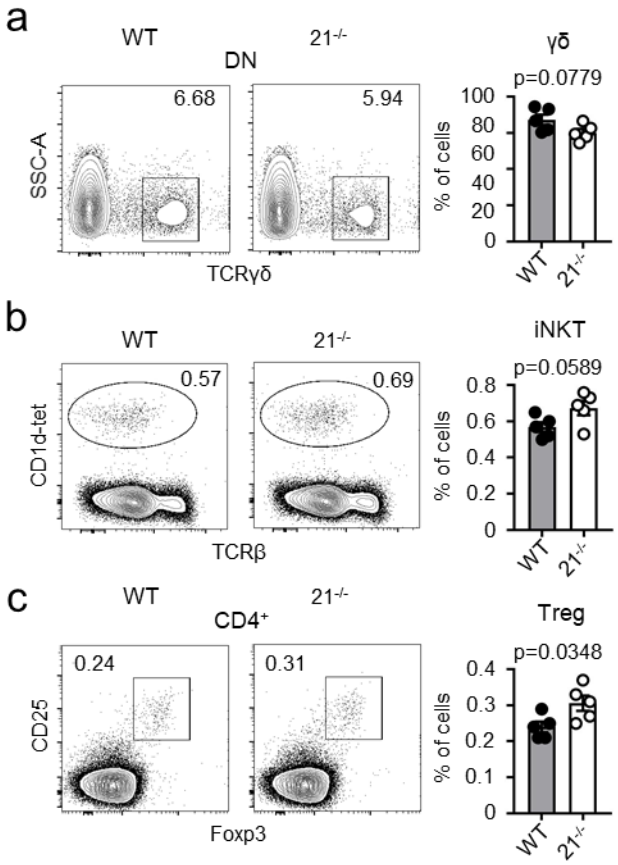

Figure 38: Frequencies of γδ and agonist-selected T cells are not impaired upon loss of miR-21. (a-c) Representative flow cytometric and statistical analyses of thymocytes from WT and miR-21$^{-/-}$ mice stained with antibodies against CD4, CD8 and TCRγδ (a), CD1d-tet and anti-TCRβ (b) or antibodies against CD4, CD25 and Foxp3 (c). Numbers in right corners of plots represent frequencies, n = 5 mice for each genotype. Data is represented as mean ± SEM. Statistical analyses were performed using unpaired t-test.

Based on the finding by (Fedeli et al., 2009) that in comparison to naïve T cells, miR-21 expression levels are elevated in agonist-selected iNKT as well as in Treg cells, we also analyzed the frequencies of agonist-selected T cells in the periphery (Figure 39). For peripheral iNKT cells (Figure 39a), we found a slight reduction in their frequency upon loss of miR-21. Consistent with our findings in the thymus, we detected elevated frequencies of peripheral Treg cells in miR-21$^{-/-}$ mice (Figure 39b).

Collectively, our data shows that despite small but significantly different results, miR-21 seems to be mostly redundant for the development of thymic γδ T cells as well as agonist-selected T cells in the thymus and periphery.

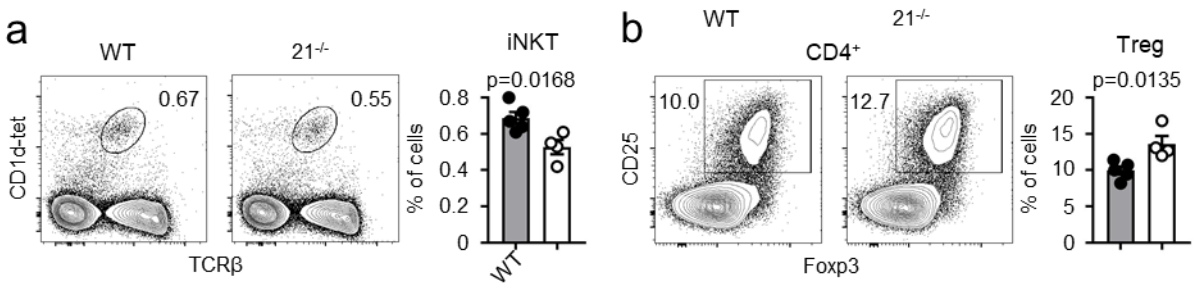

Figure 39: Frequencies of agonist-selected T cells in the periphery of miR-21$^{-/-}$ mice are slighlty impaired compared to WT mice.
(a, b) Representative flow cytometric and statistical analysis of splenocytes from WT and miR-21$^{-/-}$ mice stained with CD1d-tet and antibodies against TCRβ (a) or stained with antibodies against CD4, CD25 and Foxp3 (b). Numbers in right or left corners represent frequencies, n = 4-5 mice for each genotype. Data is represented as mean ± SEM. Statistical analyses were performed using unpaired t-test.

4.2.7 Physiological peripheral lymphoid cell frequencies are largely unaffected by the absence of miR-21.

In the next step, we tested whether miR-21 is of functional importance for peripheral lymphoid cell subsets. For this reason, we first determined frequencies of peripheral B as well as SP4 and SP8 T cells in spleen of miR-21$^{-/-}$ mice (Figure 40a and b). Consistent with our findings in thymi (Figure 34), we found similar levels of these subsets in spleens of miR-21$^{-/-}$ mice compared to WT controls. Additionally, we assessed the distribution of naïve, central memory and effector memory T-cell subsets in spleen (Figure 40c and d) and lymph nodes (LN) of miR-21$^{-/-}$ mice (Figure 40e and f). While these subsets were not affected by the absence of miR-21 in spleen, we observed significant differences in LN of miR-21$^{-/-}$ mice. In the absence of miR-21, we detected elevated frequencies of naïve T cells, whereas frequencies of central as well as effector memory T cells were reduced.

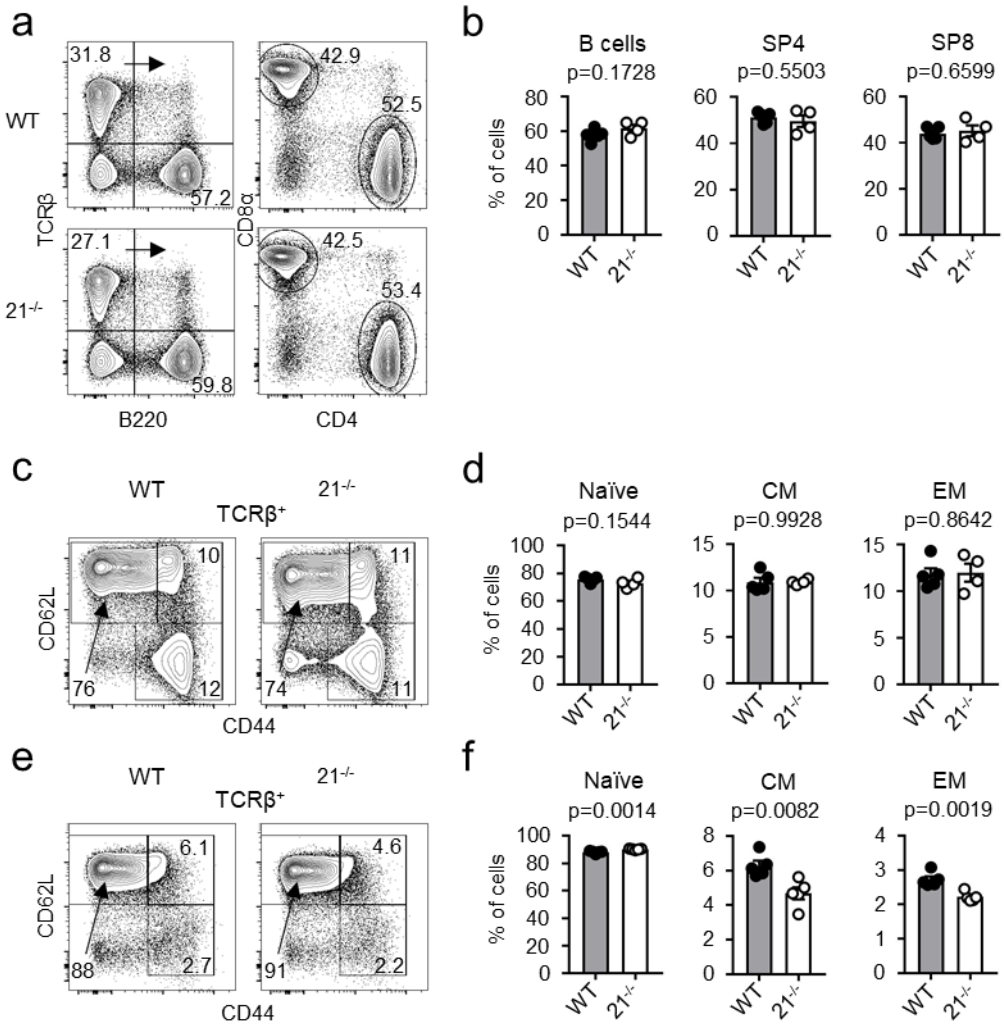

Figure 40: Analysis of peripheral lymphoid cell frequencies in the absence of miR-21.
(a) Representative flow cytometric analysis and gating strategy of splenocytes from WT and miR-21$^{-/-}$ mice stained with antibodies against B220, TCRβ, CD4 and CD8α. Numbers in quadrants or adjacent to gates represent frequencies. (b) Statistical analysis of flow cytometric results shown in (a), n = 4-5 mice for each genotype. (c-f) Representative flow cytometric analysis (c, e) and statistical analyses of flow cytometric results (d, f) of splenocytes (c, d) or LN cells (e, f) from WT and miR-21$^{-/-}$ mice stained with antibodies against TCRβ, CD44 and CD62L to identify naïve (CD44^{-}CD62L^{+}), central memory (CM, CD44^{+}CD62L^{+}) and effector memory (EM, CD44^{+}CD62L^{-}) T-cell subsets. Numbers in or adjacent to gates represent frequency, n = 4-5 mice for each genotype. Data is represented as mean ± SEM. Statistical analyses were performed using unpaired t-test.

4.2.8 Lineage fate decisions of miR-21$^{-/-}$ precursors show no alterations upon *in vitro* differentiation

Regarding the fact that alternative lineage fate decisions can occour in the thymus until the DN2a/b transition, we next asked the question whether miR-21 is important for this critical stage in T-cell development. Interestingly, as depicted in Figure 31, we found higher levels of miR-21 in DN2b cells compared to DN2a cells, which led us to hypothesize that miR-21 is involved in promoting alternative lineage fate decisions. A

key transcription factor necessary for T-lineage commitment is Bcl11b (Li et al., 2010a). For this reason, we determined the relative abundance of Bcl11b in sorted DN2a or DN2b thymocytes of miR-21-sufficient and deficient mice (Figure 41). We detected similar expression levels of Bcl11b in DN2a thymocytes of WT compared to miR-21$^{-/-}$ mice, but elevated levels in DN2b thymocytes of miR-21$^{-/-}$ mice suggesting a role of miR-21 in the promotion of alternative lineage fate decisions.

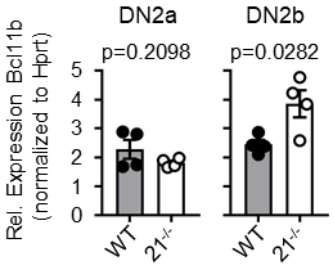

Figure 41: Elevated Bcl11b expression levels in DN2b, but not in DN2a thymocytes of miR-21$^{-/-}$ mice.
Analysis of expression of Bcl11b in sorted DN2a and DN2b cells of WT or miR-21$^{-/-}$ mice by quantitative RT-PCR. Expression levels were normalized to Hprt. Each dot represents one mouse, n = 4 mice for each genotype. Data is represented as mean ± SEM. Statistical analyses were performed using unpaired t-test.

To test this hypothesis, we monitored *in vitro* differentiation of sorted DN2a or DN2b thymocytes of miR-21-sufficient and -deficient mice using the well-established OP9 coculture system (Schmitt and Zúñiga-Pflücker, 2002). In the first step, we used OP9-DL1 BM stromal cells expressing the Notch ligand Delta-like 1. The presence of this ligand leads to the induction of T-cell lineage commitment in early thymocytes or BM-derived progenitors (here: DN2a and DN2b thymocytes). Hence, this system allows to study T-cell differentiation over time in an *in vitro* coculture approach in the absence of a thymus. We assessed the frequencies of developing T, NK and B cells every third to fourth day and detected similar frequencies of DN2a and DN2b thymocytes derived from WT and miR-21$^{-/-}$ thymi (Figure 42).

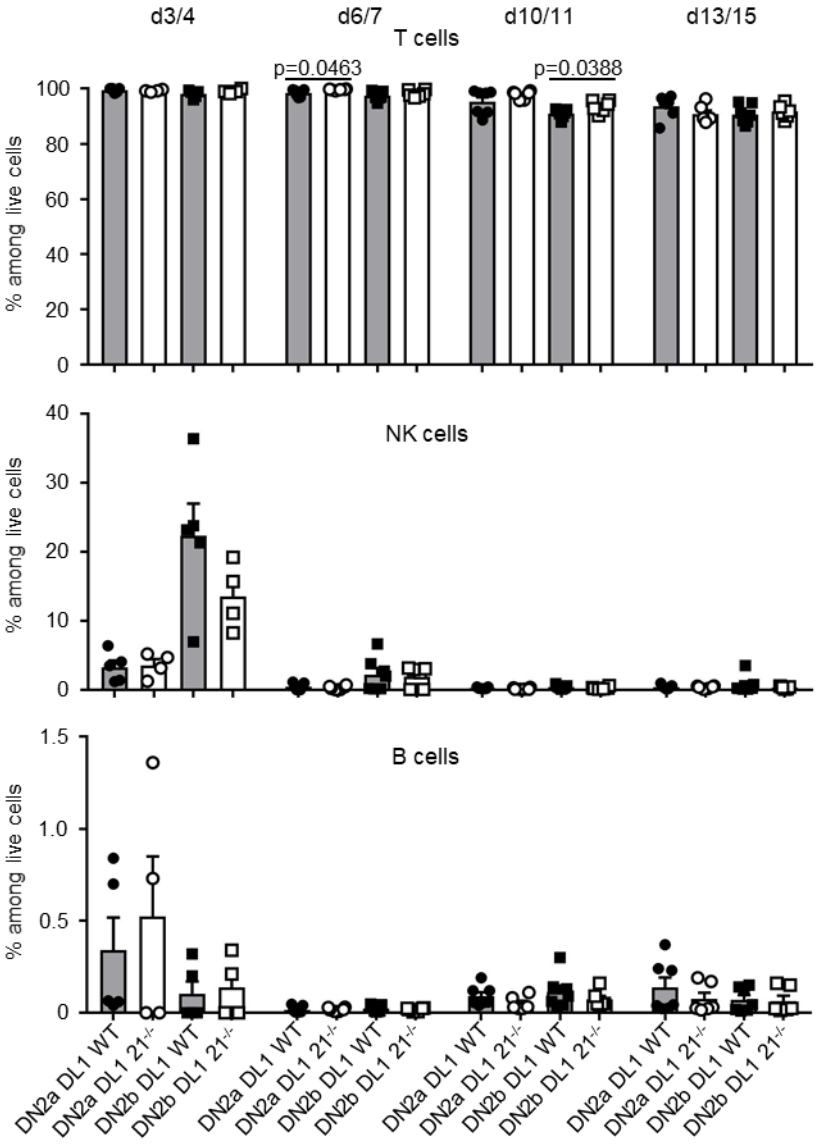

Figure 42: T-, NK- and B-cell lineage fate decisions are not impaired by loss of miR-21.
Sorted DN2a and DN2b cells were cultured on OP9-DL1 cells for up to 15 days. Generation of T, NK and B cells was determined by flow cytometry at indicated periods of time. Pooled data of two independent experiments. Each dot represents one mouse, n = 4-7 mice for each genotype. Data is represented as mean ± SEM. Statistical analyses were performed using unpaired t-test.

In parallel to OP9-DL1 cocultures, we also performed this experiment using OP9-GFP cells. These cells lack the DL1 ligand thereby promoting alternative commitment such as NK- and B-cell fate. Again, we seeded sorted DN2a or DN2b thymocytes of miR-21-sufficient and -deficient mice onto OP9-GFP cells and monitored the development of T, NK and B cells over time (Figure 43).

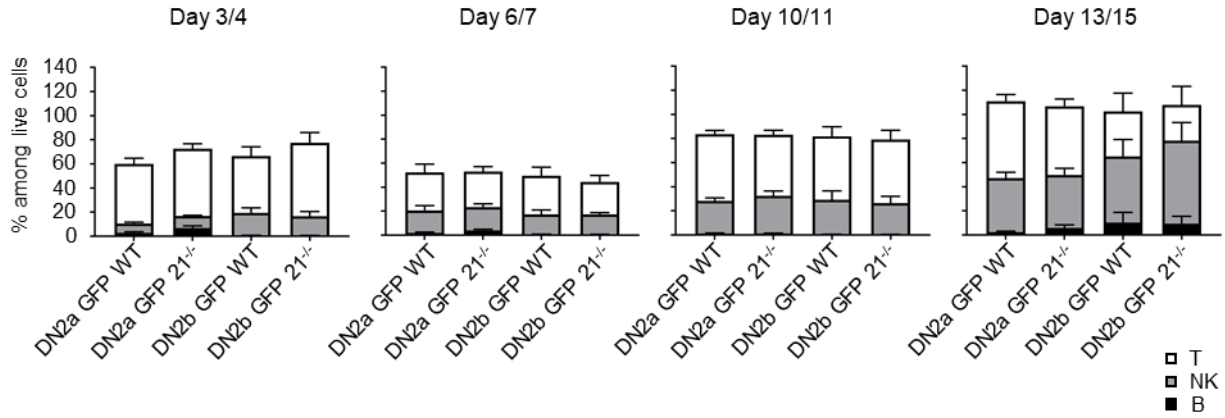

Figure 43: Alternative lineage fate decisions are unaffected by the absence of miR-21.
Sorted DN2a and DN2b cells were cultured on OP9-GFP cells for up to 15 days. Generation of T, NK and B cells was determined by flow cytometry at indicated periods of time. Bar graphs show pooled data from two independent experiments, n = 4-7 mice for each genotype. Data is represented as mean ± SEM. Statistical analyses were performed using unpaired t-test.

Consistent with our results obtained from the OP9-DL1 cocultures, alternative lineage fate decisions were mostly unaltered in the absence of miR-21 thereby arguing against a role of miR-21 in promoting alternative lineage fate decisions.

4.2.9 No cell-intrinsic defects in T-cell development in miR-21-deficient mice

In order to fully exclude compensatory effects potentially covering cell-intrinsic defects in T-cell development at steady state (Krueger et al., 2010; Zlotoff et al., 2010; Germar et al., 2011; Weber et al., 2011; Regelin et al., 2015), we performed competitive BM chimera experiments. For this, we reconstituted lethally irradiated WT recipients with 1:1 mixtures of lineage-depleted BM donor cells from WT (CD45.1) and miR-21$^{-/-}$ (CD45.2) or WT (CD45.1) and WT control (CD45.2) mice and analyzed chimeric mice eight weeks after transfer (Figure 44).

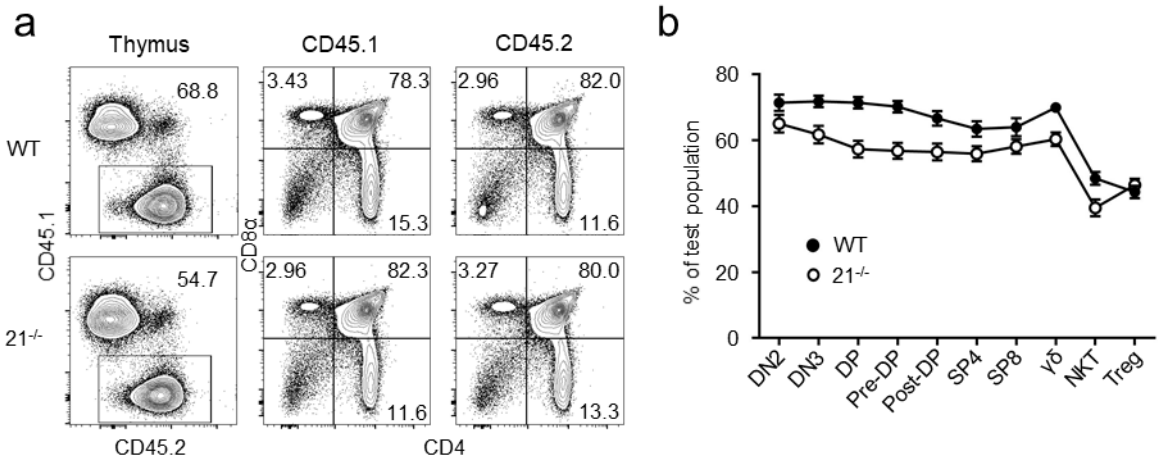

Figure 44: Physiological T-cell development of miR-21$^{-/-}$ BM cells is not affected in a competitive chimera approach *in vivo*.
(a) Representative flow cytometric analysis of competitive BM chimeras eight weeks after transfer, CD45.1: competitor population; CD45.2: test population (WT control or miR-21$^{-/-}$). Thymocytes were stained with antibodies against CD45.1, CD45.2, CD4 and CD8α. Numbers adjacent to gates and in quadrants represent frequencies. (b) Comparative analysis of thymocyte subpopulations in CD45.2 test populations (WT control or miR-21$^{-/-}$) of competitive chimeras, n = 9 mice per group. Data is represented as mean ± SEM. Statistical analyses were performed using unpaired t-test.

Thymi of chimeric mice showed similar frequencies of WT control or miR-21$^{-/-}$-reconstituted CD45.2 cells (Figure 44a). Furthermore, we found similar frequencies of DP, SP4 and SP8 T cells in CD45.1- or CD45.2-derived cells (Figure 44a). Detailed analysis of different T-cell subsets showed that miR-21$^{-/-}$- and WT-derived BM were reconstituting irradiated recipients in a comparable manner as the respective WT control (Figure 44b). Collectively, we concluded that hematopoiesis does not depend on miR-21.

4.2.10 miR-21 overexpression does not influence physiological T-cell development in BM chimeras

After an in-depth characterization of the steady-state T-cell development *in vivo* and *in vitro*, the monitoring of alternative lineage development and competitive BM chimera experiments in the absence of miR-21, we next moved on addressing the question whether miR-21 overexpression does result in aberrant T-cell development. To achieve stable overexpression of miR-21, we transduced lineage-depleted BM cells with miR-21 encoding retrovirus (or an empty vector (EV) control), both encoding enhanced GFP as a reporter. Lethally irradiated WT recipients of a different congenic background served as recipients for reconstitution. After eight weeks, we analyzed thymi (Figure 45), BM, spleen and LNs (data not shown) for different T-cell subsets

and observed no detectable changes in either GFP$^-$ (untransduced) or GFP$^+$ cells (transduced) of control or miR-21-overexpressing organs.

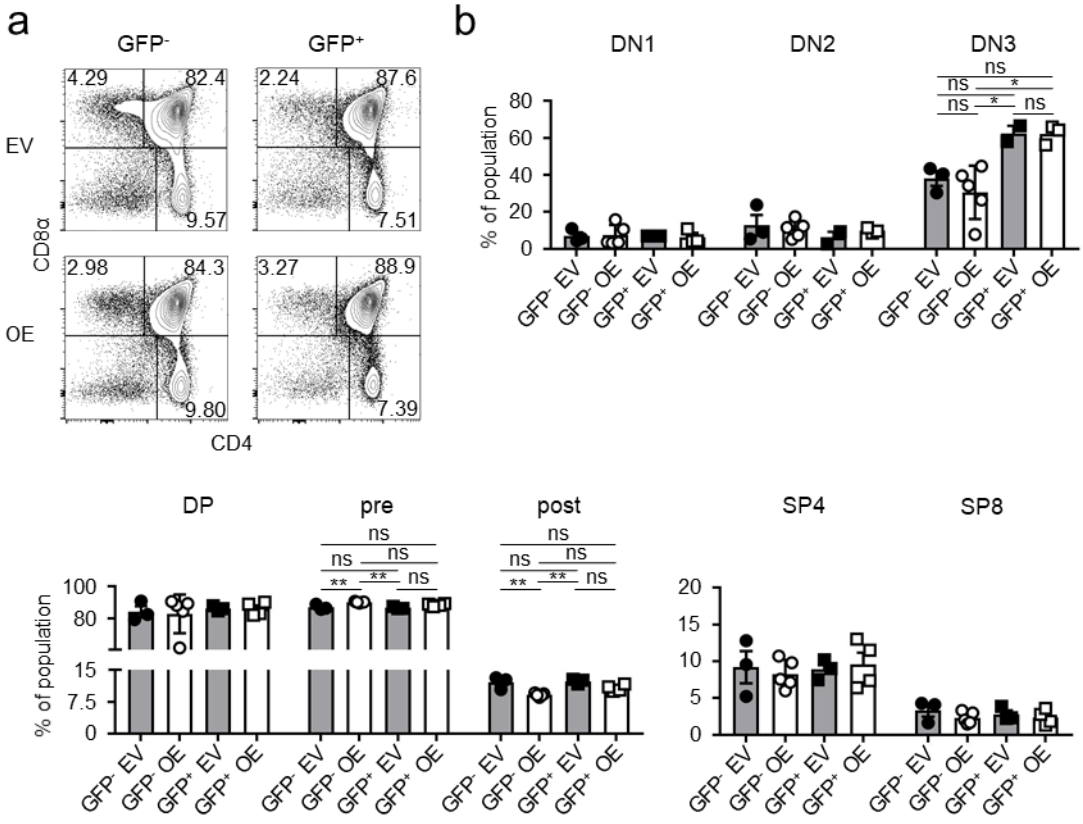

Figure 45: Overexpression of miR-21 in BM chimeras shows no influence on steady-state T-cell development.
(a) Representative flow cytometric analysis of miR-21 overexpression chimeras eight weeks after transfer. Thymocytes were stained with antibodies against CD4 and CD8α. Left panels display distribution of GFP$^-$ (untransduced) thymocytes in EV (empty vector) control or OE (miR-21-overexpression) chimeras. Right panels indicate GFP$^+$ (transduced) thymocytes. Numbers in quadrants represent frequencies. (b) Statistical analysis of flow cytometric results of DN1, DN2, DN3, DP, pre- and post-selection DP, SP4 and SP8 populations from GFP$^-$ EV, GFP$^-$ OE, GFP$^+$ EV, GFP$^+$ OE thymocyte subsets indicated as frequencies, inter alia shown in (a), n = 2-5 mice. Data is represented as mean ± SEM. Analysis of significance was performed using one-way ANOVA followed by Tukey's post hoc test. Inidicated significant results are representative of latter test (ns, not significant; *P<0.05; **P<0.01).

Therefore, it is apparent that ectopic elevation of miR-21 levels does not impair intrathymic T-cell development.

4.2.11 Endogenous T-cell regeneration is unaltered in miR-21-deficient mice

Until now, most studies about miR-21 focused on the role of this miR and its involvement in pathological settings, mainly in tumor development (Hatley et al., 2010; Medina et al., 2010; Ma et al., 2011). We next addressed the question whether miR-21

is also important for stress responses. In order to test this, we applied an experiment to induce stress and studied subsequent endogenous thymic repair *in vivo* using sublethal total body irradiation (Kadish and Basch, 1975; Huiskamp and van Ewijk, 1985; Tomooka et al., 1987; Penit and Ezine, 1989; Dudakov et al., 2012). After irradiation, WT and miR-21$^{-/-}$ mice were monitored for their thymic recovery for up to 14 days by determination of DN (Figure 46a) and DP frequencies (Figure 46b) every third to fourth day. Non-irradiated mice as well as irradiated mice that were immediately sacrificed after irradiation served as controls. In both WT and miR-21$^{-/-}$ mice, we were able to detect profound changes in frequencies of DN subsets as well as of DP, SP4 and SP8 within 14 days indicating ongoing endogenous thymic repair.

However, these changes were independent of miR-21 emphasizing a completely expendable role of miR-21 in this stress response.

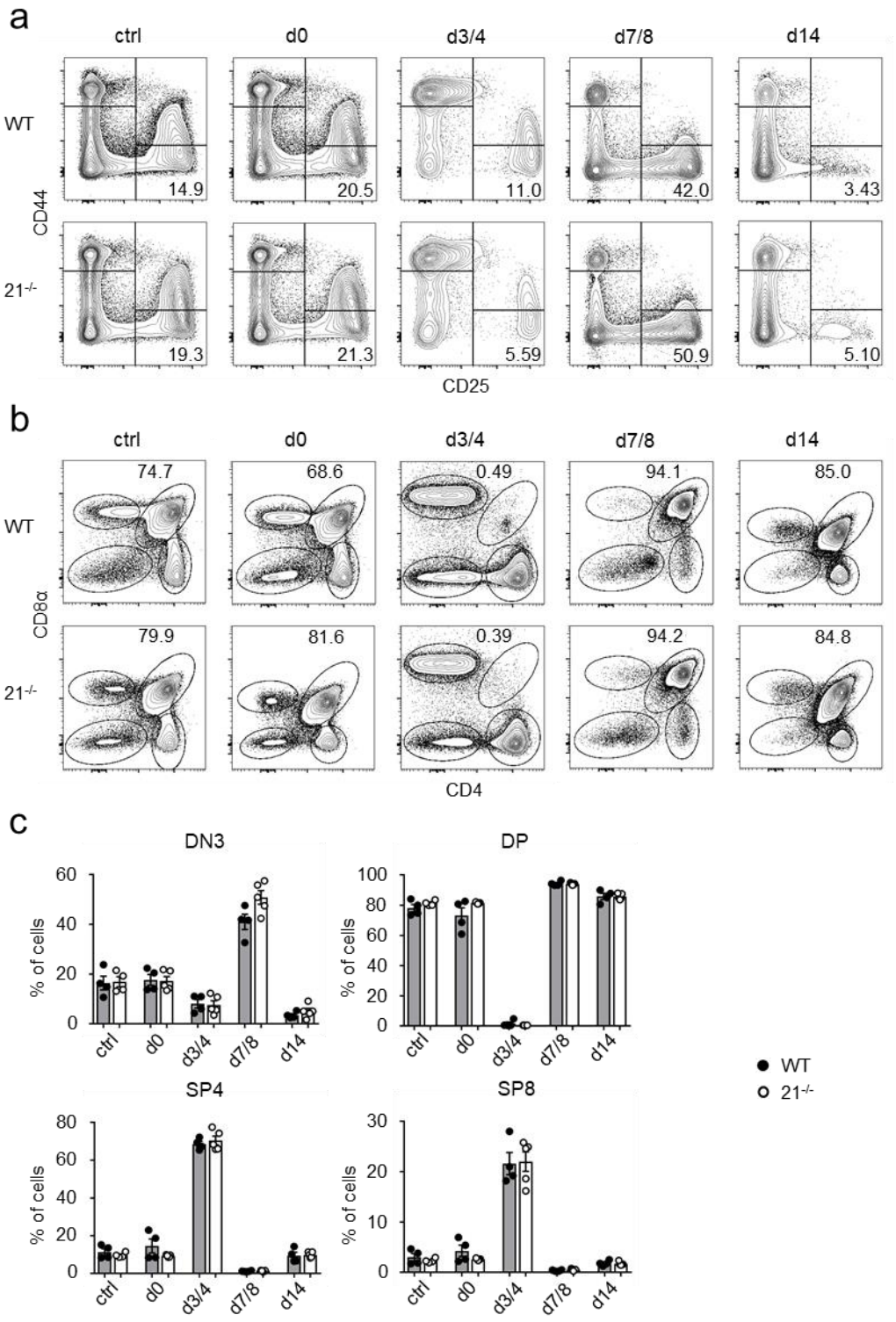

Figure 46: Endogenous T-cell regeneration in miR-21$^{-/-}$ mice is not impaired.

(a) Representative flow cytometric analysis of thymocytes from WT and miR-21$^{-/-}$ mice stained with antibodies against CD25 and CD44. Numbers in right bottom quadrants represent frequencies of DN3 thymocytes. Regeneration of DN thymocytes was assessed at indicated periods of time in non-irradiated mice or post sublethal irradiation. Pooled data of two independent experiments. (b) Representative flow cytometric analysis of thymocytes from WT and miR-21$^{-/-}$ mice stained with antibodies against CD4 and CD8α. Numbers adjacent to right gate represent frequencies of DP thymocytes. Regeneration of DP, SP4 and SP8 thymocytes was determined at indicated periods of time in non-irradiated mice or post sublethal irradiation. Pooled data of two independent experiments. (c) Statistical analysis of flow cytometric results shown in (a) and (b). Each dot represents one mouse, n = 4-5 for each genotype. Data is represented as mean ± SEM. Statistical analyses were performed using unpaired Mann-Whitney test.

4.2.12 *Ex vivo* viability of thymocytes is not affected by loss of miR-21

Previous studies have attributed miR-21 to play a key role in apoptosis by suppressing cell death (Li et al., 2009; Buscaglia and Li, 2011; Ruan et al., 2014; Song et al., 2017). In order to test, whether this is the case for thymocytes as well, we performed an apoptosis detection assay based on the analysis of propidium iodide (PI) and Annexin V (AxV) and assessed whether the absence of miR-21 is influencing the viability of SP thymocytes *ex vivo* (Figure 47). We determined the frequencies of early/mid apoptotic (defined as PI^{-}AxV^{+}) and late apoptotic cells (defined as PI^{+}AxV^{+}) in SP4 and SP8 T cells for up to 48 hrs in culture and found those to be largely unchanged in the absence of miR-21. Conversly, we detected a statistically significant but small decrease in the frequency of late apoptotic cells among SP8 cells at 48 hrs (Figure 47b).

Collectively, we concluded that miR-21 does not affect apoptosis levels of SP thymocytes *ex vivo*.

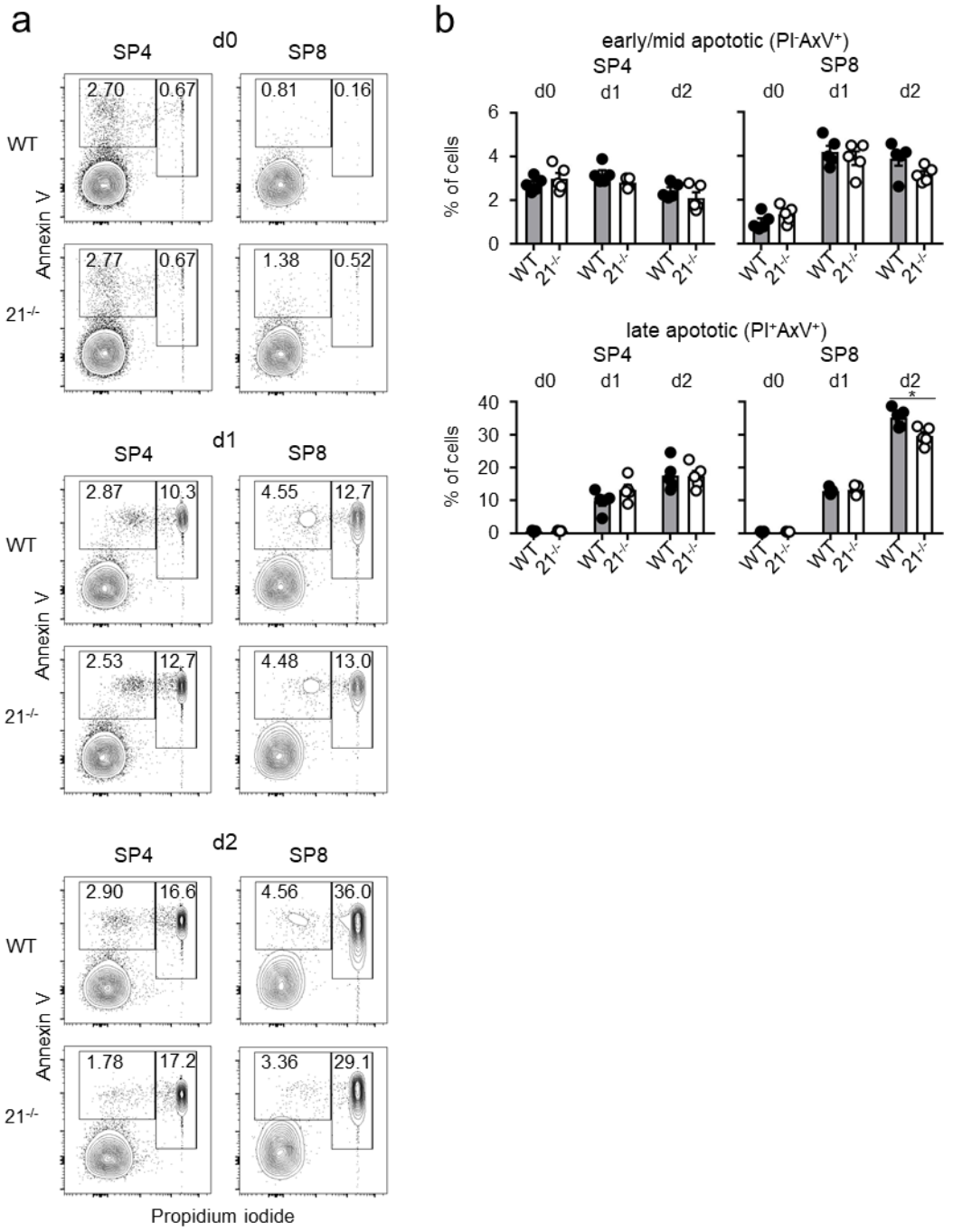

Figure 47: Frequencies of apoptotic SP T cells of miR-21$^{-/-}$ mice are similar to WT littermates.
(a) Representative flow cytometric analysis of thymocytes from WT and miR21$^{-/-}$ mice stained with antibodies against CD4, CD8α as well as propidium iodide (PI) and Annexin V (AxV). Numbers adjacent to gates represent frequencies of early/mid (defined as PI^{-}AxV^{+}) and late apoptotic cells (defined as PI^{+}AxV^{+}). Frequencies were determined at indicated days. (b) Statistical analysis of flow cytometric results shown in (a). Each dot represents one mouse, n = 5 mice for each genotype. Data is represented as mean ± SEM. Statistical analyses were performed using unpaired t-test (*P<0.05).

5 Discussion

5.1 High-resolution quantification of cell cycle dynamics during T-cell development

The development of T cells is a highly dynamic and stepwise process in which a few hundred bone-marrow derived progenitor cells colonize the thymus and undergo T-lineage commitment, TCR gene rearrangement and selection. Ultimately, millions of functional single-positive naïve T cells emigrate into the periphery. These defined steps of differentiation events are interspersed by proliferative bursts. Recent studies revealed the underlying transcriptional network of early T-cell development (Hosokawa and Rothenberg, 2021; Olariu et al., 2021; Rothenberg, 2021; Zhou et al., 2021), but a quantitative picture of T-cell development remains obscure. To fully understand T-cell population dynamics on the cell cycle level, we established a high-resolution map of cell cycle kinetics that aims to understand alterations or dysregulation of the T-cell developmental program. In this thesis, we employed *in vivo* single- and dual-nucleoside pulse labeling combined with determination of DNA replication over time in different WT thymocyte subsets at steady-state. Based on this, we assessed alterations in cell cycle kinetics of two representative mouse models with defects in the earliest thymocyte populations (DN1 and DN2) that are almost completely recovered at later stages (Krueger et al., 2010; Regelin et al., 2015). In addition, scRNA-seq helped to obtain information on cell cycle dynamics of early thymocyte subsets. Lastly, we provided cell cycle analyses in a model of endogenous thymic repair upon sublethal total body irradiation.

5.1.1 Quiescent T cells

Based on the definition that quiescent cells lack Ki-67 expression, determination of Ki-67 levels represents a useful tool to identify cell popualtions in the G0 phase (Schwarting et al., 1986; Vignon et al., 2013). Our results obtained from *in vivo* BrdU single-pulse labeling in conjunction with analyses of DNA content and Ki-67 expression levels indicate that quiescence of early T-cell developmental stages is mostly affecting DN1, DN3a and DN4 cells (Figure 10). DN1 thymocytes, that have an estimated lifetime of 9-12 days (Porritt et al., 2003), were shown to divide only ten times during their transition (Petrie and Zúñiga-Pflücker, 2007). Taking this into account, DN1 thymocytes have either a cell cycle duration of ~24 hrs or some cells are stored in a

quiescent state. A computational modeling approach of early T-cell development using data from *in vitro* differentiation cultures predicted that DN1 cells undergo a certain number of divisions before transition into DN2 stage, suggesting that cell division number and developmental progression are coupled (Manesso et al., 2013). These data indicate that there is a strong kinetic component to the transition from uncommitted TSPs to T-lineage committed thymocytes. Regarding this, quiescence in DN1 thymocytes might predominantly affect either the one stage or the other to ensure a proper reactivation upon demand. Another hypothesis is that quiescence during this early developmental stage is dependent on niche occupancy of thymocytes. A study by our group showed that in the absence of CCR7/9, niches are mostly devoid of ETPs/DN1 cells (Ziętara et al., 2015). Analyzing the remaining DN1 cells in CCR7/9 DKO mice revealed a drastic decrease in the frequencies of quiescent cells (Figure 18), supporting a dependence on niche occupancy. Transplantation experiments of WT TSPs into DKO mice might shed light on the interplay or feedback mechanism of niche occupancy and quiescence. Indeed, DKO thymi are highly receptive for WT TSPs (Ziętara et al., 2015).

For WT DN3a and DN4 thymocytes, we found similar levels of quiescent cell frequencies. Due to ongoing V(D)J recombination, the resting nature of pre-β-selection DN3a thymocytes might be required to support genomic stability during this developmental step (Visan et al., 2010). In line with that, post-β-selection DN3b thymocytes exhibit lowest frequencies of quiescent cells among all thymocyte subsets (Figure 10). Conversely, WT DN4 thymocyte subsets had similar frequencies of quiescent cells as compared to DN3a thymocytes (Figure 10). However, we assume the DN4/pre-DP stage to comprise a various mixture of cells ranging from ‘freshly’ TCRβ-chain rearranged cells, which might account for the high frequencies of quiescent cells, up to ‘older’ highly proliferating cells ensuring the generation of multiple DP thymocytes. In addition, DN4 cells are defined as negative for markers classically used for isolation (CD4, CD8, CD25, CD44). Therefore, this population is prone to potential low-level contamination by non-thymocyte cells. Interestingly, WT steady-state analysis of later stages of T-cell development such as post-selection DP and SP cells showed higher levels of quiescence pointing out that early T-cell development is more dynamically active in terms of cycling and only particular developmental steps are affected by quiescence. Moreover, in comparison to early T-cell development, where most proliferative events occur, later stages of T-cell

development ensure the establishment of a functional pool of T cells suggesting that quiescence is acquired on the path of maturation. Quiescence in its historic definition refers to an inactive, non-cycling state, in which cells are incapable to re-enter the cell cycle (Howard and Pelc, 1986; Hartwell and Weinert, 1989). Why do we then find quiescent cells during T-cell development, which constitutes a continual process with an essentially linear differentiation trajectory? Current studies suggest that the G0 phase should be rather interpreted as an actively regulated state enabling prolonged survival and an adaptive cell response on demand to maintain tissue homeostasis (Eddaoudi et al., 2018). Moreover, distinct types and depths of quiescence were described recently (Fujimaki et al., 2019). Previous studies on cell cycle kinetics could not provide any reliable information about the existence of quiescence in different developing thymocyte subpopulations (Baron and Pénit, 1990). In regard to the dynamic nature of Ki-67 expression during cell cycle (Vignon et al., 2013; Miller et al., 2018), we also tried to establish further protocols to validate our results. To this end, Pyronin Y staining which is based on flow cytometric analyses by measurement of cellular DNA and RNA content (Kim and Sederstrom, 2015; Eddaoudi et al., 2018) provided no reliable information (data not shown). A current study of our lab investigates cell cycle dynamics in thymi of fluorescent ubiquitination-based cell cycle indicator (FUCCI) mice (Tomura et al., 2013). The underlying principle is the usage of ubiquitin oscillators that control cell cycle transition. Those mice exhibit a probe expressing both tagged Geminin (labeling S/G2/M phases) and tagged hCdt1 (human Chromatin licensing and DNA replication factor 1, labeling G0/G1). Indeed, first experiments could validate our findings for DN1 and DN3a thymocytes to be partly found in the G0 phase. However, further investigations will foster our understanding about quiescent developing thymocytes.

5.1.2 Power and limitations of steady-state cell cycle analysis

Based on our *in vivo* single- and dual-pulse labeling experiments (Figure 10 and Figure 13), we were able to generate a high-resolution map of cell cycle phase contributions. Theoretically, our single-pulse labeling experiments should be mirrored by the fraction of EdU^+BrdU^+ cells (Figure 13a) due to the nature of this fraction representing the frequency of cells within a population that have been in S phase during both pulses, thus precluding any conclusions with regard to the cell's position within S phase during labeling.

This was not fully achieved for DN4 and post-selection DP thymocytes indicating that a certain level of heterogeneity cannot be excluded. Taken together, steady-state analysis confirmed previously established periodic changes between non-cycling phases of T-cell development, corresponding mostly to populations undergoing somatic TCR rearrangements and maturing SP thymocytes (MacDonald et al., 1988; Penit et al., 1988; Penit and Vasseur, 1988; Scollay et al., 1988; Baron and Pénit, 1990; Penit, 1990; Lucas et al., 1993, 1994, 1995; Pénit et al., 1995; Pénit and Vasseur, 1997; Vasseur et al., 2001). Especially for DN3a and DN3b WT thymocytes, we detected profound differences indicating that V(D)J rearrangement at the DN3a stage does not occur during DNA synthesis. This is consistent with a previous study showing that RAG-2 protein accumulates in cells in the G0/G1 phases of the cell cycle, and is degraded at the G1-S transition (Li et al., 1996; Lee and Desiderio, 1999). Some of these earlier studies focused on synchronization by eliminating cycling cells with an anti-mitotic agent which might have had deleterious effects on resting cells and thymus environment potentially skewing cell cycle kinetics. Additionally, previous studies started their analysis one day after i.p. BrdU injection, which might have contributed to increased heterogeneity (Pénit et al., 1995). Moreover, the lack of multi-color flow cytometry limited the power of the previous studies. Other studies were performed at 1 hr intervals post injection and addressed the duration of cell cycle phases of total thymocytes but do not provide information about thymocyte subpopulations (Baron and Pénit, 1990).

5.1.3 Dynamic analysis at cell cycle stage resolution

Dual nucleoside labeling enabled us to generate a high-resolution map of cell cycle entry and exit for different thymocyte subsets. Assuming that all cells cycle equally, the frequencies of $BrdU^+$ or EdU^+ cells can be used as a first benchmark to calculate cell cycle duration. Bioavailability of nucleoside analogues in rodents has been estimated to be in the range of 30-45 min (Hagan, 1984; Matiašová et al., 2014). Hence, the fraction of $BrdU^+EdU^-$ cells has entered S phase 30-45 min after the EdU pulse, but no later than 30-45 min after the BrdU pulse, defining a window of S-phase entry of approximately 1 hour.

A possible limitation for this calculation is given by the fact of DNA replication speed being different among early and late S-phase cells (Li et al., 2014). However, based on this, rates of S-phase entry indicated that DN2 (4.8% $BrdU^+$), DN3b (7.01%

$BrdU^+$) and DN4 (5.91% $BrdU^+$) thymocytes go through cell cycle more than once a day with approximately 1.5 to 3.4 divisions per day (calculated based on mean entry per hour by frequency of $BrdU^+$, daily rate and labeling time).

Whereas the overall pattern of EdU^+ and $BrdU^+$ frequencies mirrored the frequencies of EdU^+BrdU^+ cells, we detected exceptions for DN1, post-selection DP and SP4 thymocytes. For DN1 and SP4 thymocytes, due to the low cell numbers of incorporated cells, definitive conclusions for possible underlying mechanisms are difficult to draw. However, one may speculate that in the case of SP4 cells, EdU^+ cells represent the final cycle before cells enter final maturation and the frequency of quiescent cells increases. Indeed, for SP4 thymocytes, frequencies of quiescent cells were high in comparison to other thymocyte subsets (Figure 10). Moreover, as mentioned before in this discussion, among early developmental stages, DN1 thymocytes also had high frequencies of quiescent cells.

Interestingly, for post-selection DP thymocytes, calculating ratios between S-phase cells (EdU^+BrdU^+) and S-phase entry ($BrdU^+$) or exit (EdU^+) provides an initial estimate of the relative S-phase length (Figure 13e, f). High ratios imply that the duration of S phase is large compared to overall cycle. Low ratios indicate that other cell cycle phases, presumably G1, are comparatively longer. This suggests that post-selection DP thymocytes among all thymocyte subsets exhibit a prolonged S phase in line with minute entry and exit of cells into the S phase. Additionally, this finding points out that post-selection DP cells might stall or arrest in S phase. Indeed, our finding is consistent with a study that showed the existence of cycling cells that probably transit into a resting state upon selection (Penit, 1990). Additionally, post-selection DP thymocytes exhibit highest frequencies of quiescent cells, further supporting the assumption that quiescence is acquired on the path of maturation.

5.1.4 Quantification of cell cycle lengths

In addition to information about cell cycle dynamics obtained from steady-state single- and dual-pulse nucleoside labeling, combination of dual-pulse labeling with analysis of temporally resolved DNA replication provided accurate information on re-entry in G1 and S phase (Figure 15) as well as the duration of G1 and S phase (Figure 16, Figure 22). Direct analysis of DNA synthesis over time revealed short S phases of approximately 6.5 hrs for DN3b and DN4 cells. These findings are consistent with extremely rapid turnover of these populations (Shortman et al., 1990;

Pénit et al., 1995). Based on our aforementioned calculations in this section, DN2 cells were considered cells with more than one division per day, comparable to DN3b and DN4 cells. On the other hand, a longer S-phase duration of 8-9.5 hrs was observed for DN2, DN3a and pre-selection DP thymocytes (Figure 16). Thus, these data suggest that S-phase shortening below a certain limit is a feature restricted to extremely fast proliferating DN3b and DN4 cells. Curiously, post-selection DP cells contained more DNA already at early time points of analysis and cells remained in S-phase considerably longer than other populations (>11 hrs) (Figure 16). This finding is consistent with our aforementioned explanations in this discussion. The underlying mechanism of this peculiarity remains unknown but led us to conclude that post-selection DP thymocytes undergo S-phase stalling probably as consequence of massive death due to selection at this particular stage.

Note that, based on earlier studies, we employed a linear regression model to determine S-phase duration (Begg et al., 1985; Baron and Pénit, 1990). However, in all data sets a sigmoidal fit corresponding to a slow start in DNA replication and a deceleration prior to completion of S phase might be more accurate (Li et al., 2014). However, as calculation of S-phase duration is based on the slope, linear regression provides a sufficiently good estimate for S-phase length.

We have employed three complimentary apoproaches for cell cycle analysis *in vivo*: a) Single-pulse labeling reveals a static snapshot of cell cycle phase distribution, but precludes conclusions regarding dynamic changes. b) Dual-pulse labeling reveals rates of cell cycle entry in a given population and allows to estimate cell cycle length, but only under the assumption that the population of interest is homogeneously cycling. c) Dual-pulse labeling in combination with DNA labeling directly reveals DNA replication speed as well as re-entry into S phase after G1. Thus, it provides the most in-depth information, but remains limited to a population actively cycling during administration of the initial pulses. Interestingly, dual-pulse labeling followed by DNA content analysis revealed a certain degree of heterogeneity of some populations in our analyses (Figure 14 and Figure 17) indicating that cell cycle kinetics are much more dynamic than previously described. Therefore, we have to consider that despite being phenotypically discriminated by defined markers (e.g., DN4 and pre-selection DP thymocytes), the developmental program at those transition stages results in heterogeneity of a cell's individual cell cycle behavior. In a recent experiment, we also tried to extend our dual-pulse labeling analyses for a 16 and 20 hrs timepoint (data not

shown). This experiment revealed a high level of heterogeneity further underlining our observations. In the future, the aforementioned FUCCI mice (Tomura et al., 2013) in addition with a biomathematical model (Robert et al., 2021) might help us to study this finding in more detail.

5.1.5 Cell cycle in models of perturbations of homeostasis

We addressed how paucity in the earliest thymocyte populations (DN1 and DN2) recovers towards the DN3 stage in two representative mouse models, CCR7/9 DKO as well as miR-17~92-deficient mice. Consistent with earlier findings, the frequency of cells in S phase was most evidently elevated in DN3a DKO cells in both single- as well as dual-pulse data (Figure 18 and Figure 19) (Krueger et al., 2010). However, we detected subtle alterations in cell cycle phase composition of DN3a thymocytes but also in other thymocyte populations. This led us to conclude that it is the DN3a population, in which the most prominent acceleration in cell cycle speed occurs. The dual-pulse approach in conjunction with analysis of DNA replication revealed consistently shorter S-phase duration for all DN subsets from DKO thymi in a range of 0.73 to 1.16 hrs (Figure 21), most prominently for DN3a thymocytes. We conclude from our analysis that DN3a cells display the largest alteration in overall cell cycle length, which at least partially explains recovery of later DN thymocyte subsets when thymus colonization is impaired. Taken together, we provided insight into a specific stage of the cell cycle associated with increased thymocyte turnover to compensate homeostatic pressure in terms of composition of early thymocyte populations.

miR-17~92-deficient mice are comparable with DKO mice, although the observed phenotype is more likely due to a partial defect in cytokine signaling rather than migration (Regelin et al., 2015). Our preliminary results indicate a different cell cycle adjustment than observed for CCR7/9 DKO mice. The absence of miR-17~92 results in S-phase alterations on the level of DN3b and DN4 thymocytes. A possible explanation for the non-responsiveness of the DN3a compartment in miR-17~92-deficient mice might be a functional defect of those cells. Indeed, at least post-β-selection proliferation of DN3 cells is dependent on c-Myc and cyclin D3 (Sicinska et al., 2003; Kozar et al., 2004; Dose et al., 2006). However, β-selection is not affected in thymi of miR-17~92-deficient mice (Regelin et al., 2015).

Another example of thymus recovery was given by a model for thymus size restoration after pre-conditioning. The dynamics of thymocyte reconstitution during this

process have been mapped and molecular feedback mechanisms between cell types have been proposed (Penit and Vasseur, 1988; Penit and Ezine, 1989; Dudakov et al., 2012; Wertheimer et al., 2018; Kaneko et al., 2019). DP thymocytes form the predominant population affected by irradiation and recently, it has been suggested that their level of apoptosis signals feedback regulation of thymus regeneration in an IL-22-dependent manner (Chidgey et al., 2007; Dudakov et al., 2012; Kinsella and Dudakov, 2020; Kinsella et al., 2021). Accordingly, affected cell populations as well as underlying mechanisms are different in this model of restoration of tissue homeostasis.

In this thesis, we could provide new insights how pre-conditioning affects cell cycle dynamics on various levels such as S-phase kinetics (Figure 29) as well as by elongation of S-phase speed (Figure 30). Up to now, high-resolution cell cycle kinetics in a model of thymic repair were never performed. In difference to the genetic perturbations, where most effects were attributed to the DN3a (CCR7/9 DKO) or DN3b/DN4 stage (miR-17~92$^{\Delta/\Delta}$), upon endogenous repair, DN3a cells were altered in terms of elevated frequencies, higher levels of S-phase entry (Figure 29) and prolonged S-phase duration (Figure 30). In addition, DN3b stage thymocytes were largely unaffected, whereas frequencies of DN4 thymocytes upon irradiation were reduced. Indeed, consistent with DN3a cells, we found a prolonged S-phase duration of DN4 cells (Figure 29 and Figure 30).

To conclude, our results illustrate the remarkable ability of the thymus to maintain tissue homeostasis despite developmental defects or disruptions. In order to better understand population dynamics during T-cell development at steady-state, in CCR7/9- and miR-17~92-deficient mice as well as during regeneration, we established a quantitative high-resolution map of cell cycle dynamics. To this end, we employed dual-nucleoside pulse labeling combined with determination of DNA replication over time. In addition, we used scRNA-seq to obtain information on cell cycle dynamics of rare thymocyte subsets. As indicated above, we currently establish a population-based biomathematical model based on the presented data in order to fully explain cell cycle dynamics during T-cell development. The underlying idea is to bridge the gap of knowledge between experimentally verified statements and predictions. Ultimately, this will help to explain multiple different aspects of T-cell development from a cell cycle’s perspective.

5.2 miR-21: Dynamically expressed in the thymus but largely redundant for intrathymic T-cell development

miRNAs have emerged as key posttranscriptional regulators of the immune system. In light of this, several miRNAs were described as functionally important for T-cell development (Li et al., 2007; Ebert et al., 2009; Ziętara et al., 2013; Regelin et al., 2015; Schaffert et al., 2015; Mildner et al., 2017). Given the dynamic expression of miR-21 during T-cell development (Figure 31) (Neilson et al., 2007; Kuchen et al., 2010; Kirigin et al., 2012), we hypothesized that miR-21 has a regulatory function in the thymus. A commercially available miR-21 knockout mouse model allowed us to determine the role of this miRNA for the development of T cells in the thymus and the maintenance of T cells in the periphery. We complemented our steady-state experiments by competitive bone marrow chimera experiments in the context of miR-21 deficiency and overexpression. In addition, we investigated the function of miR-21 in negative selection *in vivo* as well as in T-cell differentiation in coculture experiments *in vitro*. Furthermore, we assessed a potential role of miR-21 in a model of endogenous regeneration of the thymus after sublethal irradiation to identify implications of miR-21 to regulate cellular stress responses.

Despite being prominently expressed in thymocytes, the role of miR-21 remains elusive. We showed that miR-21 is largely dispensable for intrathymic T-cell development (Kunze-Schumacher et al., 2018) except for some statistically significant differences in frequencies of DN2 as well as Treg cells in miR-21-deficient mice. Given the abrupt decrease in thymic expression levels of miR-21 towards the DP stage prior to re-expression in SP T cells, we further hypothesized a potential role of miR-21 during selection. Indeed, we observed reduced expression levels of CD5 (Figure 35b), a surrogate marker for TCR signal strength (Azzam et al., 1998). To our surprise, functional assays such as anti-CD3-mediated induction of negative selection could not support this hypothesis (Figure 37).

A recent study supports our findings and defines the role of miR-21 in acting as a critical rheostat facilitating the T- and iNKT-cell response towards low-affinity antigens (Fedeli et al., 2021). Especially for iNKT cells, miR-21 is the most highly upregulated miRNA compared to conventional T cells (Fedeli et al., 2009). Surprisingly, absence of miR-21 does not result in altered frequencies of iNKT cells as shown by us and others (Kunze-Schumacher et al., 2018; Fedeli et al., 2021) (Figure 38). In the recent study by Fedeli et al. (2021), miR-21 was identified to sustain CD28-dependent costimulation

pathways and KO mice showed enhanced resistance towards experimental autoimmune encephalomyelitis. These experiments support our findings of miR-21 rather acting in fine-tuning T-cell responses than controlling a particular step of T-cell development. Indeed, miR-21 has previously been described as negative regulator of T-cell activation, survival factor for memory cells as well as downstream effector of PD-1 signaling (Iliopoulos et al., 2011; Smigielska-Czepiel et al., 2013; Carissimi et al., 2014; Wang et al., 2014).

Interestingly, miR-21 transcription is regulated by two promoters: Whereas one is found within its host gene *Vmp1*, another one is located in an intron of *Vmp1* (Ozsolak et al., 2008; Ribas et al., 2012; Wang et al., 2020). A recent study discovered that expression of miR-21 found in immune cells is most likely attributed to the proximal intronic promoter (Rose et al., 2021). Ozsolak et al. proposed a model that suggested the use of proximal promoters to be an orientational consequence of evolution (Ozsolak et al., 2008). In line with this model, miRNAs from longer host transcripts are sustained by closer promoters to ensure high miRNA levels. But what is the consequence of high miR-21 expression? In pathological conditions, miR-21 is well-characterized as genuine oncogene due to its overexpression in many tumor types including neuroblastoma, glioblastoma, colorectal, lung, breast, pancreas, leukemia and lymphoma (Chan et al., 2005; Iorio et al., 2005; Si et al., 2007; Schetter et al., 2008; Hatley et al., 2010; Ma et al., 2011). In line with this, miR-21 is the only miRNA upregulated in six different tumor types among 540 human samples (Volinia et al., 2006). In mice, overexpression of miR-21 induces the formation of a pre-B-cell lymphoma (Medina et al., 2010). Their findings show complete tumor regression after miR-21 inactivation pointing towards miR-21 being a potential target to treat human cancers by pharmacological inhibition. This effect is most likely attributed to miR-21 playing a key role in apoptosis by suppressing cell death (Li et al., 2009; Buscaglia and Li, 2011; Ruan et al., 2014; Song et al., 2017). On the other hand, miR-21 overexpression promoted tumor formation in a non-small-cell lung cancer model (Hatley et al., 2010). Interestingly, this study observed decreased expression of caspase-3 in lung tumors upon overexpression of miR-21 and verified targeting of genes by miR-21 that are involved in apoptosis. In our studies, we detected no difference in levels of cleaved caspase-3 for DP thymocytes in miR-21-sufficient and -deficient mice pointing towards no alterations in apoptosis levels (Figure 37c and d). Conversely, our results evinced a small but statistically significant decrease in the

frequency of late apoptotic cells among SP8 cells upon *ex vivo* culture of thymocytes (Figure 47). Whether this holds true for DN thymocyte stages was not investigated. However, this outcome suggests that thymic miR-21 does not support cell proliferation in physiological settings. In addition, miR-21 is a potential disease target in the cardiovascular system regulating the ERK-MAP kinase signaling pathway in cardiac fibroblasts (Thum et al., 2008). Treatment of mice with miR-21 antagonists rescues mice with diabetic nephropathy (Kölling et al., 2017) and reduces the clinical severity of autoimmune encephalomyelitis, a mouse model of multiple sclerosis (Murugaiyan et al., 2015). Assuming an exclusive role in pathological conditions why is miR-21 prominently expressed in thymocytes? To delve further into this, we investigated the potential role of miR-21 in a model of endogenous thymic regeneration to mimic restoration of immune competence after stress or pre-conditioning for hematopoietic stem cell transplantation (Gruver and Sempowski, 2008). Again, we detected no significant differences in frequencies of DN and DP thymocytes between WT and miR-21-deficient mice indicating that miR-21 is largely dispensable for thymic regeneration (Figure 46). In line with this, a study assessed a potential role of miR-21 in a model of pathological cardiac remodeling as response of the heart towards stress (Patrick et al., 2010). In line with our observations, in the absence of miR-21, cardiac remodeling is not influenced.

In search of an explanation for the apparent discrepancy between dynamic expression but lack of a regulatory function in the thymus, we raise the question whether mechanisms exist that compensate for the absence of miR-21 in our KO mouse model. In line with this, small RNA-seq experiments might shed light on alterations in miRNA networks and could reveal new insights about miRNA composition. We also speculated about cell-context-dependent miRNA binding and function for miR-21 as it was found for miR-155 (Hsin et al., 2018). For miR-155, target genes were differently repressed in dendritic cells, macrophages, B and T cells pointing towards cell-type-specific regulation by this miRNA. Interestingly, alternative cleavage and polyadenylation did not affect miR-155's binding capacity. Especially, shortening of 3′ UTRs through alternative polyadenylation was found to result in the absence of miRNA-binding sites and target de-repression during immune cell activation (Sandberg et al., 2008), but this was not observed for miR-155. A previous study also suggested adenosine methylation on mRNAs to impact miRNA function (Ke et al., 2015). Additionally, altered precursor processing influenced the targets

repressed by a miRNA (Kirigin et al., 2012). For miR-21, the study by Kirigin et al. observed an enormous impact of altered seed sequence on predicted targets. Whether these are possible explanations for miR-21-mediated gene regulation needs to be further investigated. Up to now, comparative target analyses about miR-21 are missing to address these questions.

Consistent with the assumption of a cell-context-dependent mode of action for miR-21, it has been published that miR-21-mediated repression of its targets failed in healthy mouse liver cells while being functional in a tumor cell line. Whereas miR-21 in healthy tissue is selectively absent from mRNAs associated with multiple ribosomes, miR-21's ability to repress its targets in cancer cells is greatly enhanced due to association with polysomes (Androsavich et al., 2012). Interestingly, in healthy liver cells from miR-21-deficient mice or upon pharmacological inhibition of miR-21, absence of target repression was not due to different regulation of canonical seed-matched mRNAs. In line with our speculations about thymic miR-21, activity of miR-21 in the liver appears to be largely restricted to pathological settings such as cancer. Furthermore, miR-21 seems to act in a threshold-like manner ranging from a weak silencer in healthy tissue to a broad repressor with enhanced RNA silencing activity upon overexpression in cancer. Whether thymic miR-21 lacks association with polysomes has to be further elucidated.

A possible explanation for differential ribosomal occupancy and the absence of a clear phenotype for miR-21 in the thymus is given by two recent studies that both consider association of a particular miRNA with either low or high molecular weight RNA-induced silencing complexes (RISCs) thereby exerting different regulatory function (La Rocca et al., 2015; Toivakka et al., 2020). Low molecular weight RISCs refer to miRNAs bound to Argonaute proteins in the absence of association with other RISC components. In consequence, association with its target mRNA is hampered and miRNAs appear inactive. Whereas resting T cells predominantly contain low molecular weight RISCs, upon activation of T cells, these RISCs assemble with additional proteins, mRNA and the translation machinery to high molecular weight RISCs. Thereby, target repression by miRNAs is ensured while levels of total miR expression are constant (La Rocca et al., 2015; Toivakka et al., 2020). However, at least some miRNAs seem to favor one association over the other (Toivakka et al., 2020). To investigate RISC assembly, determination of molecular weight profiles of Argonaute proteins in WT thymi using Superose 6-based size exclusion chromatography could

be performed. Hence, we hypothesized that miR-21 is mostly found in low molecular weight RISC in the thymus. Furthermore, these studies underline that a dynamic expression is not predictive of the capacity of a given miRNA to repress its targets. Taking this into account, the lack of an apparent phenotype for miR-21 can be explained by a lack of association with its target mRNA. Indeed, miR-21 in activated T cells was still mostly associated with low molecular weight RISCs (La Rocca et al., 2015). Additionally, miR-21 in thyroid cancer cell lines was mostly detected in low molecular weight RISCs and the least abundant miRNA in high molecular RISC fractions (Powell et al., 2020).

In addition, it has been demonstrated that 5’-end phosphorylation of a miRNA is crucial for its incorporation into the RISC (Salzman et al., 2016). Accordingly, mature miR-34 was found to be mostly inactive due to the lack of 5'-phosphate. Interestingly, upon demand (e.g. DNA damage), this inactive pool of existing transcribed miR-34 was then rapidly activated through phosphorylation. Further experiments such as northern blotting to assess 5’-end phosphorylation status are required to investigate whether miR-21 is also mostly found in an inactive form in the thymus.

In conclusion, the role of miR-21 in the thymus is still enigmatic. It has to be further elucidated how miR-21 is post-transcriptionally modified to fully explain the functional limitation of this miRNA under normal physiological conditions despite prominent and dynamic expression in the thymus. Finally, we would like to share the title of a commentary reflecting this part of the thesis: “The magic and mystery of miR-21” (Morrisey, 2010).

6 References

Adolfsson, J., Månsson, R., Buza-Vidas, N., Hultquist, A., Liuba, K., Jensen, C.T., Bryder, D., Yang, L., Borge, O.-J., and Thoren, L.A.M., et al. (2005). Identification of Flt3+ lympho-myeloid stem cells lacking erythro-megakaryocytic potential a revised road map for adult blood lineage commitment. *Cell* 121, 295-306

Aifantis, I., Mandal, M., Sawai, K., Ferrando, A., and Vilimas, T. (2006). Regulation of T-cell progenitor survival and cell-cycle entry by the pre-T-cell receptor. *Immunological reviews* 209, 159-169

Akinduro, O., Weber, T.S., Ang, H., Haltalli, M.L.R., Ruivo, N., Duarte, D., Rashidi, N.M., Hawkins, E.D., Duffy, K.R., and Lo Celso, C. (2018). Proliferation dynamics of acute myeloid leukaemia and haematopoietic progenitors competing for bone marrow space. *Nature communications* 9, 519

Allman, D., Sambandam, A., Kim, S., Miller, J.P., Pagan, A., Well, D., Meraz, A., and Bhandoola, A. (2003). Thymopoiesis independent of common lymphoid progenitors. *Nature immunology* 4, 168-174

Amado, T., Amorim, A., Enguita, F.J., Romero, P.V., Inácio, D., Miranda, M.P. de, Winter, S.J., Simas, J.P., Krueger, A., and Schmolka, N., et al. (2020). MicroRNA-181a regulates IFN-γ expression in effector CD8+ T cell differentiation. *Journal of molecular medicine (Berlin, Germany)* 98, 309-320

Androsavich, J.R., Chau, B.N., Bhat, B., Linsley, P.S., and Walter, N.G. (2012). Disease-linked microRNA-21 exhibits drastically reduced mRNA binding and silencing activity in healthy mouse liver. *RNA (New York, N.Y.)* 18, 1510-1526

Asangani, I.A., Rasheed, S.A.K., Nikolova, D.A., Leupold, J.H., Colburn, N.H., Post, S., and Allgayer, H. (2008). MicroRNA-21 (miR-21) post-transcriptionally downregulates tumor suppressor Pdcd4 and stimulates invasion, intravasation and metastasis in colorectal cancer. *Oncogene* 27, 2128-2136

Azzam, H.S., Grinberg, A., Lui, K., Shen, H., Shores, E.W., and Love, P.E. (1998). CD5 expression is developmentally regulated by T cell receptor (TCR) signals and TCR avidity. *The Journal of experimental medicine* 188, 2301-2311

Baron, C., and Pénit, C. (1990). Study of the thymocyte cell cycle by bivariate analysis of incorporated bromodeoxyuridine and DNA content. *European journal of immunology* 20, 1231-1236

Baumjohann, D., and Ansel, K.M. (2013). MicroRNA-mediated regulation of T helper cell differentiation and plasticity. *Nature reviews. Immunology* 13, 666-678

Baumjohann, D., and Ansel, K.M. (2014). MicroRNA regulation of the germinal center response. *Current opinion in immunology* 28, 6-11

Begg, A.C., McNally, N.J., Shrieve, D.C., and Kärcher, H. (1985). A method to measure the duration of DNA synthesis and the potential doubling time from a single sample. *Cytometry* 6, 620-626

Bell, J.J., and Bhandoola, A. (2008). The earliest thymic progenitors for T cells possess myeloid lineage potential. *Nature* 452, 764-767

Benz, C., Heinzel, K., and Bleul, C.C. (2004). Homing of immature thymocytes to the subcapsular microenvironment within the thymus is not an absolute requirement for T cell development. *European journal of immunology* 34, 3652-3663

Besseyrias, V., Fiorini, E., Strobl, L.J., Zimber-Strobl, U., Dumortier, A., Koch, U., Arcangeli, M.-L., Ezine, S., Macdonald, H.R., and Radtke, F. (2007). Hierarchy of Notch-Delta interactions promoting T cell lineage commitment and maturation. *The Journal of experimental medicine* 204, 331-343

Bhandoola, A., Boehmer, H. von, Petrie, H.T., and Zúñiga-Pflücker, J.C. (2007). Commitment and developmental potential of extrathymic and intrathymic T cell precursors: plenty to choose from. *Immunity* 26, 678-689

Blume, J., Ziętara, N., Witzlau, K., Liu, Y., Sanchez, O.O., Puchałka, J., Winter, S.J., Kunze-Schumacher, H., Saran, N., and Düber, S., et al. (2019). miR-191 modulates B-cell development and targets transcription factors E2A, Foxp1, and Egr1. *European journal of immunology* 49, 121-132

Blume, J., zur Lage, S., Witzlau, K., Georgiev, H., Weiss, S., Łyszkiewicz, M., Ziętara, N., and Krueger, A. (2016). Overexpression of Vα14Jα18 TCR promotes development of iNKT cells in the absence of miR-181a/b-1. *Immunology and cell biology* 94, 741-746

Boer, R.J. de, Ganusov, V.V., Milutinović, D., Hodgkin, P.D., and Perelson, A.S. (2006). Estimating lymphocyte division and death rates from CFSE data. *Bulletin of mathematical biology* 68, 1011-1031

Bradford, J.A., and Clarke, S.T. (2011). Dual-pulse labeling using 5-ethynyl-2'-deoxyuridine (EdU) and 5-bromo-2'-deoxyuridine (BrdU) in flow cytometry. *Current protocols in cytometry* Chapter 7, Unit 7.38

Buchholz, V.R., Schumacher, T.N.M., and Busch, D.H. (2016). T Cell Fate at the Single-Cell Level. *Annual review of immunology* 34, 65-92

Buscaglia, L.E.B., and Li, Y. (2011). Apoptosis and the target genes of microRNA-21. *Chinese journal of cancer* 30, 371-380

Busch, K., Klapproth, K., Barile, M., Flossdorf, M., Holland-Letz, T., Schlenner, S.M., Reth, M., Höfer, T., and Rodewald, H.-R. (2015). Fundamental properties of unperturbed haematopoiesis from stem cells in vivo. *Nature* 518, 542-546

Butler, A., Hoffman, P., Smibert, P., Papalexi, E., and Satija, R. (2018). Integrating single-cell transcriptomic data across different conditions, technologies, and species. *Nature biotechnology* 36, 411-420

Cai, X., Hagedorn, C.H., and Cullen, B.R. (2004). Human microRNAs are processed from capped, polyadenylated transcripts that can also function as mRNAs. *RNA (New York, N.Y.)* 10, 1957-1966

Carissimi, C., Carucci, N., Colombo, T., Piconese, S., Azzalin, G., Cipolletta, E., Citarella, F., Barnaba, V., Macino, G., and Fulci, V. (2014). miR-21 is a negative modulator of T-cell activation. *Biochimie* 107 Pt B, 319-326

Carmona, L.M., Fugmann, S.D., and Schatz, D.G. (2016). Collaboration of RAG2 with RAG1-like proteins during the evolution of V(D)J recombination. *Genes & development* 30, 909-917

Ceredig, R., Lowenthal, J.W., Nabholz, M., and MacDonald, H.R. (1985). Expression of interleukin-2 receptors as a differentiation marker on intrathymic stem cells. *Nature* 314, 98-100

Chan, J.A., Krichevsky, A.M., and Kosik, K.S. (2005). MicroRNA-21 is an antiapoptotic factor in human glioblastoma cells. *Cancer research* 65, 6029-6033

Chen, C.-Z., Li, L., Lodish, H.F., and Bartel, D.P. (2004). MicroRNAs modulate hematopoietic lineage differentiation. *Science (New York, N.Y.)* 303, 83-86

Chen, E.L.Y., Thompson, P.K., and Zúñiga-Pflücker, J.C. (2019). RBPJ-dependent Notch signaling initiates the T cell program in a subset of thymus-seeding progenitors. *Nature immunology* 20, 1456-1468

Chidgey, A., Dudakov, J., Seach, N., and Boyd, R. (2007). Impact of niche aging on thymic regeneration and immune reconstitution. *Seminars in immunology* 19, 331-340

Cobb, B.S., Nesterova, T.B., Thompson, E., Hertweck, A., O'Connor, E., Godwin, J., Wilson, C.B., Brockdorff, N., Fisher, A.G., and Smale, S.T., et al. (2005). T cell lineage choice and differentiation in the absence of the RNase III enzyme Dicer. *The Journal of experimental medicine* 201, 1367-1373

Cossarizza, A., Chang, H.-D., Radbruch, A., Abrignani, S., Addo, R., Akdis, M., Andrä, I., Andreata, F., Annunziato, F., and Arranz, E., et al. (2021). Guidelines for the use of flow cytometry and cell sorting in immunological studies (third edition). *European journal of immunology* online version

Cossarizza, A., Chang, H.-D., Radbruch, A., Acs, A., Adam, D., Adam-Klages, S., Agace, W.W., Aghaeepour, N., Akdis, M., and Allez, M., et al. (2019). Guidelines for the use of flow cytometry and cell sorting in immunological studies (second edition). *European journal of immunology* 49, 1457-1973

Davalos-Misslitz, A.C.M., Worbs, T., Willenzon, S., Bernhardt, G., and Förster, R. (2007). Impaired responsiveness to T-cell receptor stimulation and defective negative selection of thymocytes in CCR7-deficient mice. *Blood* 110, 4351-4359

Dong, L., Wang, X., Tan, J., Li, H., Qian, W., Chen, J., Chen, Q., Wang, J., Xu, W., and Tao, C., et al. (2014). Decreased expression of microRNA-21 correlates with the imbalance of Th17 and Treg cells in patients with rheumatoid arthritis. *Journal of cellular and molecular medicine* 18, 2213-2224

Dose, M., Khan, I., Guo, Z., Kovalovsky, D., Krueger, A., Boehmer, H. von, Khazaie, K., and Gounari, F. (2006). c-Myc mediates pre-TCR-induced proliferation but not developmental progression. *Blood* 108, 2669-2677

Dudakov, J.A., Hanash, A.M., Jenq, R.R., Young, L.F., Ghosh, A., Singer, N.V., West, M.L., Smith, O.M., Holland, A.M., and Tsai, J.J., et al. (2012). Interleukin-22 drives endogenous thymic regeneration in mice. *Science (New York, N.Y.)* 336, 91-95

Ebert, P.J.R., Jiang, S., Xie, J., Li, Q.-J., and Davis, M.M. (2009). An endogenous positively selecting peptide enhances mature T cell responses and becomes an autoantigen in the absence of microRNA miR-181a. *Nature immunology* 10, 1162-1169

Eddaoudi, A., Canning, S.L., and Kato, I. (2018). Flow Cytometric Detection of G0 in Live Cells by Hoechst 33342 and Pyronin Y Staining. *Methods in molecular biology (Clifton, N.J.)* 1686, 49-57

Egerton, M., Scollay, R., and Shortman, K. (1990). Kinetics of mature T-cell development in the thymus. *Proceedings of the National Academy of Sciences of the United States of America* 87, 2579-2582

Fedeli, M., Kuka, M., Finardi, A., Albano, F., Viganò, V., Iannacone, M., Furlan, R., Dellabona, P., and Casorati, G. (2021). miR-21 sustains CD28 signalling and low-affinity T-cell responses at the expense of self-tolerance. *Clinical & translational immunology* 10, e1321

Fedeli, M., Napolitano, A., Wong, M.P.M., Marcais, A., Lalla, C. de, Colucci, F., Merkenschlager, M., Dellabona, P., and Casorati, G. (2009). Dicer-dependent microRNA pathway controls invariant NKT cell development. *Journal of immunology (Baltimore, Md. : 1950)* 183, 2506-2512

Fischer, D.S., Fiedler, A.K., Kernfeld, E.M., Genga, R.M.J., Bastidas-Ponce, A., Bakhti, M., Lickert, H., Hasenauer, J., Maehr, R., and Theis, F.J. (2019). Inferring population dynamics from single-cell RNA-sequencing time series data. *Nature biotechnology* 37, 461-468

Flommersfeld, S., Böttcher, J.P., Ersching, J., Flossdorf, M., Meiser, P., Pachmayr, L.O., Leube, J., Hensel, I., Jarosch, S., and Zhang, Q., et al. (2021). Fate mapping of single NK cells identifies a type 1 innate lymphoid-like lineage that bridges innate and adaptive recognition of viral infection. *Immunity* 54, 2288-2304.e7

Frankel, L.B., Christoffersen, N.R., Jacobsen, A., Lindow, M., Krogh, A., and Lund, A.H. (2008). Programmed cell death 4 (PDCD4) is an important functional target of the microRNA miR-21 in breast cancer cells. *The Journal of biological chemistry* 283, 1026-1033

Freeden-Jeffry, U. von, Solvason, N., Howard, M., and Murray, R. (1997). The earliest T lineage-committed cells depend on IL-7 for Bcl-2 expression and normal cell cycle progression. *Immunity* 7, 147-154

Fujimaki, K., Li, R., Chen, H., Della Croce, K., Zhang, H.H., Xing, J., Bai, F., and Yao, G. (2019). Graded regulation of cellular quiescence depth between proliferation and senescence by a lysosomal dimmer switch. *Proceedings of the National Academy of Sciences of the United States of America* 116, 22624-22634

Ganusov, V.V., Pilyugin, S.S., Boer, R.J. de, Murali-Krishna, K., Ahmed, R., and Antia, R. (2005). Quantifying cell turnover using CFSE data. *Journal of immunological methods* 298, 183-200

Germar, K., Dose, M., Konstantinou, T., Zhang, J., Wang, H., Lobry, C., Arnett, K.L., Blacklow, S.C., Aifantis, I., and Aster, J.C., et al. (2011). T-cell factor 1 is a

gatekeeper for T-cell specification in response to Notch signaling. *Proceedings of the National Academy of Sciences of the United States of America* 108, 20060-20065

Gitlin, A.D., Mayer, C.T., Oliveira, T.Y., Shulman, Z., Jones, M.J.K., Koren, A., and Nussenzweig, M.C. (2015). HUMORAL IMMUNITY. T cell help controls the speed of the cell cycle in germinal center B cells. *Science (New York, N.Y.)* 349, 643-646

Gitlin, A.D., Shulman, Z., and Nussenzweig, M.C. (2014). Clonal selection in the germinal centre by regulated proliferation and hypermutation. *Nature* 509, 637-640

Glaesener, S., Jaenke, C., Habener, A., Geffers, R., Hagendorff, P., Witzlau, K., Imelmann, E., Krueger, A., and Meyer-Bahlburg, A. (2018). Decreased production of class-switched antibodies in neonatal B cells is associated with increased expression of miR-181b. *PloS one* 13, e0192230

Godfrey, D.I., Kennedy, J., Mombaerts, P., Tonegawa, S., and Zlotnik, A. (1994). Onset of TCR-beta gene rearrangement and role of TCR-beta expression during CD3-CD4-CD8- thymocyte differentiation. *Journal of immunology (Baltimore, Md. : 1950)* 152, 4783-4792

Godfrey, D.I., Kennedy, J., Suda, T., and Zlotnik, A. (1993). A developmental pathway involving four phenotypically and functionally distinct subsets of CD3-CD4-CD8- triple-negative adult mouse thymocytes defined by CD44 and CD25 expression. *Journal of immunology (Baltimore, Md. : 1950)* 150, 4244-4252

Gossens, K., Naus, S., Corbel, S.Y., Lin, S., Rossi, F.M.V., Kast, J., and Ziltener, H.J. (2009). Thymic progenitor homing and lymphocyte homeostasis are linked via S1P-controlled expression of thymic P-selectin/CCL25. *The Journal of experimental medicine* 206, 761-778

Grewers, Z., and Krueger, A. (2020). MicroRNA miR-181-A Rheostat for TCR Signaling in Thymic Selection and Peripheral T-Cell Function. *International journal of molecular sciences* 21

Grimson, A., Farh, K.K.-H., Johnston, W.K., Garrett-Engele, P., Lim, L.P., and Bartel, D.P. (2007). MicroRNA targeting specificity in mammals: determinants beyond seed pairing. *Molecular cell* 27, 91-105

Groettrup, M., Ungewiss, K., Azogui, O., Palacios, R., Owen, M.J., Hayday, A.C., and Boehmer, H. von (1993). A novel disulfide-linked heterodimer on pre-T cells consists of the T cell receptor beta chain and a 33 kd glycoprotein. *Cell* 75, 283-294

Gruver, A.L., and Sempowski, G.D. (2008). Cytokines, leptin, and stress-induced thymic atrophy. *Journal of leukocyte biology* 84, 915-923

Guo, H., Ingolia, N.T., Weissman, J.S., and Bartel, D.P. (2010). Mammalian microRNAs predominantly act to decrease target mRNA levels. *Nature* 466, 835-840

Haas, J.D., Nistala, K., Petermann, F., Saran, N., Chennupati, V., Schmitz, S., Korn, T., Wedderburn, L.R., Förster, R., and Krueger, A., et al. (2011). Expression of miRNAs miR-133b and miR-206 in the Il17a/f locus is co-regulated with IL-17 production in αβ and γδ T cells. *PloS one* 6, e20171

Hackett, E.E., and Sheedy, F.J. (2017). miR-21 alters circulating Treg function in vascular disease-hope for restoring immunoregulatory responses in atherosclerosis? *Annals of translational medicine* 5, 21

Hagan, M.P. (1984). Cell proliferation kinetics analyzed with BrdU and near-UV light treatment. *Bibliotheca haematologica*, 384-401

Hartwell, L.H., and Weinert, T.A. (1989). Checkpoints: controls that ensure the order of cell cycle events. *Science (New York, N.Y.)* 246, 629-634

Hatley, M.E., Patrick, D.M., Garcia, M.R., Richardson, J.A., Bassel-Duby, R., van Rooij, E., and Olson, E.N. (2010). Modulation of K-Ras-dependent lung tumorigenesis by MicroRNA-21. *Cancer cell* 18, 282-293

Hayday, A.C., and Pennington, D.J. (2007). Key factors in the organized chaos of early T cell development. *Nature immunology* 8, 137-144

He, L., Thomson, J.M., Hemann, M.T., Hernando-Monge, E., Mu, D., Goodson, S., Powers, S., Cordon-Cardo, C., Lowe, S.W., and Hannon, G.J., et al. (2005). A microRNA polycistron as a potential human oncogene. *Nature* 435, 828-833

Heinzel, S., Marchingo, J.M., Horton, M.B., and Hodgkin, P.D. (2018). The regulation of lymphocyte activation and proliferation. *Current opinion in immunology* 51, 32-38

Hoffman, E.S., Passoni, L., Crompton, T., Leu, T.M., Schatz, D.G., Koff, A., Owen, M.J., and Hayday, A.C. (1996). Productive T-cell receptor beta-chain gene rearrangement: coincident regulation of cell cycle and clonality during development in vivo. *Genes & development* 10, 948-962

Hosokawa, H., and Rothenberg, E.V. (2021). How transcription factors drive choice of the T cell fate. *Nature reviews. Immunology* 21, 162-176

Howard, A., and Pelc, S.R. (1986). Synthesis of Desoxyribonucleic Acid in Normal and Irradiated Cells and Its Relation to Chromosome Breakage. *International Journal of Radiation Biology and Related Studies in Physics, Chemistry and Medicine* 49, 207-218

Hozumi, K., Mailhos, C., Negishi, N., Hirano, K., Yahata, T., Ando, K., Zuklys, S., Holländer, G.A., Shima, D.T., and Habu, S. (2008). Delta-like 4 is indispensable in thymic environment specific for T cell development. *The Journal of experimental medicine* 205, 2507-2513

Hsin, J.-P., Lu, Y., Loeb, G.B., Leslie, C.S., and Rudensky, A.Y. (2018). The effect of cellular context on miR-155-mediated gene regulation in four major immune cell types. *Nature immunology* 19, 1137-1145

Huesmann, M., Scott, B., Kisielow, P., and Boehmer, H. von (1991). Kinetics and efficacy of positive selection in the thymus of normal and T cell receptor transgenic mice. *Cell* 66, 533-540

Huiskamp, R., and van Ewijk, W. (1985). Repopulation of the mouse thymus after sublethal fission neutron irradiation. I. Sequential appearance of thymocyte subpopulations. *Journal of immunology (Baltimore, Md. : 1950)* 134, 2161-2169

Igarashi, H., Gregory, S.C., Yokota, T., Sakaguchi, N., and Kincade, P.W. (2002). Transcription from the RAG1 locus marks the earliest lymphocyte progenitors in bone marrow. *Immunity* 17, 117-130

Ikawa, T., Hirose, S., Masuda, K., Kakugawa, K., Satoh, R., Shibano-Satoh, A., Kominami, R., Katsura, Y., and Kawamoto, H. (2010). An essential developmental checkpoint for production of the T cell lineage. *Science (New York, N.Y.)* 329, 93-96

Iliopoulos, D., Kavousanaki, M., Ioannou, M., Boumpas, D., and Verginis, P. (2011). The negative costimulatory molecule PD-1 modulates the balance between immunity and tolerance via miR-21. *European journal of immunology* 41, 1754-1763

Iorio, M.V., Ferracin, M., Liu, C.-G., Veronese, A., Spizzo, R., Sabbioni, S., Magri, E., Pedriali, M., Fabbri, M., and Campiglio, M., et al. (2005). MicroRNA gene expression deregulation in human breast cancer. *Cancer research* 65, 7065-7070

Jackson, P.K. (2008). The hunt for cyclin. *Cell* 134, 199-202

Kadish, J.L., and Basch, R.S. (1975). Thymic regeneration after lethal irradiation evidence for an intra-thymic radioresistant T cell precursor. *Journal of immunology (Baltimore, Md. : 1950)* 114, 452-458

Kaneko, K.B., Tateishi, R., Miyao, T., Takakura, Y., Akiyama, N., Yokota, R., Akiyama, T., and Kobayashi, T.J. (2019). Quantitative analysis reveals reciprocal regulations underlying recovery dynamics of thymocytes and thymic environment in mice. *Communications biology* 2, 444

Ke, S., Alemu, E.A., Mertens, C., Gantman, E.C., Fak, J.J., Mele, A., Haripal, B., Zucker-Scharff, I., Moore, M.J., and Park, C.Y., et al. (2015). A majority of m6A residues are in the last exons, allowing the potential for 3' UTR regulation. *Genes & development* 29, 2037-2053

Kertesz, M., Iovino, N., Unnerstall, U., Gaul, U., and Segal, E. (2007). The role of site accessibility in microRNA target recognition. *Nature genetics* 39, 1278-1284

Kim, K.H., and Sederstrom, J.M. (2015). Assaying Cell Cycle Status Using Flow Cytometry. *Current protocols in molecular biology* 111, 28.6.1-28.6.11

Kinsella, S., and Dudakov, J.A. (2020). When the Damage Is Done: Injury and Repair in Thymus Function. *Frontiers in immunology* 11, 1745

Kinsella, S., Evandy, C.A., Cooper, K., Iovino, L., deRoos, P.C., Hopwo, K.S., Granadier, D.W., Smith, C.W., Rafii, S., and Dudakov, J.A. (2021). Attenuation of apoptotic cell detection triggers thymic regeneration after damage. *Cell Reports* 37, 109789

Kirigin, F.F., Lindstedt, K., Sellars, M., Ciofani, M., Low, S.L., Jones, L., Bell, F., Pauli, F., Bonneau, R., and Myers, R.M., et al. (2012). Dynamic microRNA gene transcription and processing during T cell development. *Journal of immunology (Baltimore, Md. : 1950)* 188, 3257-3267

Koch, U., Fiorini, E., Benedito, R., Besseyrias, V., Schuster-Gossler, K., Pierres, M., Manley, N.R., Duarte, A., Macdonald, H.R., and Radtke, F. (2008). Delta-like 4 is the essential, nonredundant ligand for Notch1 during thymic T cell lineage commitment. *The Journal of experimental medicine* 205, 2515-2523

Koenecke, C., and Krueger, A. (2018). MicroRNA in T-Cell Development and T-Cell Mediated Acute Graft-Versus-Host Disease. *Frontiers in immunology* 9, 992

Kölling, M., Kaucsar, T., Schauerte, C., Hübner, A., Dettling, A., Park, J.-K., Busch, M., Wulff, X., Meier, M., and Scherf, K., et al. (2017). Therapeutic miR-21 Silencing Ameliorates Diabetic Kidney Disease in Mice. *Molecular therapy : the journal of the American Society of Gene Therapy* 25, 165-180

Kozar, K., Ciemerych, M.A., Rebel, V.I., Shigematsu, H., Zagozdzon, A., Sicinska, E., Geng, Y., Yu, Q., Bhattacharya, S., and Bronson, R.T., et al. (2004). Mouse development and cell proliferation in the absence of D-cyclins. *Cell* 118, 477-491

Kreslavsky, T., Gleimer, M., Miyazaki, M., Choi, Y., Gagnon, E., Murre, C., Sicinski, P., and Boehmer, H. von (2012). β-Selection-induced proliferation is required for αβ T cell differentiation. *Immunity* 37, 840-853

Krueger, A. (2011). A missing link in thymic dendritic cell development. *European journal of immunology* 41, 2145-2147

Krueger, A. (2018). Thymus Colonization: Who, How, How Many? *Archivum immunologiae et therapiae experimentalis* 66, 81-88

Krueger, A., and Boehmer, H. von (2007). Identification of a T lineage-committed progenitor in adult blood. *Immunity* 26, 105-116

Krueger, A., Garbe, A.I., and Boehmer, H. von (2006). Phenotypic plasticity of T cell progenitors upon exposure to Notch ligands. *The Journal of experimental medicine* 203, 1977-1984

Krueger, A., Willenzon, S., Lyszkiewicz, M., Kremmer, E., and Förster, R. (2010). CC chemokine receptor 7 and 9 double-deficient hematopoietic progenitors are severely impaired in seeding the adult thymus. *Blood* 115, 1906-1912

Krueger, A., Ziętara, N., and Łyszkiewicz, M. (2017). T Cell Development by the Numbers. *Trends in immunology* 38, 128-139

Kuchen, S., Resch, W., Yamane, A., Kuo, N., Li, Z., Chakraborty, T., Wei, L., Laurence, A., Yasuda, T., and Peng, S., et al. (2010). Regulation of microRNA expression and abundance during lymphopoiesis. *Immunity* 32, 828-839

Kueh, H.Y., Champhekar, A., Champhekhar, A., Nutt, S.L., Elowitz, M.B., and Rothenberg, E.V. (2013). Positive feedback between PU.1 and the cell cycle controls myeloid differentiation. *Science (New York, N.Y.)* 341, 670-673

Kueh, H.Y., Yui, M.A., Ng, K.K.H., Pease, S.S., Zhang, J.A., Damle, S.S., Freedman, G., Siu, S., Bernstein, I.D., and Elowitz, M.B., et al. (2016). Asynchronous combinatorial action of four regulatory factors activates Bcl11b for T cell commitment. *Nature immunology* 17, 956-965

Kumarswamy, R., Volkmann, I., and Thum, T. (2011). Regulation and function of miRNA-21 in health and disease. *RNA biology* 8, 706-713

Kunze-Schumacher, H., and Krueger, A. (2020). The Role of MicroRNAs in Development and Function of Regulatory T Cells - Lessons for a Better Understanding of MicroRNA Biology. *Frontiers in immunology* 11, 2185

Kunze-Schumacher, H., Winter, S.J., Imelmann, E., and Krueger, A. (2018). miRNA miR-21 Is Largely Dispensable for Intrathymic T-Cell Development. *Frontiers in immunology* 9, 2497

La Rocca, G., Olejniczak, S.H., González, A.J., Briskin, D., Vidigal, J.A., Spraggon, L., DeMatteo, R.G., Radler, M.R., Lindsten, T., and Ventura, A., et al. (2015). In vivo, Argonaute-bound microRNAs exist predominantly in a reservoir of low molecular weight complexes not associated with mRNA. *Proceedings of the National Academy of Sciences of the United States of America* 112, 767-772

Lai, A.Y., and Kondo, M. (2007). Identification of a bone marrow precursor of the earliest thymocytes in adult mouse. *Proceedings of the National Academy of Sciences of the United States of America* 104, 6311-6316

Landgraf, P., Rusu, M., Sheridan, R., Sewer, A., Iovino, N., Aravin, A., Pfeffer, S., Rice, A., Kamphorst, A.O., and Landthaler, M., et al. (2007). A mammalian microRNA expression atlas based on small RNA library sequencing. *Cell* 129, 1401-1414

Lavaert, M., Liang, K.L., Vandamme, N., Park, J.-E., Roels, J., Kowalczyk, M.S., Li, B., Ashenberg, O., Tabaka, M., and Dionne, D., et al. (2020). Integrated scRNA-Seq Identifies Human Postnatal Thymus Seeding Progenitors and Regulatory Dynamics of Differentiating Immature Thymocytes. *Immunity* 52, 1088-1104.e6

Lee, C.-W., Wohlan, K., Dallmann, I., Förster, R., Ganser, A., Krueger, A., Scherr, M., Eder, M., and Koenecke, C. (2016). miR-181a Expression in Donor T Cells Modulates Graft-versus-Host Disease after Allogeneic Bone Marrow Transplantation. *Journal of immunology (Baltimore, Md. : 1950)* 196, 3927-3934

Lee, J., and Desiderio, S. (1999). Cyclin A/CDK2 Regulates V(D)J Recombination by Coordinating RAG-2 Accumulation and DNA Repair. *Immunity* 11, 771-781

Leif, R.C., Stein, J.H., and Zucker, R.M. (2004). A short history of the initial application of anti-5-BrdU to the detection and measurement of S phase. *Cytometry. Part A : the journal of the International Society for Analytical Cytology* 58, 45-52

León, K., Faro, J., and Carneiro, J. (2004). A general mathematical framework to model generation structure in a population of asynchronously dividing cells. *Journal of theoretical biology* 229, 455-476

Li, B., Zhao, H., Rybak, P., Dobrucki, J.W., Darzynkiewicz, Z., and Kimmel, M. (2014). Different rates of DNA replication at early versus late S-phase sections: multiscale modeling of stochastic events related to DNA content/EdU (5-ethynyl-2'deoxyuridine) incorporation distributions. *Cytometry. Part A : the journal of the International Society for Analytical Cytology* 85, 785-797

Li, J., Huang, H., Sun, L., Yang, M., Pan, C., Chen, W., Wu, D., Lin, Z., Zeng, C., and Yao, Y., et al. (2009). MiR-21 indicates poor prognosis in tongue squamous cell carcinomas as an apoptosis inhibitor. *Clinical cancer research : an official journal of the American Association for Cancer Research* 15, 3998-4008

Li, L., Leid, M., and Rothenberg, E.V. (2010a). An early T cell lineage commitment checkpoint dependent on the transcription factor Bcl11b. *Science (New York, N.Y.)* 329, 89-93

Li, P., Burke, S., Wang, J., Chen, X., Ortiz, M., Lee, S.-C., Lu, D., Campos, L., Goulding, D., and Ng, B.L., et al. (2010b). Reprogramming of T cells to natural killer-like cells upon Bcl11b deletion. *Science (New York, N.Y.)* 329, 85-89

Li, Q.-J., Chau, J., Ebert, P.J.R., Sylvester, G., Min, H., Liu, G., Braich, R., Manoharan, M., Soutschek, J., and Skare, P., et al. (2007). miR-181a is an intrinsic modulator of T cell sensitivity and selection. *Cell* 129, 147-161

Li, Z., Dordai, D.I., Lee, J., and Desiderio, S. (1996). A Conserved Degradation Signal Regulates RAG-2 Accumulation during Cell Division and Links V(D)J Recombination to the Cell Cycle. *Immunity* 5, 575-589

Lind, E.F., Prockop, S.E., Porritt, H.E., and Petrie, H.T. (2001). Mapping precursor movement through the postnatal thymus reveals specific microenvironments supporting defined stages of early lymphoid development. *The Journal of experimental medicine* 194, 127-134

Liu, C., Saito, F., Liu, Z., Lei, Y., Uehara, S., Love, P., Lipp, M., Kondo, S., Manley, N., and Takahama, Y. (2006a). Coordination between CCR7- and CCR9-mediated chemokine signals in prevascular fetal thymus colonization. *Blood* 108, 2531-2539

Liu, Y., Goff, R.D., Zhou, D., Mattner, J., Sullivan, B.A., Khurana, A., Cantu, C., Ravkov, E.V., Ibegbu, C.C., and Altman, J.D., et al. (2006b). A modified alpha-galactosyl ceramide for staining and stimulating natural killer T cells. *Journal of immunological methods* 312, 34-39

Löffler, D., Brocke-Heidrich, K., Pfeifer, G., Stocsits, C., Hackermüller, J., Kretzschmar, A.K., Burger, R., Gramatzki, M., Blumert, C., and Bauer, K., et al. (2007). Interleukin-6 dependent survival of multiple myeloma cells involves the Stat3-mediated induction of microRNA-21 through a highly conserved enhancer. *Blood* 110, 1330-1333

Lu, Z., Liu, M., Stribinskis, V., Klinge, C.M., Ramos, K.S., Colburn, N.H., and Li, Y. (2008). MicroRNA-21 promotes cell transformation by targeting the programmed cell death 4 gene. *Oncogene* 27, 4373-4379

Lucas, B., James, K.D., Cosway, E.J., Parnell, S.M., Tumanov, A.V., Ware, C.F., Jenkinson, W.E., and Anderson, G. (2016). Lymphotoxin β Receptor Controls T Cell Progenitor Entry to the Thymus. *Journal of immunology (Baltimore, Md. : 1950)* 197, 2665-2672

Lucas, B., Vasseur, F., and Penit, C. (1993). Normal sequence of phenotypic transitions in one cohort of 5-bromo-2'-deoxyuridine-pulse-labeled thymocytes. Correlation with T cell receptor expression. *Journal of immunology (Baltimore, Md. : 1950)* 151, 4574-4582

Lucas, B., Vasseur, F., and Penit, C. (1994). Production, selection, and maturation of thymocytes with high surface density of TCR. *Journal of immunology (Baltimore, Md. : 1950)* 153, 53-62

Lucas, B., Vasseur, F., and Penit, C. (1995). Stochastic coreceptor shut-off is restricted to the CD4 lineage maturation pathway. *The Journal of experimental medicine* 181, 1623-1633

Luis, T.C., Luc, S., Mizukami, T., Boukarabila, H., Thongjuea, S., Woll, P.S., Azzoni, E., Giustacchini, A., Lutteropp, M., and Bouriez-Jones, T., et al. (2016). Initial seeding of the embryonic thymus by immune-restricted lympho-myeloid progenitors. *Nature immunology* 17, 1424-1435

Łyszkiewicz, M., Winter, S.J., Witzlau, K., Föhse, L., Brownlie, R., Puchałka, J., Verheyden, N.A., Kunze-Schumacher, H., Imelmann, E., and Blume, J., et al. (2019). miR-181a/b-1 controls thymic selection of Treg cells and tunes their suppressive capacity. *PLoS biology* 17, e2006716

Łyszkiewicz, M., Ziętara, N., Föhse, L., Puchałka, J., Diestelhorst, J., Witzlau, K., Prinz, I., Schambach, A., and Krueger, A. (2015). Limited niche availability suppresses murine intrathymic dendritic-cell development from noncommitted progenitors. *Blood* 125, 457-464

Ma, X., Kumar, M., Choudhury, S.N., Becker Buscaglia, L.E., Barker, J.R., Kanakamedala, K., Liu, M.-F., and Li, Y. (2011). Loss of the miR-21 allele elevates the expression of its target genes and reduces tumorigenesis. *Proceedings of the National Academy of Sciences of the United States of America* 108, 10144-10149

MacDonald, H.R., Budd, R.C., and Howe, R.C. (1988). A CD3- subset of CD4-8+ thymocytes: a rapidly cycling intermediate in the generation of CD4+8+ cells. *European journal of immunology* 18, 519-523

Manesso, E., Chickarmane, V., Kueh, H.Y., Rothenberg, E.V., and Peterson, C. (2013). Computational modelling of T-cell formation kinetics: output regulated by initial proliferation-linked deferral of developmental competence. *Journal of the Royal Society, Interface* 10, 20120774

Martin, C.H., Aifantis, I., Scimone, M.L., Andrian, U.H. von, Reizis, B., Boehmer, H. von, and Gounari, F. (2003). Efficient thymic immigration of B220+ lymphoid-restricted bone marrow cells with T precursor potential. *Nature immunology* 4, 866-873

Massa, S., Balciunaite, G., Ceredig, R., and Rolink, A.G. (2006). Critical role for c-kit (CD117) in T cell lineage commitment and early thymocyte development in vitro. *European journal of immunology* 36, 526-532

Matiašová, A., Sevc, J., Mikeš, J., Jendželovský, R., Daxnerová, Z., and Fedoročko, P. (2014). Flow cytometric determination of 5-bromo-2'-deoxyuridine pharmacokinetics in blood serum after intraperitoneal administration to rats and mice. *Histochemistry and cell biology* 142, 703-712

Matsuzaki, Y., Gyotoku, J., Ogawa, M., Nishikawa, S., Katsura, Y., Gachelin, G., and Nakauchi, H. (1993). Characterization of c-kit positive intrathymic stem cells that are restricted to lymphoid differentiation. *The Journal of experimental medicine* 178, 1283-1292

Mavrakis, K.J., Wolfe, A.L., Oricchio, E., Palomero, T., Keersmaecker, K. de, McJunkin, K., Zuber, J., James, T., Khan, A.A., and Leslie, C.S., et al. (2010). Genome-wide RNA-mediated interference screen identifies miR-19 targets in Notch-induced T-cell acute lymphoblastic leukaemia. *Nature cell biology* 12, 372-379

McCaughtry, T.M., Baldwin, T.A., Wilken, M.S., and Hogquist, K.A. (2008). Clonal deletion of thymocytes can occur in the cortex with no involvement of the medulla. *The Journal of experimental medicine* 205, 2575-2584

Medina, P.P., Nolde, M., and Slack, F.J. (2010). OncomiR addiction in an in vivo model of microRNA-21-induced pre-B-cell lymphoma. *Nature* 467, 86-90

Meyer, A., Herkt, S., Kunze-Schumacher, H., Kohrs, N., Ringleb, J., Schneider, L., Kuvardina, O.N., Oellerich, T., Häupl, B., and Krueger, A., et al. (2020). The transcription factor TAL1 and miR-17-92 create a regulatory loop in hematopoiesis. *Scientific reports* 10, 21438

Mildner, A., Chapnik, E., Varol, D., Aychek, T., Lampl, N., Rivkin, N., Bringmann, A., Paul, F., Boura-Halfon, S., and Hayoun, Y.S., et al. (2017). MicroRNA-142 controls thymocyte proliferation. *European journal of immunology* 47, 1142-1152

Miller, I., Min, M., Yang, C., Tian, C., Gookin, S., Carter, D., and Spencer, S.L. (2018). Ki67 is a Graded Rather than a Binary Marker of Proliferation versus Quiescence. *Cell Reports* 24, 1105-1112.e5

Miller, J. (1961). Immunological function of the thymus. *The Lancet* 278, 748-749

Mingueneau, M., Kreslavsky, T., Gray, D., Heng, T., Cruse, R., Ericson, J., Bendall, S., Spitzer, M.H., Nolan, G.P., and Kobayashi, K., et al. (2013). The transcriptional landscape of αβ T cell differentiation. *Nature immunology* 14, 619-632

Misslitz, A., Pabst, O., Hintzen, G., Ohl, L., Kremmer, E., Petrie, H.T., and Förster, R. (2004). Thymic T cell development and progenitor localization depend on CCR7. *The Journal of experimental medicine* 200, 481-491

Mori, S., Shortman, K., and Wu, L. (2001). Characterization of thymus-seeding precursor cells from mouse bone marrow. *Blood* 98, 696-704

Morrisey, E.E. (2010). The magic and mystery of miR-21. *The Journal of clinical investigation* 120, 3817-3819

Mu, P., Han, Y.-C., Betel, D., Yao, E., Squatrito, M., Ogrodowski, P., Stanchina, E. de, D'Andrea, A., Sander, C., and Ventura, A. (2009). Genetic dissection of the miR-17~92 cluster of microRNAs in Myc-induced B-cell lymphomas. *Genes & development* 23, 2806-2811

Mukherji, S., Ebert, M.S., Zheng, G.X.Y., Tsang, J.S., Sharp, P.A., and van Oudenaarden, A. (2011). MicroRNAs can generate thresholds in target gene expression. *Nature genetics* 43, 854-859

Murugaiyan, G., da Cunha, A.P., Ajay, A.K., Joller, N., Garo, L.P., Kumaradevan, S., Yosef, N., Vaidya, V.S., and Weiner, H.L. (2015). MicroRNA-21 promotes Th17 differentiation and mediates experimental autoimmune encephalomyelitis. *The Journal of clinical investigation* 125, 1069-1080

Neilson, J.R., Zheng, G.X.Y., Burge, C.B., and Sharp, P.A. (2007). Dynamic regulation of miRNA expression in ordered stages of cellular development. *Genes & development* 21, 578-589

Niu, N., and Qin, X. (2013). New insights into IL-7 signaling pathways during early and late T cell development. *Cellular & molecular immunology* 10, 187-189

Nossal, G.J. (1994). Negative selection of lymphocytes. *Cell* 76, 229-239

Olariu, V., Yui, M.A., Krupinski, P., Zhou, W., Deichmann, J., Andersson, E., Rothenberg, E.V., and Peterson, C. (2021). Multi-scale Dynamical Modeling of T Cell Development from an Early Thymic Progenitor State to Lineage Commitment. *Cell Reports* 34, 108622

Olive, V., Bennett, M.J., Walker, J.C., Ma, C., Jiang, I., Cordon-Cardo, C., Li, Q.-J., Lowe, S.W., Hannon, G.J., and He, L. (2009). miR-19 is a key oncogenic component of mir-17-92. *Genes & development* 23, 2839-2849

Ozsolak, F., Poling, L.L., Wang, Z., Liu, H., Liu, X.S., Roeder, R.G., Zhang, X., Song, J.S., and Fisher, D.E. (2008). Chromatin structure analyses identify miRNA promoters. *Genes & development* 22, 3172-3183

Patrick, D.M., Montgomery, R.L., Qi, X., Obad, S., Kauppinen, S., Hill, J.A., van Rooij, E., and Olson, E.N. (2010). Stress-dependent cardiac remodeling occurs in the absence of microRNA-21 in mice. *The Journal of clinical investigation* 120, 3912-3916

Pearse, M., Wu, L., Egerton, M., Wilson, A., Shortman, K., and Scollay, R. (1989). A murine early thymocyte developmental sequence is marked by transient expression of the interleukin 2 receptor. *Proceedings of the National Academy of Sciences of the United States of America* 86, 1614-1618

Pei, W., Shang, F., Wang, X., Fanti, A.-K., Greco, A., Busch, K., Klapproth, K., Zhang, Q., Quedenau, C., and Sauer, S., et al. (2020). Resolving Fates and Single-Cell Transcriptomes of Hematopoietic Stem Cell Clones by PolyloxExpress Barcoding. *Cell stem cell* 27, 383-395.e8

Pei, W., Wang, X., Rössler, J., Feyerabend, T.B., Höfer, T., and Rodewald, H.-R. (2019). Using Cre-recombinase-driven Polylox barcoding for in vivo fate mapping in mice. *Nature protocols* 14, 1820-1840

Penit, C. (1988). Localization and phenotype of cycling and post-cycling murine thymocytes studied by simultaneous detection of bromodeoxyuridine and surface antigens. *The journal of histochemistry and cytochemistry : official journal of the Histochemistry Society* 36, 473-478

Penit, C. (1990). Positive selection is an early event in thymocyte differentiation: high TCR expression by cycling immature thymocytes precedes final maturation by several days. *International immunology* 2, 629-638

Penit, C., and Ezine, S. (1989). Cell proliferation and thymocyte subset reconstitution in sublethally irradiated mice: compared kinetics of endogenous and intrathymically transferred progenitors. *Proceedings of the National Academy of Sciences of the United States of America* 86, 5547-5551

Penit, C., and Vasseur, F. (1988). Sequential events in thymocyte differentiation and thymus regeneration revealed by a combination of bromodeoxyuridine DNA labeling and antimitotic drug treatment. *Journal of immunology (Baltimore, Md. : 1950)* 140, 3315-3323

Penit, C., Vasseur, F., and Papiernik, M. (1988). In vivo dynamics of CD4-8- thymocytes. Proliferation, renewal and differentiation of different cell subsets

studied by DNA biosynthetic labeling and surface antigen detection. *European journal of immunology* 18, 1343-1350

Pénit, C., Lucas, B., and Vasseur, F. (1995). Cell expansion and growth arrest phases during the transition from precursor (CD4-8-) to immature (CD4+8+) thymocytes in normal and genetically modified mice. *Journal of immunology (Baltimore, Md. : 1950)* 154, 5103-5113

Pénit, C., and Vasseur, F. (1997). Expansion of mature thymocyte subsets before emigration to the periphery. *Journal of immunology (Baltimore, Md. : 1950)* 159, 4848-4856

Pennycook, B.R., and Barr, A.R. (2020). Restriction point regulation at the crossroads between quiescence and cell proliferation. *FEBS letters*

Perry, S.S., Wang, H., Pierce, L.J., Yang, A.M., Tsai, S., and Spangrude, G.J. (2004). L-selectin defines a bone marrow analog to the thymic early T-lineage progenitor. *Blood* 103, 2990-2996

Petrie, H.T., Livak, F., Burtrum, D., and Mazel, S. (1995). T cell receptor gene recombination patterns and mechanisms: cell death, rescue, and T cell production. *The Journal of experimental medicine* 182, 121-127

Petrie, H.T., and Zúñiga-Pflücker, J.C. (2007). Zoned out: functional mapping of stromal signaling microenvironments in the thymus. *Annual review of immunology* 25, 649-679

Porritt, H.E., Gordon, K., and Petrie, H.T. (2003). Kinetics of steady-state differentiation and mapping of intrathymic-signaling environments by stem cell transplantation in nonirradiated mice. *The Journal of experimental medicine* 198, 957-962

Porritt, H.E., Rumfelt, L.L., Tabrizifard, S., Schmitt, T.M., Zúñiga-Pflücker, J.C., and Petrie, H.T. (2004). Heterogeneity among DN1 prothymocytes reveals multiple progenitors with different capacities to generate T cell and non-T cell lineages. *Immunity* 20, 735-745

Powell, B.H., Turchinovich, A., Wang, Y., Liao, Z., Dar, M.A., La Rocca, G., Umanah, G.E., Zeiger, M.A., Umbricht, C.B., and Witwer, K.W. (2020). mir-21 is associated with inactive low molecular weight Argonaute complexes in thyroid cancer cell lines. bioRxiv preprint
doi:https://doi.org/10.1101/2020.03.24.006072

Prockop, S.E., Palencia, S., Ryan, C.M., Gordon, K., Gray, D., and Petrie, H.T. (2002). Stromal cells provide the matrix for migration of early lymphoid progenitors through the thymic cortex. *Journal of immunology (Baltimore, Md. : 1950)* 169, 4354-4361

Qiu, X., Mao, Q., Tang, Y., Wang, L., Chawla, R., Pliner, H.A., and Trapnell, C. (2017). Reversed graph embedding resolves complex single-cell trajectories. *Nature methods* 14, 979-982

Radtke, F., Wilson, A., Stark, G., Bauer, M., van Meerwijk, J., MacDonald, H.R., and Aguet, M. (1999). Deficient T cell fate specification in mice with an induced inactivation of Notch1. *Immunity* 10, 547-558

Rappez, L., Rakhlin, A., Rigopoulos, A., Nikolenko, S., and Alexandrov, T. (2020). DeepCycle reconstructs a cyclic cell cycle trajectory from unsegmented cell images using convolutional neural networks. *Molecular systems biology* 16, e9474

Regelin, M., Blume, J., Pommerencke, J., Vakilzadeh, R., Witzlau, K., Łyszkiewicz, M., Ziętara, N., Saran, N., Schambach, A., and Krueger, A. (2015). Responsiveness of Developing T Cells to IL-7 Signals Is Sustained by miR-17∼92. *Journal of immunology (Baltimore, Md. : 1950)* 195, 4832-4840

Ribas, J., Ni, X., Castanares, M., Liu, M.M., Esopi, D., Yegnasubramanian, S., Rodriguez, R., Mendell, J.T., and Lupold, S.E. (2012). A novel source for miR-21 expression through the alternative polyadenylation of VMP1 gene transcripts. *Nucleic acids research* 40, 6821-6833

Robert, P.A., Kunze-Schumacher, H., Greiff, V., and Krueger, A. (2021). Modeling the Dynamics of T-Cell Development in the Thymus. *Entropy (Basel, Switzerland)* 23

Rodewald, H.R., Ogawa, M., Haller, C., Waskow, C., and DiSanto, J.P. (1997). Pro-thymocyte expansion by c-kit and the common cytokine receptor gamma chain is essential for repertoire formation. *Immunity* 6, 265-272

Rodewald, H.-R., and Fehling, H.J. (1998). Molecular and Cellular Events in Early Thymocyte Development 11Received for publication October 14, 1997. In (Elsevier), pp. 1–112

Rose, S.A., Wroblewska, A., Dhainaut, M., Yoshida, H., Shaffer, J.M., Bektesevic, A., Ben-Zvi, B., Rhoads, A., Kim, E.Y., and Yu, B., et al. (2021). A microRNA expression and regulatory element activity atlas of the mouse immune system. *Nature immunology* 22, 914-927

Rossi, F.M.V., Corbel, S.Y., Merzaban, J.S., Carlow, D.A., Gossens, K., Duenas, J., So, L., Yi, L., and Ziltener, H.J. (2005). Recruitment of adult thymic progenitors is regulated by P-selectin and its ligand PSGL-1. *Nature immunology* 6, 626-634

Rothenberg, E.V. (2021). Single-cell insights into the hematopoietic generation of T-lymphocyte precursors in mouse and human. *Experimental hematology* 95, 1-12

Rouas, R., Fayyad-Kazan, H., El Zein, N., Lewalle, P., Rothé, F., Simion, A., Akl, H., Mourtada, M., El Rifai, M., and Burny, A., et al. (2009). Human natural Treg microRNA signature: role of microRNA-31 and microRNA-21 in FOXP3 expression. *European journal of immunology* 39, 1608-1618

Rowell, E.A., and Wells, A.D. (2006). The role of cyclin-dependent kinases in T-cell development, proliferation, and function. *Critical reviews in immunology* 26, 189-212

Ru, H., Chambers, M.G., Fu, T.-M., Tong, A.B., Liao, M., and Wu, H. (2015). Molecular Mechanism of V(D)J Recombination from Synaptic RAG1-RAG2 Complex Structures. *Cell* 163, 1138-1152

Ruan, Q., Wang, P., Wang, T., Qi, J., Wei, M., Wang, S., Fan, T., Johnson, D., Wan, X., and Shi, W., et al. (2014). MicroRNA-21 regulates T-cell apoptosis by directly targeting the tumor suppressor gene Tipe2. *Cell death & disease* 5, e1095

Rubin, S.M., Sage, J., and Skotheim, J.M. (2020). Integrating Old and New Paradigms of G1/S Control. *Molecular cell* 80, 183-192

Salzman, D.W., Nakamura, K., Nallur, S., Dookwah, M.T., Metheetrairut, C., Slack, F.J., and Weidhaas, J.B. (2016). miR-34 activity is modulated through 5'-end phosphorylation in response to DNA damage. *Nature communications* 7, 10954

Sandberg, R., Neilson, J.R., Sarma, A., Sharp, P.A., and Burge, C.B. (2008). Proliferating cells express mRNAs with shortened 3' untranslated regions and fewer microRNA target sites. *Science (New York, N.Y.)* 320, 1643-1647

Sandrock, I., Ziętara, N., Łyszkiewicz, M., Oberdörfer, L., Witzlau, K., Krueger, A., and Prinz, I. (2015). MicroRNA-181a/b-1 Is Not Required for Innate γδ NKT Effector Cell Development. *PloS one* 10, e0145010

Saran, N., Łyszkiewicz, M., Pommerencke, J., Witzlau, K., Vakilzadeh, R., Ballmaier, M., Boehmer, H. von, and Krueger, A. (2010). Multiple extrathymic precursors contribute to T-cell development with different kinetics. *Blood* 115, 1137-1144

Saran, N., Pommerencke, J., Witzlau, K., Regelin, M., and Krueger, A. (2012). Extra-thymic physiological T lineage progenitor activity is exclusively confined to cells expressing either CD127, CD90, or high levels of CD117. *PloS one* 7, e30864

Sarmiento, M., Glasebrook, A.L., and Fitch, F.W. (1980). IgG or IgM monoclonal antibodies reactive with different determinants on the molecular complex bearing Lyt 2 antigen block T cell-mediated cytolysis in the absence of complement. *Journal of immunology (Baltimore, Md. : 1950)* 125, 2665-2672

Sawicka, M., Stritesky, G.L., Reynolds, J., Abourashchi, N., Lythe, G., Molina-París, C., and Hogquist, K.A. (2014). From pre-DP, post-DP, SP4, and SP8 Thymocyte Cell Counts to a Dynamical Model of Cortical and Medullary Selection. *Frontiers in immunology* 5, 19

Schaffert, S.A., Loh, C., Wang, S., Arnold, C.P., Axtell, R.C., Newell, E.W., Nolan, G., Ansel, K.M., Davis, M.M., and Steinman, L., et al. (2015). mir-181a-1/b-1 Modulates Tolerance through Opposing Activities in Selection and Peripheral T Cell Function. *Journal of immunology (Baltimore, Md. : 1950)* 195, 1470-1479

Schatz, D.G. (2004). V(D)J recombination. *Immunological reviews* 200, 5-11

Schatz, D.G., and Ji, Y. (2011). Recombination centres and the orchestration of V(D)J recombination. *Nature reviews. Immunology* 11, 251-263

Schetter, A.J., Leung, S.Y., Sohn, J.J., Zanetti, K.A., Bowman, E.D., Yanaihara, N., Yuen, S.T., Chan, T.L., Kwong, D.L.W., and Au, G.K.H., et al. (2008). MicroRNA expression profiles associated with prognosis and therapeutic outcome in colon adenocarcinoma. *JAMA* 299, 425-436

Schlenner, S.M., Madan, V., Busch, K., Tietz, A., Läufle, C., Costa, C., Blum, C., Fehling, H.J., and Rodewald, H.-R. (2010). Fate mapping reveals separate origins of T cells and myeloid lineages in the thymus. *Immunity* 32, 426-436

Schmitt, T.M., and Zúñiga-Pflücker, J.C. (2002). Induction of T Cell Development from hematopoietic progenitor cells by Delta-like-1 in vitro. *Immunity* 17, 749-756

Schwarting, R., Gerdes, J., Niehus, J., Jaeschke, L., and Stein, H. (1986). Determination of the growth fraction in cell suspensions by flow cytometry using the monoclonal antibody Ki-67. *Journal of immunological methods* 90, 65-70

Schwarz, B.A., and Bhandoola, A. (2004). Circulating hematopoietic progenitors with T lineage potential. *Nature immunology* 5, 953-960

Schwarz, B.A., Sambandam, A., Maillard, I., Harman, B.C., Love, P.E., and Bhandoola, A. (2007). Selective thymus settling regulated by cytokine and chemokine receptors. *Journal of immunology (Baltimore, Md. : 1950)* 178, 2008-2017

Scimone, M.L., Aifantis, I., Apostolou, I., Boehmer, H. von, and Andrian, U.H. von (2006). A multistep adhesion cascade for lymphoid progenitor cell homing to the thymus. *Proceedings of the National Academy of Sciences of the United States of America* 103, 7006-7011

Scollay, R., and Shortman, K. (1985). Identification of early stages of T lymphocyte development in the thymus cortex and medulla. *Journal of immunology (Baltimore, Md. : 1950)* 134, 3632-3642

Scollay, R., Smith, J., and Stauffer, V. (1986). Dynamics of early T cells: prothymocyte migration and proliferation in the adult mouse thymus. *Immunological reviews* 91, 129-157

Scollay, R., Wilson, A., D'Amico, A., Kelly, K., Egerton, M., Pearse, M., Wu, L., and Shortman, K. (1988). Developmental status and reconstitution potential of subpopulations of murine thymocytes. *Immunological reviews* 104, 81-120

Scollay, R.G., Butcher, E.C., and Weissman, I.L. (1980). Thymus cell migration. Quantitative aspects of cellular traffic from the thymus to the periphery in mice. *European journal of immunology* 10, 210-218

Serwold, T., Ehrlich, L.I.R., and Weissman, I.L. (2009). Reductive isolation from bone marrow and blood implicates common lymphoid progenitors as the major source of thymopoiesis. *Blood* 113, 807-815

Shortman, K., Egerton, M., Spangrude, G.J., and Scollay, R. (1990). The generation and fate of thymocytes. *Seminars in immunology* 2, 3-12

Si, M.-L., Zhu, S., Wu, H., Lu, Z., Wu, F., and Mo, Y.-Y. (2007). miR-21-mediated tumor growth. *Oncogene* 26, 2799-2803

Sicinska, E., Aifantis, I., Le Cam, L., Swat, W., Borowski, C., Yu, Q., Ferrando, A.A., Levin, S.D., Geng, Y., and Boehmer, H. von, et al. (2003). Requirement for cyclin D3 in lymphocyte development and T cell leukemias. *Cancer cell* 4, 451-461

Singer, A., Adoro, S., and Park, J.-H. (2008). Lineage fate and intense debate: myths, models and mechanisms of CD4- versus CD8-lineage choice. *Nature reviews. Immunology* 8, 788-801

Smigielska-Czepiel, K., van den Berg, A., Jellema, P., Slezak-Prochazka, I., Maat, H., van den Bos, H., van der Lei, R.J., Kluiver, J., Brouwer, E., and Boots, A.M.H., et al. (2013). Dual role of miR-21 in CD4+ T-cells: activation-induced miR-21 supports survival of memory T-cells and regulates CCR7 expression in naive T-cells. *PloS one* 8, e76217

Song, J., Shao, Q., Li, C., Liu, H., Li, J., Wang, Y., Song, W., Li, L., Wang, G., and Shao, Z., et al. (2017). Effects of microRNA-21 on apoptosis by regulating the expression of PTEN in diffuse large B-cell lymphoma. *Medicine* 96, e7952

Stritesky, G.L., Jameson, S.C., and Hogquist, K.A. (2012). Selection of self-reactive T cells in the thymus. *Annual review of immunology* 30, 95-114

Stritesky, G.L., Xing, Y., Erickson, J.R., Kalekar, L.A., Wang, X., Mueller, D.L., Jameson, S.C., and Hogquist, K.A. (2013). Murine thymic selection quantified using a unique method to capture deleted T cells. *Proceedings of the National Academy of Sciences of the United States of America* 110, 4679-4684

Surdziel, E., Cabanski, M., Dallmann, I., Lyszkiewicz, M., Krueger, A., Ganser, A., Scherr, M., and Eder, M. (2011). Enforced expression of miR-125b affects myelopoiesis by targeting multiple signaling pathways. *Blood* 117, 4338-4348

Svensson, M., Marsal, J., Uronen-Hansson, H., Cheng, M., Jenkinson, W., Cilio, C., Jacobsen, S.E.W., Sitnicka, E., Anderson, G., and Agace, W.W. (2008). Involvement of CCR9 at multiple stages of adult T lymphopoiesis. *Journal of leukocyte biology* 83, 156-164

Teague, T.K., Tan, C., Marino, J.H., Davis, B.K., Taylor, A.A., Huey, R.W., and van de Wiele, C.J. (2010). CD28 expression redefines thymocyte development during the pre-T to DP transition. *International immunology* 22, 387-397

Teteloshvili, N., Smigielska-Czepiel, K., Yuan, Y., Seitz, A., Jong, D. de, Rutgers, B., Jellema, P., van der Lei, R.J., Slezak-Prochazka, I., and Brouwer, E., et al. (2017). Argonaute 2 immunoprecipitation revealed large tumor suppressor kinase 1 as a novel proapoptotic target of miR-21 in T cells. *The FEBS journal* 284, 555-567

Thum, T., Gross, C., Fiedler, J., Fischer, T., Kissler, S., Bussen, M., Galuppo, P., Just, S., Rottbauer, W., and Frantz, S., et al. (2008). MicroRNA-21 contributes to myocardial disease by stimulating MAP kinase signalling in fibroblasts. *Nature* 456, 980-984

Toivakka, M., Gordon, K., Kumar, S., Zamoyska, R., and Buck, A. (2020). Analysis of High Molecular Weight RNA-induced silencing complex (HMW-RISC) in CD8 + T cells identifies miR-7 as a modulator of T cell activation. bioRxiv preprint doi: https://doi.org/10.1101/2020.05.17.100339

Tomooka, S., Matsuzaki, G., Kishihara, K., Tanaka, K., Yoshikai, Y., Taniguchi, K., Himeno, K., and Nomoto, K. (1987). Sequential appearance of thymocyte subpopulations and T cell antigen receptor gene messages in the mouse thymus after sublethal irradiation. *Journal of immunology (Baltimore, Md. : 1950)* 139, 3986-3990

Tomura, M., Sakaue-Sawano, A., Mori, Y., Takase-Utsugi, M., Hata, A., Ohtawa, K., Kanagawa, O., and Miyawaki, A. (2013). Contrasting quiescent G0 phase with mitotic cell cycling in the mouse immune system. *PloS one* 8, e73801

Tsang, J.S., Ebert, M.S., and van Oudenaarden, A. (2010). Genome-wide dissection of microRNA functions and cotargeting networks using gene set signatures. *Molecular cell* 38, 140-153

Turka, L.A., Schatz, D.G., Oettinger, M.A., Chun, J.J., Gorka, C., Lee, K., McCormack, W.T., and Thompson, C.B. (1991). Thymocyte expression of RAG-1 and RAG-2: termination by T cell receptor cross-linking. *Science (New York, N.Y.)* 253, 778-781

Uehara, S., Grinberg, A., Farber, J.M., and Love, P.E. (2002). A role for CCR9 in T lymphocyte development and migration. *Journal of immunology (Baltimore, Md. : 1950)* 168, 2811-2819

Umland, O., Mwangi, W.N., Anderson, B.M., Walker, J.C., and Petrie, H.T. (2007). The blood contains multiple distinct progenitor populations with clonogenic B and T lineage potential. *Journal of immunology (Baltimore, Md. : 1950)* 178, 4147-4152

Vasseur, F., Le Campion, A., and Pénit, C. (2001). Scheduled kinetics of cell proliferation and phenotypic changes during immature thymocyte generation. *European journal of immunology* 31, 3038-3047

Veerman, K.M., Williams, M.J., Uchimura, K., Singer, M.S., Merzaban, J.S., Naus, S., Carlow, D.A., Owen, P., Rivera-Nieves, J., and Rosen, S.D., et al. (2007). Interaction of the selectin ligand PSGL-1 with chemokines CCL21 and CCL19 facilitates efficient homing of T cells to secondary lymphoid organs. *Nature immunology* 8, 532-539

Vignon, C., Debeissat, C., Georget, M.-T., Bouscary, D., Gyan, E., Rosset, P., and Herault, O. (2013). Flow cytometric quantification of all phases of the cell cycle and apoptosis in a two-color fluorescence plot. *PloS one* 8, e68425

Visan, I., Yuan, J.S., Liu, Y., Stanley, P., and Guidos, C.J. (2010). Lunatic fringe enhances competition for delta-like Notch ligands but does not overcome defective pre-TCR signaling during thymocyte beta-selection in vivo. *Journal of immunology (Baltimore, Md. : 1950)* 185, 4609-4617

Vogel, K.U., Bell, L.S., Galloway, A., Ahlfors, H., and Turner, M. (2016). The RNA-Binding Proteins Zfp36l1 and Zfp36l2 Enforce the Thymic β-Selection Checkpoint by Limiting DNA Damage Response Signaling and Cell Cycle Progression. *Journal of immunology (Baltimore, Md. : 1950)* 197, 2673-2685

Volinia, S., Calin, G.A., Liu, C.-G., Ambs, S., Cimmino, A., Petrocca, F., Visone, R., Iorio, M., Roldo, C., and Ferracin, M., et al. (2006). A microRNA expression signature of human solid tumors defines cancer gene targets. *Proceedings of the National Academy of Sciences of the United States of America* 103, 2257-2261

Wada, H., Masuda, K., Satoh, R., Kakugawa, K., Ikawa, T., Katsura, Y., and Kawamoto, H. (2008). Adult T-cell progenitors retain myeloid potential. *Nature* 452, 768-772

Wallis, V.J., Leuchars, E., Chwalinski, S., and Davies, A.J. (1975). On the sparse seeding of bone marrow and thymus in radiation chimaeras. *Transplantation* 19, 2-11

Wang, C., Peng, R., Zeng, M., Zhang, Z., Liu, S., Jiang, D., Lu, Y., and Zou, F. (2020). An autoregulatory feedback loop of miR-21/VMP1 is responsible for the abnormal expression of miR-21 in colorectal cancer cells. *Cell death & disease* 11, 1067

Wang, L., He, L., Zhang, R., Liu, X., Ren, Y., Liu, Z., Zhang, X., Cheng, W., and Hua, Z.-C. (2014). Regulation of T lymphocyte activation by microRNA-21. *Molecular immunology* 59, 163-171

Weber, B.N., Chi, A.W.-S., Chavez, A., Yashiro-Ohtani, Y., Yang, Q., Shestova, O., and Bhandoola, A. (2011). A critical role for TCF-1 in T-lineage specification and differentiation. *Nature* 476, 63-68

Weber, T.S., Jaehnert, I., Schichor, C., Or-Guil, M., and Carneiro, J. (2014). Quantifying the length and variance of the eukaryotic cell cycle phases by a stochastic model and dual nucleoside pulse labelling. *PLoS computational biology* 10, e1003616

Wertheimer, T., Velardi, E., Tsai, J., Cooper, K., Xiao, S., Kloss, C.C., Ottmüller, K.J., Mokhtari, Z., Brede, C., and deRoos, P., et al. (2018). Production of BMP4 by endothelial cells is crucial for endogenous thymic regeneration. *Science immunology* 3

Winter, J., Jung, S., Keller, S., Gregory, R.I., and Diederichs, S. (2009). Many roads to maturity: microRNA biogenesis pathways and their regulation. *Nature cell biology* 11, 228-234

Winter, S.J. (2020). The role of miR-181a/b-1 in thymic development (Frankfurt am Main: Universitätsbibliothek Johann Christian Senckenberg)

Winter, S.J., and Krueger, A. (2019). Development of Unconventional T Cells Controlled by MicroRNA. *Frontiers in immunology* 10, 2520

Winter, S.J., Kunze-Schumacher, H., Imelmann, E., Grewers, Z., Osthues, T., and Krueger, A. (2019). MicroRNA miR-181a/b-1 controls MAIT cell development. *Immunology and cell biology* 97, 190-202

Witkowski, M., Witkowski, M., Saffarzadeh, M., Friebel, J., Tabaraie, T., Ta Bao, L., Chakraborty, A., Dörner, A., Stratmann, B., and Tschoepe, D., et al. (2020). Vascular miR-181b controls tissue factor-dependent thrombogenicity and inflammation in type 2 diabetes. *Cardiovascular diabetology* 19, 20

Wu, L., Antica, M., Johnson, G.R., Scollay, R., and Shortman, K. (1991). Developmental potential of the earliest precursor cells from the adult mouse thymus. *The Journal of experimental medicine* 174, 1617-1627

Yui, M.A., Feng, N., and Rothenberg, E.V. (2010). Fine-scale staging of T cell lineage commitment in adult mouse thymus. *Journal of immunology (Baltimore, Md. : 1950)* 185, 284-293

Zhao, B., Yoganathan, K., Li, L., Lee, J.Y., Zúñiga-Pflücker, J.C., and Love, P.E. (2019). Notch and the pre-TCR coordinate thymocyte proliferation by induction of the SCF subunits Fbxl1 and Fbxl12. *Nature immunology* 20, 1381-1392

Zhou, W., Gao, F., Romero-Wolf, M., Jo, S., and Rothenberg, E.V. (2021). Single-cell perturbation dissects transcription factor control of progression speed and trajectory choice in early T-cell development. bioRxiv preprint doi: https://doi.org/10.1101/2021.09.03.458944

Ziętara, N., Łyszkiewicz, M., Puchałka, J., Witzlau, K., Reinhardt, A., Förster, R., Pabst, O., Prinz, I., and Krueger, A. (2015). Multicongenic fate mapping quantification of dynamics of thymus colonization. *The Journal of experimental medicine* 212, 1589-1601

Ziętara, N., Łyszkiewicz, M., Witzlau, K., Naumann, R., Hurwitz, R., Langemeier, J., Bohne, J., Sandrock, I., Ballmaier, M., and Weiss, S., et al. (2013). Critical role for miR-181a/b-1 in agonist selection of invariant natural killer T cells. *Proceedings of the National Academy of Sciences of the United States of America* 110, 7407-7412

Zlotoff, D.A., Sambandam, A., Logan, T.D., Bell, J.J., Schwarz, B.A., and Bhandoola, A. (2010). CCR7 and CCR9 together recruit hematopoietic progenitors to the adult thymus. *Blood* 115, 1897-1905

7 Abbreviations

7-AAD	7-Aminoactinomycin D
Ago	Argonaute protein
ANOVA	Analysis of variance
APC	Allophycocyanin
AxV	Annexin V
BM	Bone marrow
BrdU	5-Bromo-2'-deoxyuridine
BV	Brilliant violet
CD	Cluster of Differentiation
CDK	Cyclin-dependent kinase
Cdkn	Cyclin-dependent kinase inhibitor
cDNA	Complementary DNA
CFSE	5-(and 6)-Carboxyfluorescein diacetate succinimidyl ester
CLP	Common lymphoid progenitor
CM	Central memory
CMJ	Corticomedullary junction
cTEC	Cortical thymic epithelial cell
Cy	Cyanine
DAPI	4′,6-diamidino-2-phenylindole
DGCR8	DiGeorge syndrome critical region 8
DKO	Double knockout
DL	Delta-like ligand
DMEM	Dulbecco’s Modified Eagle Medium
DMSO	Dimethyl sulfoxide
DN	Double negative ($CD4^-CD8^-$)
DNA	Deoxyribonucleic acid
dNTP	Desoxyribonukleosidtriphosphat
DP	Double positive ($CD4^+CD8^+$)
EdU	5-Ethynyl-2'-deoxyuridine
EM	Effector memory
ETP	Early T-lineage progenitor
EV	Empty vector
FACS	Fluorescence-activated cell sorting
FCS	Fetal calf serum
FITC	Fluorescein isothiocyanate
Foxp3	Forkhead box protein 3
FSC-A	Forward scatter area

FSC-H	Forward scatter height
FUCCI	Fluorescent ubiquitination-based cell cycle indicator
G	Growth or gap
GFP	Green fluorescent protein
hCDT1	Human Chromatin licensing and DNA replication factor 1
HEK	Human embryonic kidney
HPRT	Hypoxanthine guanine phosphoribosyl transferase
HSC	Hematopoietic stem cell
IL	Interleukin
iNKT	Invariant natural killer T cell
kDa	Kilodalton
KO	Knockout
Lin	Lineage
LMPP	Lymphoid-primed multipotent progenitor
LN	Lymph node
LSK	Lineage negative, Sca1 positive, c-kit negative
LTR	Long terminal repeat
M	Mitosis
MAIT	Mucosal-associated invariant T cell
MEM	Minimum essential media
MHC	Major histocompatibility complex
miR / miRNA	MicroRNA
MKI67	Marker of proliferation Ki-67
MPP	Multipotent progenitor
MRE	miRNA recognition element
mRNA	Messenger RNA
mTEC	Medullary thymic epithelial cell
NK	Natural killer
ns	Not significant
OE	Overexpression
OP	Osteopetrotic
P/S	Penicillin/streptomycin
PB	Pacific blue
PBS	Phosphate buffered saline
PDCD4	Programmed cell death protein 4
PE	Phycoerythrin
PerCP	Peridinin chlorophyll protein
PI	Propidium iodide
pMHC	Peptide-Major histocompatibility complex

PTEN	Phosphatase and Tensin homolog
qRT-PCR	Quantitative Real-Time PCR
RAG	Recombination-activating gene
RBC	Red blood cell
RISC	RNA-induced silencing complex
RM	Relative movement
RNA	Ribonucleic acid
RT	Room temperature
S	Synthesis
SCF	Stem cell factor
scRNA-seq	Single-cell RNA-sequencing
SP	Single positive (CD4 or CD8)
SPRY1	Sprouty RTK Signaling Antagonist 1
SSC-A	Side scatter area
SSC-H	Side scatter height
TCR	T-cell receptor
TMEM	Transmembrane protein
TRBP	Transactivation response element RNA-binding protein
Treg	Regulatory T cell
TSP	Thymus seeding progenitor
UTR	Untranslated region
VMP	Vacuole membrane protein
WT	Wild-type

8 List of figures

9 List of tables

10 Appendix

% of cells in S <2 hrs	DN1	DN2	DN3a	DN3b	DN4	Pre-sel. DP	Post-sel. DP	SP8	SP4
DN1									
DN2	<0.0001								
DN3a	0.9812	<0.0001							
DN3b	<0.0001	0.0008	<0.0001						
DN4	<0.0001	0.1938	<0.0001	<0.0001					
Pre-sel. DP	0.8614	<0.0001	0.9995	<0.0001	<0.0001				
Post-sel. DP	0.06	<0.0001	0.0944	<0.0001	<0.0001	0.3142			
SP8	0.8485	<0.0001	0.9991	<0.0001	<0.0001	>0.9999	0.3924		
SP4	>0.9999	<0.0001	0.9607	<0.0001	<0.0001	0.7771	0.0285	0.7619	

Rate of entry <1 hr	DN1	DN2	DN3a	DN3b	DN4	Pre-sel. DP	Post-sel. DP	SP8	SP4
DN1									
DN2	<0.0001								
DN3a	0.9998	<0.0001							
DN3b	<0.0001	0.0005	<0.0001						
DN4	<0.0001	0.4378	<0.0001	0.3334					
Pre-sel. DP	0.9948	<0.0001	>0.9999	<0.0001	<0.0001				
Post-sel. DP	>0.9999	<0.0001	0.9052	<0.0001	<0.0001	0.6316			
SP8	>0.9999	<0.0001	0.9969	<0.0001	<0.0001	0.9401	0.9997		
SP4	0.9895	<0.0001	0.7138	<0.0001	<0.0001	0.4716	0.9977	0.9636	

Rate of exit <1 hr	DN1	DN2	DN3a	DN3b	DN4	Pre-sel. DP	Post-sel. DP	SP8	SP4
DN1									
DN2	0.6151								
DN3a	0.0001	0.0015							
DN3b	0.0054	<0.0001	<0.0001						
DN4	0.9483	0.0006	<0.0001	0.0088					
Pre-sel. DP	0.0136	0.3043	0.5881	<0.0001	<0.0001				
Post-sel. DP	<0.0001	<0.0001	0.9994	<0.0001	<0.0001	0.1788			
SP8	<0.0001	<0.0001	0.9739	<0.0001	<0.0001	0.064	>0.9999		
SP4	0.005	0.1159	>0.9999	<0.0001	<0.0001	0.9714	0.9969	0.9673	

Figure 48: Statistical analyses of steady-state thymocyte cell cycle dynamics.
Summary of ordinary one-way ANOVA followed by Tukey's multiple comparisons test. Results obtained from data shown in Figure 13. Numbers represent adjusted P-values by Tukey's Test. Significant results are indicated by colored background.

G1-phase re-entry	DN2	DN3a	DN3b	DN4	Pre-sel. DP	Post-sel. DP
DN2						
DN3a	0.7541					
DN3b	0.5393	0.9991				
DN4	0.0647	0.5686	0.7803			
Pre-sel. DP	0.5593	0.9998	>0.9999	0.6688		
Post-sel. DP	0.0003	<0.0001	<0.0001	<0.0001	<0.0001	

S-phase re-entry	DN2	DN3a	DN3b	DN4	Pre-sel. DP	Post-sel. DP
DN2						
DN3a	0.7036					
DN3b	<0.0001	<0.0001				
DN4	<0.0001	<0.0001	0.1074			
Pre-sel. DP	0.0002	0.0065	0.0308	<0.0001		
Post-sel. DP	0.836	0.9994	<0.0001	<0.0001	0.0017	

Figure 49: Statistical analyses of G1- and S-phase re-entry.
Summary of ordinary one-way ANOVA followed by Tukey's multiple comparisons test. Results obtained from data shown in Figure 15. Numbers represent adjusted P-values by Tukey's Test. Significant results are indicated by colored background. Data from the 6 hrs time point was utilized for comparison.

S-phase duration	DN2	DN3a	DN3b	DN4	Pre-sel. DP	Post-sel. DP
DN2						
DN3a	0.9997					
DN3b	0.2455	0.1478				
DN4	0.1743	0.101	>0.9999			
Pre-sel. DP	0.9998	0.9930	0.3713	0.2753		
Post-sel. DP	0.417	0.2725	0.9992	0.9934	0.5765	

Figure 50: Statistical analyses of RM values.
Summary of ordinary one-way ANOVA followed by Tukey's multiple comparisons test. Results obtained from data shown in Figure 16. Numbers represent adjusted P-values by Tukey's Test. Significant results are indicated by colored background. RM values obtained from the 4 hrs time point were used for comparison.

% of cells in S <2 hrs	DN2	DN3a	DN3b	DN4	Pre-sel. DP	Post-sel. DP	SP8	SP4
DN2								
DN3a	<0.0001							
DN3b	<0.0001	<0.0001						
DN4	0.0092	<0.0001	<0.0001					
Pre-sel. DP	<0.0001	0.9906	<0.0001	<0.0001				
Post-sel. DP	<0.0001	>0.9999	<0.0001	<0.0001	0.9763			
SP8	<0.0001	0.6446	<0.0001	<0.0001	0.9785	0.548		
SP4	<0.0001	0.0375	<0.0001	<0.0001	0.2396	0.0246	0.8381	

Rate of entry <1 hr	DN2	DN3a	DN3b	DN4	Pre-sel. DP	Post-sel. DP	SP8	SP4
DN2								
DN3a	<0.0001							
DN3b	<0.0001	<0.0001						
DN4	0.9991	<0.0001	<0.0001					
Pre-sel. DP	<0.0001	0.9974	<0.0001	<0.0001				
Post-sel. DP	<0.0001	0.063	<0.0001	<0.0001	0.2515			
SP8	<0.0001	0.0142	<0.0001	<0.0001	0.0786	0.9998		
SP4	<0.0001	0.0021	<0.0001	<0.0001	0.015	0.9703	0.9992	

Rate of exit <1 hr	DN2	DN3a	DN3b	DN4	Pre-sel. DP	Post-sel. DP	SP8	SP4
DN2								
DN3a	<0.0001							
DN3b	<0.0001	<0.0001						
DN4	0.2272	<0.0001	<0.0001					
Pre-sel. DP	<0.0001	0.9706	<0.0001	<0.0001				
Post-sel. DP	<0.0001	0.8717	<0.0001	<0.0001	0.2396			
SP8	<0.0001	0.7511	<0.0001	<0.0001	0.1386	>0.9999		
SP4	<0.0001	0.9147	<0.0001	<0.0001	0.2896	>0.9999	>0.9999	

Figure 51: Statistical analyses of DKO thymocyte cell cycle dynamics.
Summary of ordinary one-way ANOVA followed by Tukey's multiple comparisons test. Results obtained from data shown in Figure 19. Numbers represent adjusted P-values by Tukey's Test. Significant results are indicated by colored background.

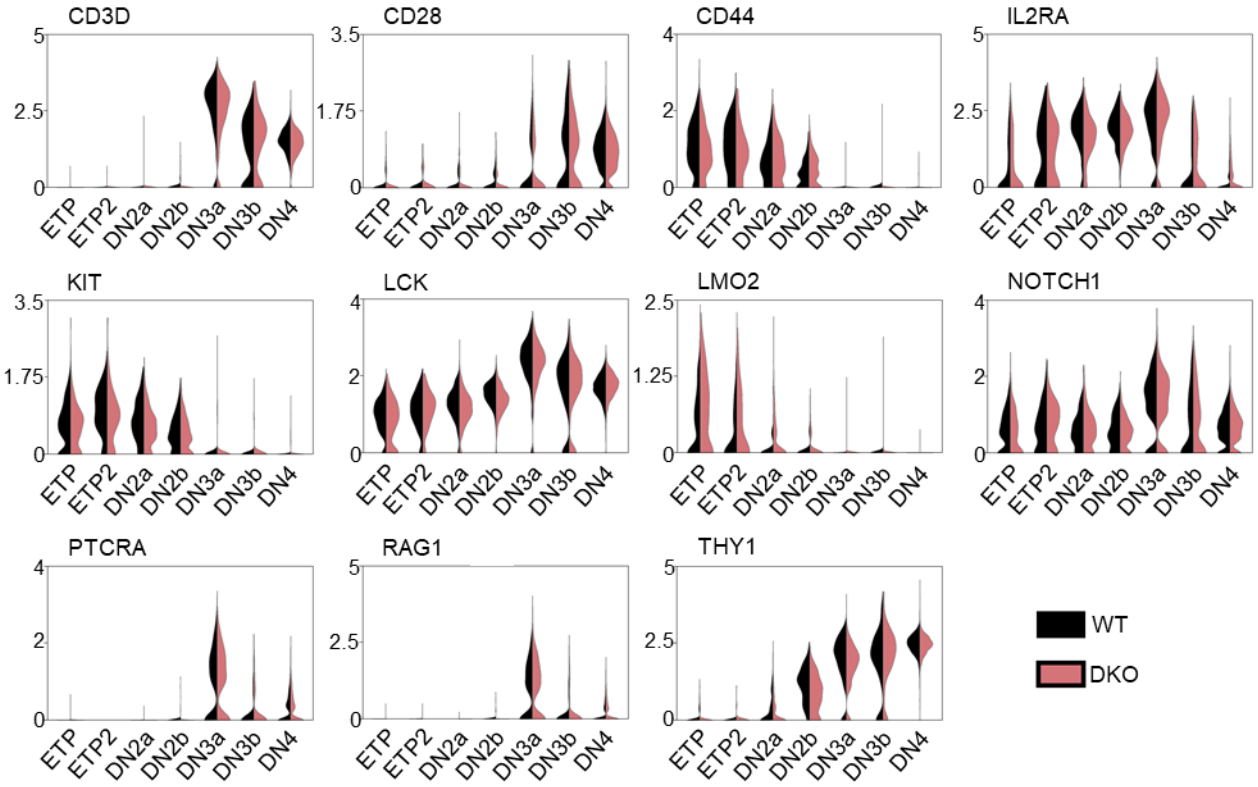

Figure 52: Gene expression of common markers to identify thymocyte supopulations.
Violin plots represent expression patterns of specific genes as indicated in the seven different WT (black) and DKO (pink) thymocyte subsets.

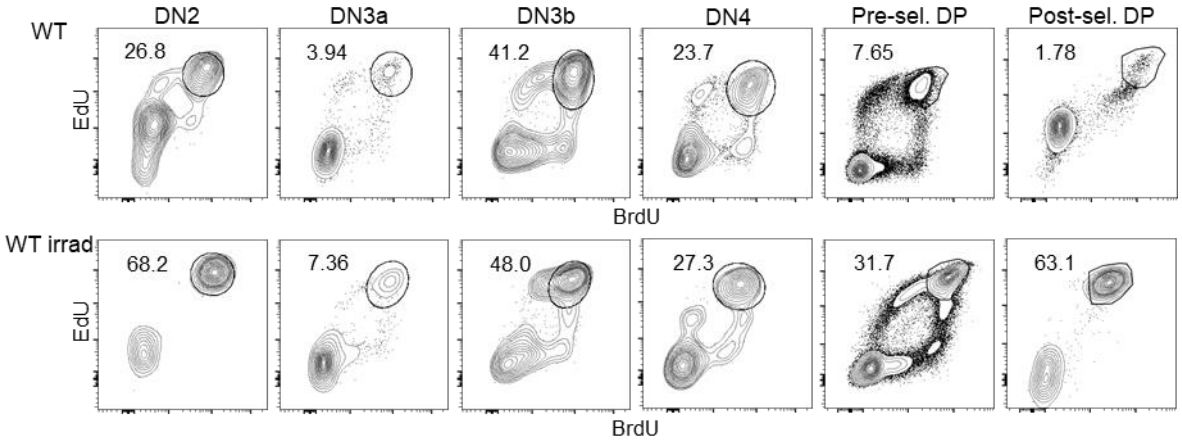

Figure 53: S-phase profiling of thymocyte subsets of control and irradiated WT mice.
Representative flow cytometric analysis of WT and irradiated WT thymocyte subsets stained for BrdU and EdU incorporation (data shown in Figure 29). Numbers in plots indicate frequencies of EdU^+BrdU^+ cells.

% of cells in S <2 hrs	DN2	DN3a	DN3b	DN4	Pre-sel. DP	Post-sel. DP
DN2						
DN3a	<0.0001					
DN3b	0.0005	<0.0001				
DN4	<0.0001	0.0001	<0.0001			
Pre-sel. DP	<0.0001	<0.0001	0.0015	0.6177		
Post-sel. DP	0.0462	<0.0001	0.6565	<0.0001	<0.0001	

Rate of entry <1 hr	DN2	DN3a	DN3b	DN4	Pre-sel. DP
DN2					
DN3a	>0.9999				
DN3b	0.0001	0.0001			
DN4	<0.0001	<0.0001	<0.0001		
Pre-sel. DP	0.0118	0.0122	0.5829	<0.0001	

Rate of exit <1 hr	DN2	DN3a	DN3b	DN4	Pre-sel. DP
DN2					
DN3a	0.2778				
DN3b	<0.0001	<0.0001			
DN4	0.0002	<0.0001	0.0301		
Pre-sel. DP	0.0021	<0.0001	0.003	0.9487	

Figure 54: Statistical analyses of S-phase kinetics upon irradiation.
Summary of ordinary one-way ANOVA followed by Tukey's multiple comparisons test. Results obtained from data shown in Figure 29. Numbers represent adjusted P-values by Tukey's test. Significant results are indicated by colored background.

14 Eidesstattliche Versicherung

Ich erkläre hiermit an Eides Statt, dass ich die vorgelegte Dissertation mit dem Titel „Molecular and Cellular Control of Intrathymic T-Cell Development“ selbstständig angefertigt und mich keiner anderen Hilfsmittel als der in ihr angegebenen bedient habe, insbesondere, dass alle Entlehnungen aus anderen Schriften mit Angabe der betreffenden Schrift gekennzeichnet sind.

Ich versichere, nicht die Hilfe einer kommerziellen Promotionsvermittlung in Anspruch genommen zu haben.

Frankfurt am Main, den _____ _____

(Unterschrift)